

684-7  
NATIONAL ADVISORY COMMITTEE FOR AERONAUTICS

# WARTIME REPORT

ORIGINALLY ISSUED

October 1940 as  
Advance Confidential Report

DRAG ANALYSIS OF SINGLE-ENGINE MILITARY AIRPLANES

TESTED IN THE NACA FULL-SCALE WIND TUNNEL

By C. H. Dearborn and Abe Silverstein

Langley Memorial Aeronautical Laboratory  
Langley Field, Va.

CASE FILE  
COPY



WASHINGTON

NACA WARTIME REPORTS are reprints of papers originally issued to provide rapid distribution of advance research results to an authorized group requiring them for the war effort. They were previously held under a security status but are now unclassified. Some of these reports were not technically edited. All have been reproduced without change in order to expedite general distribution.

# DRAG ANALYSIS OF SINGLE-ENGINE MILITARY AIRPLANE

## TESTED IN THE NACA FULL-SCALE WIND TUNNEL

By C. H. Dearborn and Abe Silverstein

### INTRODUCTION

Tests have been made in the NACA full-scale wind tunnel on 11 single-engine military airplanes to investigate methods for increasing their high speed. The airplanes were tested for the Navy Bureau of Aeronautics and the Army Air Corps, and separate reports have been forwarded to these agencies. Repetition of similar inefficient design features on many of the airplanes indicated the desirability of analyzing and combining all of the results into a single paper for distribution to designers. The data for the various airplanes are not consistent in scope since the extent of the tests depended on the possibility of making alterations to the particular airplane and the time available for the tests.

The discrepancies between the computed high speeds for ideal airplane arrangements and the speeds actually reached by standard military types are well known, and it is largely the purpose of this paper to indicate the sources of these differences. The compromises involved in the engineering design of the airplanes that were tested often led to disadvantageous combinations of their basic components. The advantages of elegant refinements to the basic aerodynamic elements in other cases were nullified by inattention to detail, and established aerodynamic principles were violated to simplify structural problems. In the tests the modifications were usually limited to those which practically could be applied to the existing airplanes, and the gains that were realized were by no means the maximum. Changes were guided by fundamental information obtained from studies throughout the laboratory on cowlings, ducts, etc. It will be possible to utilize some of the data directly in design; however, it is believed that the results are of greater importance in indicating errors to be avoided. As a guide, comparisons are made wherever possible between the test arrangements and the ideal.

The investigations included numerous studies of cooling and cowlings arrangements for air- and liquid-cooled

power plant installations. Scoops for carburetor intakes, for intercoolers, for Prestone radiators, and for oil coolers were tested on many of the airplanes. Measurements of the wing drag by the momentum method were made for each of the airplanes, and measurements of the transition point and the critical compressibility velocity were included to aid in evaluating the wing drag at high speeds. Considerable data were also obtained on the drag of retracted and partially retracted landing gears, windshields, cockpit enclosures, airdials, air leaks, and armament installations.

The drag increments were measured at tunnel speeds between 60 and 100 miles per hour. Increased performances predicted by the tunnel tests from modifications of several of the airplanes were later substantially verified in flight tests.

## AIRPLANES AND EQUIPMENT

Pertinent descriptive data on the airplanes tested are shown in the photographs of the wind-tunnel set-ups (fig. 1), and in the three-view drawings (fig. 2). The airplanes are identified by numbers. The photographs (fig. 1) show most of the airplanes in the condition as received at the full-scale tunnel (designated original condition); however, a few are shown in various stages of modification as described in the figure titles. Sketches and photographs showing details of various components are included with the discussion.

The NACA full-scale wind tunnel is described in reference 1.

## METHODS AND TESTS

In the tests the focal points of excessive drag on the airplane were searched for, after which they were refaired and improved as much as was possible in a practical way. In some cases, components were removed from the airplane and their drag increments measured.

Initially, short tufts and tuft masts were distributed over the surfaces of the airplane and visual and

photographic observations taken of their motion. Disturbed or turbulent motion of the tufts with the airplane in the high-speed attitude normally indicated excessive drag. In the diagnosis of the flow disturbances a rake of total-pressure tubes was used, which could be moved to any position around the airplane. These pressure observations were used qualitatively as a quick means for locating flow break-down, and quantitatively for calculation of the drag coefficient. The drags of the wings and all wing protuberances were measured in this way. The technique of these measurements is described in reference 2.

The air flows through the duct and cowlings installations and the pressure drops through the cooling units were measured. A rake of static- and total-pressure tubes at the duct outlet was most satisfactory for measuring the air-flow quantity, and the pressure drop was measured as the difference between the total pressure ahead of a cooling unit and the total pressure at the outlet. When existing coolers were not adaptable to modified arrangements, they were simulated by perforated plates having the same pressure drop. Ducts and cowlings were usually tested both in the normally open and completely sealed condition, so that the drag due to the cooling air flow could be determined.

The usual balance measurements were made to obtain lift, drag, and pitching-moment characteristics over the angle-of-attack range from zero lift through the stall. Scale effects were measured for a range of tunnel speeds between 60 and 100 miles per hour. Most of the tests were made without operating propellers, but for several of the airplanes power-on data were also obtained.

In order to aid in extrapolating the wing drag to higher Reynolds numbers and to study in greater detail the origin of the wing drag, measurements were made in the wing boundary layer and the transition points were determined over a range of air speeds and angles of attack. (See reference 3.) Measurements were also made of the static pressure distribution at critical points on the airplane to aid in estimating the speed at which compressibility effects on the airplane might become important. These measurements were made either by means of flush orifices or small surface static tubes attached with the static holes approximately 1/16 inch above the surface.



## RESULTS AND DISCUSSION

The over-all drag coefficients of the original airplanes and the increments in drag coefficient due to modifying or removing various airplane components are summarized in table I. The tabulated drag coefficients are given for a high-speed lift coefficient of 0.15 and from tests at a tunnel speed of 100 miles per hour. These drag increments are in most cases also given in the text in pounds at a speed of 100 miles per hour to provide a basis of comparison that will be independent of the airplane wing areas. Typical curves showing scale effect for one of the airplanes between tunnel speeds of 60 and 100 miles per hour are shown in figure 3.

An example of a typical test sequence followed to evaluate the drag of the various airplane components on airplane 8 is shown in figure 4.

Based on the test results and other more fundamental laboratory investigations, various sources of aerodynamic inefficiency are discussed in the following chapters.

## POWER-PLANT INSTALLATION

The most important drag reductions were effected by improvements in the airplane power-plant installation. These included modifications to NACA cowlings, oil-cooler ducts, carburetor air scoops, exhaust stacks, etc. Discussion of the drag of power-plant installations may be separated under the subjects of internal and external air flows. A brief résumé of fundamentals is given when possible to aid in interpreting the test results.

### Internal Air Flow

Cooling drag and duct losses.— The power usefully absorbed in a cooling unit is  $Q\Delta p$ , in which  $Q$  is the air quantity and  $\Delta p$  is the pressure drop across the cooling unit. The actual power absorbed in the installation is larger, owing to duct and wake losses, and may reach the upper value of  $2Qq_0$  when the entire momentum of the cooling air is lost. The term  $q_0$  is the dynamic pressure corresponding to the flight speed. The total power absorbed

between any two sections in a duct, based on calculations of the momentum loss, is given by the expression,

$$P = 2Q \sqrt{q_0} \left[ \sqrt{H_1} - \sqrt{H_2} \right] \quad (1)$$

in which  $H_1$  and  $H_2$  are the total pressures at the two sections.

Numerous equations have been derived to express duct efficiency, all of which include the useful power  $Q\Delta p$  in the numerator. The efficiency of the internal duct flow is

$$\eta_i = \frac{Q\Delta p}{2Q \sqrt{q_0} \left[ \sqrt{H_0} - \sqrt{H_3} \right]} \quad (2)$$

in which  $H_0$  is the free stream total pressure and  $H_3$  is the total pressure at the duct outlet; the over-all efficiency including the effect of the installation on the external drag is

$$\eta = \frac{Q\Delta p}{\Delta D V_0} \quad (3)$$

in which  $\Delta D$  is the total drag increment added by the cooling installation. An optimum cooling system design is one in which  $Q\Delta p$  is as small as possible and  $\eta$  approaches unity. To achieve low values of  $Q\Delta p$ , cooling units of large frontal area should be used; the upper limit of size is definitely fixed by the power required to carry the weight of the radiator. Assuming that the  $L/D$  ratio of the airplane is unchanged by the addition of the cooling unit, the power required to carry the radiator weight is approximately

$$P_w = 1.5 w \left( \frac{C_D}{C_L} \right) V_0 \quad (4)$$

in which  $w$  is the weight of the radiator. The optimum radiator is the one for which  $(Q\Delta p + P_w)$  is a minimum (reference 4).

In order to realize values of  $\eta$  approaching unity,

extreme care must be taken in the duct design. In practice it is difficult to approach this value with anything but a straight duct of optimum design. The following precautions should be taken to minimize duct losses:

1. Avoid bends in the high-speed sections of the duct since the total-pressure loss in a turn is proportional to  $V^2$ .
2. Use guide vanes in all the duct bends. For good vane design, see figure 5. If a dividing vane of single sheet-metal thickness is used it should be provided with a rounded nose.
3. Avoid sudden changes in duct size; limit 2-dimensional expansions to an included angle of  $10^\circ$  and 3-dimensional expansions to 7 degrees; when duct expansions exceed these values, use dividing plates in the duct. An exception is a low-velocity expansion just ahead of a high-resistance, in which case the allowable angles are considerably higher. (See fig. 6.) Actually, the allowable duct expansion depends on the boundary-layer conditions on the duct walls. The allowable expansion angles given assume that the boundary layer fills the duct as it does in a long pipe, and expansions may be made at considerably greater angles at a duct inlet before a boundary layer is formed.
4. Design the duct entry so that the air flow does not create pressure peaks on the external or internal lips of the duct entrance (reference 5).
5. Duct inlets should be located whenever possible on a stagnation point. Duct inlets located at other than the stagnation point must be designed to recover the full total pressure corresponding to the flight speed.
6. Internal shutters to control the duct air flow should not be used, as they regulate the flow by destroying total pressure, which is wasteful of power. (See equation (1).)
7. The duct should have a smooth internal surface and circular cross section when possible.

8. The air flow should be discharged along the contour of the aerodynamic body at the duct outlet, and the afterbody at the duct outlet undercut slightly to avoid a pressure peak. (See fig. 7(a).)

9. When the flow distribution into the duct entrance is asymmetrical, as in the case of an opening in a boundary layer, dividing plates both ahead of and behind the cooling unit are required.

Air-flow control.— The quantity of air flow through a duct can be efficiently controlled only by varying the area of the duct outlet. All other devices, such as control by position or area of the inlet, internal shutters, etc., are inefficient and will result in low duct efficiencies. Since at the outlet

$$Q = A_3 V_3$$

and if the discharge is made in a region of free-stream static pressure, the outlet velocity

$$V_3 = \sqrt{\frac{2}{\rho} H_3}$$

it is obvious that any decrease in the outlet velocity must be made at a sacrifice of total pressure  $H_3$ . From equation (1) it is further obvious that a decrease in  $H_3$  results in an increase in power absorbed in the duct.

The duct outlet area,  $A_3$ , for a required flow  $Q$ , may be calculated approximately from the equation,

$$A_3 = 1.1 \frac{Q}{\sqrt{\frac{2}{\rho} (H_3 - p_3)}} \quad (5)$$

in which  $p_3$  is the static pressure at the duct outlet. The constant 1.1 is introduced to allow for the venturi contraction behind usual tapered outlets such as figure 7(b). It may be omitted if the outlet is shaped so as to produce parallel flow, as in figure 7(c). The value of  $H_3$  must be calculated from the duct losses and pressure drop across the cooling unit.

The necessity for designing a duct outlet which can be adjusted to provide just sufficient air quantity for

cooling in high-speed flight cannot be overemphasized. This is particularly true if the duct efficiency is low,

since the power absorbed varies as  $\frac{A_R V_R^3}{\eta}$  in which  $V_R$  is the velocity through the cooling unit and  $A_R$  is its area. Cowling flaps and duct outlet controls are absolute necessities on higher speed airplanes. Numerous test results demonstrate this fact.

In the case of airplane 3, which was not provided with cowling flaps, an exit slot averaging about 2-1/2 inches in width was provided to give sufficient cooling air for the climb. For the high-speed condition the cowling gap was reduced to 1/2 inch by fairing out the fuselage width as shown in figure 19(d). This cowling gap showed that a satisfactory pressure drop across the engine of 9 inches of water was obtained for the high-speed condition. This change in the cowling gap by refairing the fuselage reduced the drag coefficient of the airplane by 0.0017. A large part of this increment was due to the decreased internal flow losses; however, a small part of the increment may have been due to the improved external flow conditions with the smaller gap. The air-cooled engine cowling of airplane 6 was provided with a main slot and an accessory control slot having a width of approximately 1-1/2 and 1-1/8 inches, respectively. No cowling flaps were provided. The drag of the entire airplane was increased by the increment of 0.0025, owing to the air flow through the cowling. Calculations based on air flow required for this engine indicated that the outlet area could be reduced to almost one-third of its original size and the power required for cooling reduced from about 7.1 percent of the total airplane drag to approximately 1.6 percent.

In the case of airplane 9, cooling of an Allison engine was provided for by a Prestone radiator located in a wing duct without outlet control (fig. 8). In the original duct the outlet opening height was approximately 6 percent of the chord, the air quantity about 17,000 cubic feet per minute in the high-speed condition, and the drag increment 0.0023. By reducing the outlet opening to about 3 percent of the chord, sufficient air quantity (10,250 cubic feet per minute) for cooling in the high-speed condition was obtained and the drag due to the wing duct was decreased to 0.0008. The variations in the drag of the wing duct with outlet size and air quantity are shown in figure 9. For this installation a large part of the difference be-

tween the measured internal drag and the ideal drag is due to the presence of structural members in the duct (fig. 8).

The excessive drag without an outlet control for flow regulation is further demonstrated by the modified oil-cooler installation on airplane 8 (fig. 10). The variation of the drag increment with exit opening and air quantity is shown in figure 11. Included is a curve showing the ideal power required for cooling. As is noted later, the large difference between the ideal and measured drag indicates a relatively inefficient system. Still another case is the inefficient intercooling installation on airplane 10. As originally installed on the airplane, the intercooler drag increment equalled 0.0012. In this condition the intercooler duct was discharging into a wheel well at a short distance behind the cooling unit (fig. 16) without any energy recovery. Of this total a drag coefficient increment of approximately 0.0007 was attributed to the internal flow of about 6400 cubic feet per minute through the ducts. By satisfactory control of the outlet of the duct the power required for cooling could be reduced to about 0.0002 for the correct quantity of air flow.

The drag and air-flow characteristics of the under-slung Prestone radiator ducts for airplane 11 are shown in figure 12. For this airplane a study was made of two Prestone radiator installations (figs. 13 and 14) designated as forward and rear according to their location on the fuselage. In the forward installation two 9- by 19-1/2-inch elliptical radiators were used, and in the rear installation a single 20-1/2-inch diameter radiator was used. The results show drag increments of 0.0011 and 0.0010 for the forward and the rear installation when both are adjusted to the correct air flow. The large increase in drag which would have occurred if outlet control were not used on these ducts is shown by the steep slope of the curve of drag increment against air flow (fig. 12).

The heat dissipated in a cooling duct is a further factor controlling the air flow since, when heat is added to the cooling air, the mass flow is decreased and for equal cooling the exit area must be increased. This subject is discussed in reference 6.

Recovery of waste heat energy.— The useful energy output of the gasoline engine is less than a third of the heat energy of the fuel, and the remainder is wastefully discharged in the cooling air and engine exhaust. Some

progress has recently been made in recovering a part of the waste energy in the form of jet propulsion. The theory indicates and experiments have verified the possibility of recovering more than 10 percent of the engine power by rearward discharge of the exhaust gases. The optimum recovery occurs when individual exhaust stacks are used for each cylinder, and limited data are available to indicate the exhaust stack discharge area for maximum thrust. In the case of airplane 8, flight tests showed the high speed was increased approximately 15 miles per hour at an altitude of 17,000 feet by the use of individual stacks pointing rearward (reference 7).

The efficiency of recovery of waste heat from the cooling air may be calculated by the method of Moredith (reference 8). The theory indicates that thrust is derived by adding the waste heat to the cooling air at a pressure above that of the external stream, and the theory has been verified in some degree by experiment (reference 6). The gains are not large but may be sufficient with a well-designed cooling system on a high-speed airplane to compensate for the cooling losses.

Air induction system.— Good military performance requires that maximum engine horsepower be maintained at high altitudes. For this purpose blowers and intercoolers are provided to maintain the density of the mixture air for the engine at or slightly above the sea-level density. An important source of available blower pressure is the dynamic pressure of the air stream. This pressure is available for ramming at any of the airplane stagnation points, and failure to utilize it fully is doubly harmful. An aerodynamic power loss occurs in handling the engine air at lower than free-stream total pressure according to equation (1), and an engine power loss occurs corresponding to the reduced pressure at the carburetor. Values of the ram pressure available at standard temperatures for different altitudes and at various flight speeds are shown in figure 15.

In the usual two-stage blower engine installation the engine air passes progressively through the carburetor intake, the primary blower, the intercooler, through the carburetor, and then through the secondary blower to the engine. The air is heated by the adiabatic compression in the primary blower, and for efficient operation this heat should be removed in the intercooler. If the air temperature at the engine is allowed to rise because of

insufficient intercooling, the difficulties are numerous and include:

1. Lower density of intake air to the engine leading to lower engine power.
2. Earlier knocking of engine with a given fuel. It is desirable to avoid air intake temperatures above 120° F.
3. Greater secondary blower power required for a given increase of intake air density.

Most of the difficulties of supercharger installations will vanish if efficient blowers are developed, and in fact it may be possible then to completely eliminate the intercooler. Since the change of the air temperature with altitude is approximately adiabatic, the intercooler principally serves to remove heat added because of the blower inefficiency. The low blower efficiency is harmful since it not only necessitates the complicated intercooler installation but directly requires greater engine power for the blower operation. Power is first taken from the engine to heat up the carburetor air and further power is absorbed in the intercooler to cool it again.

The difficulties in the intercooler installations tested in the full-scale tunnel were normally those due to space restrictions. On single-seater airplanes such as airplanes 8, 9, and 10, the space available for the inclusion of large rectangular intercoolers was limited. This led to awkward and inefficient ducts in both the cooling and engine air passages (fig. 16). The intercoolers were generally attached to an airplane which previously was equipped with an unsupercharged engine. In cases such as these the expected failure of the intercooler installation vitiates the entire design.

#### External Flow

The drag added to an airplane by the power plant installation owing to changes in the external flow is not readily calculable. The drag is essentially due to interference, and the detrimental effects of external flow disturbances depend on the magnitude and location of the disturbing element and upon the stability of the flow behind it. The basic condition to which airplanes equipped



with various power-plant installations should be compared is an ideal streamline airplane having sufficient size to accommodate the pilot and military equipment. Any changes in the fuselage size or shape required to accommodate the engine installation must be charged against it.

In this connection a few data on the minimum drag coefficients of ideal combinations may be of interest. It is realized that comparisons of drag coefficients which neglect the wing loading are of little interest; however, most of the comparisons made apply to wing loadings of about 30. In the variable-density tunnel tests on combinations of wing, fuselage, and tail (reference 9), it was found that a drag coefficient of 0.0128 could be reached for an ideal midwing airplane combined with an NACA 111 fuselage. Tests on airplane 9 in the full-scale tunnel in its fully streamline condition (fig. 1(i)) gave a minimum drag coefficient of 0.0145; however, the wake measurements over the wing showed that the manufacturing roughness and wing protuberances accounted for 0.0013, and similar fuselage irregularities would probably account for another substantial item. In a polished-model condition its drag coefficient might lie between the values of 0.0125 and 0.0130. For airplane 8 with a slightly larger fuselage a minimum drag coefficient of 0.0155 was measured for the airplane in a similar smooth condition but with the canopy in place (fig. 1(h)). This would probably reduce to 0.0135 for a model tested in a polished condition.

A large difference may exist between the drag coefficient of a smooth polished model tested in a wind tunnel (even assuming the transition point is fixed at the same location) and the drag coefficient of an airplane built according to the best modern flush riveted practice but including such items as pitot tubes, aileron gaps, windshield roughness, manufacturing irregularities, etc. This item, which is in the nature of a hidden drag increment, accounts in part for the failure of smooth model tests to predict the high-speed drag of airplanes with the conventional extrapolation made according to the skin-friction law.

Assuming that the engine installation can be housed in an ideal fuselage shape of somewhat larger diameter or length than the ideal fuselage required for the pilot and military equipment, it is necessary to charge the engine installation with the added skin-friction drag due to the greater fuselage surface area. This may become a significant item if an attempt is made to obtain optimum efficiency and emphasizes the necessity for small-diameter engines.

The drag increments on modern military airplanes due to larger fuselage size are smaller than those introduced due to changes in the ideal streamline shape such as occur, for example, when poorly designed scoops are added near the airplane nose. The generalization may be made that any change in the airplane shape which tends to increase the adverse pressure gradients or the maximum value of the negative pressure occurring on the body will increase the drag, with the effects becoming more serious as speeds approach 450 to 500 miles per hour. The separate items in the various power-plant installations which may create drag by changing the airplane shape and disturbing the external flow are considered in the following.

Air-cooled engine cowlings.— The conventional installation of an air-cooled engine at the nose of the fuselage results in an airplane with a shape somewhat more blunt than is the best from the standpoint of drag. This is substantiated by the fact that the negative pressures on the best NACA cowling reach values from  $-0.6q_0$  to  $-0.8q_0$  in contrast with values of less than  $0.2q_0$  on good streamline noses. In the belief that these negative pressure increases lead to higher drag, streamline noses were added to two of the airplanes tested in the full-scale wind tunnel (figs. 1(h) and 1(j)) to ascertain the drag increment due to the NACA cowling with no air flowing. In the case of airplane 8 the drag coefficient was decreased by an increment of 0.0020 owing to the addition of the streamline nose. In the case of airplane 10 the addition of the streamline nose decreased the drag by a smaller increment of 0.0013; however, as can be seen by comparisons of figures 1(h) and 1(j), the nose on airplane 10 was not of a type which would as effectively reduce the negative pressure as that on airplane 8.

As previously mentioned, the comparisons were made with no air flowing over the engine, and an attempt was made in the case of airplane 8 to improve the shape of the cowling so as to approach more nearly the drag of the solid streamline nose and at the same time provide a method of cooling the engine. Long-nose cowlings of shape similar to those shown in figure 17 were tried in an effort to maintain a good external shape and at the same time to provide sufficient air flow. It was found that the long-nose cowlings with air flowing through them showed no decrease in drag over that of the conventional NACA cowling, indicating that some peculiar internal or external flow phenomena existed to nullify the gains which apparently should

be realized from the improved external shape. This investigation was of a preliminary nature and more detailed investigations are now in progress at the laboratory.

For conventional NACA cowlings installations, it has been found that the best net efficiency and the minimum negative pressures are realized for cowling C, which was developed from tests in the NACA high-speed tunnel and reported in reference 10.

In a further attempt toward improving the blunt shape of the NACA cowlings, tests were made with spinners of various sizes attached to the propeller (fig. 18). These spinners varied in size from 17 inches diameter corresponding to the conventional de-icing spinner up to 38.6 inches diameter. For a part of the tests with the spinners, cuffs were also added to the propeller. The results showed that the medium spinner increased the over-all propulsive efficiency by about 3 percent in the high-speed condition and provided sufficient cooling pressure. The larger spinners produced about the same increase in propulsive efficiency but did not provide adequate cooling air to the engine. The addition of the cuffs did not increase the propulsive efficiency in the high-speed condition, although it would be expected that the available pressure for ground cooling would be increased. The relatively small increases in propulsive efficiency noted by adding the spinners are not believed to be the ultimate that can be obtained in this way since the NACA cowlings will no doubt require modifications when used in conjunction with spinners. Study on this problem is scheduled for further research.

With the use of the NACA cowlings and its attendant large negative pressure rise, it is exceedingly important that the fuselage behind the cowlings be correctly designed to avoid sharp pressure gradients and to return the negative pressure to free-stream pressure with a minimum of disturbance. The high adverse pressure gradients are conducive to flow separation with a resultant drag penalty. An attempt was made in the case of airplane 8 to improve the afterbody shape by lengthening the fuselage approximately 5 feet by means of a conical extension (fig. 19(b)); this resulted in a decrease of drag coefficient of 0.0005 for the airplane with the NACA cowlings without cooling air. For the airplane with the solid streamline nose the drag was the same with or without the lengthened afterbody. A further small change was made by enlarging the tail of the cockpit canopy to decrease the divergent air-flow angle.

This had no measurable effect in the case of the NACA cowling; however, the change increased the drag of the airplane by 0.0006 in the case of the streamline nose installation.

Some air-cooled engine airplanes when viewed from the top show a distinct necking-in of the fuselage aft of the cowling. On airplane 5 the fuselage was modified so as to eliminate this necking-in feature, as shown in figure 19(c). The straight-line fuselage elements extend from the front of the fuselage to points of tangency aft on the fuselage. This change reduced the drag coefficient of the airplane by 0.0009. A similar change was made on airplane 6 (fig. 19(a)) which reduced its drag coefficient by 0.0006.

Air inlets.— The rules for the design of duct inlets are not so well established as those for the design of the outlets. The principles are known, however, and have been verified by experiments. It is a primary requirement of a duct inlet that it recover the full total pressure corresponding to the flight speed of the airplane. If the total pressure at the inlet is less than  $H_0$  there will be a power loss calculable by means of equation (1). The opening should therefore be located at an existing stagnation point such as the wing leading edge or the nose of the fuselage, or at an artificial stagnation point created by means of a scoop. The use of scoops is discouraged, however, by the requirement that the flow into and around duct inlets should not create local gradients in the pressure distribution over the body or increase the values of the negative pressures above those of the body without the inlet. A well-designed opening at the nose of a wing or fuselage will in fact tend to reduce the negative pressures over the body near an opening since a part of the air is bypassed through the duct and the external velocities are lower (fig. 20).

Large adverse pressure gradients (negative to positive) cause a transition from laminar to turbulent flow, and tend to precipitate flow separation. Large negative pressures on a body further lead to compressibility effects at low critical speeds, and require that the afterbody be long to reduce the adverse pressure gradients. While awaiting a theory for specifying the shape required for openings of different size and air-flow quantity the experiments of reference 5 may serve as a guide. By properly proportioning the opening, inlet velocity ratios  $V_1/V_0$  may be varied over a wide range without increasing the

external drag. When the internal duct passages cannot be designed to expand the air efficiently it may be desirable to provide low inlet velocity ratio to reduce the duct losses.

The corners and sides of rectangular duct inlets should be carefully rounded and faired into the body. If an optimum high-speed opening cannot be designed to accommodate the climb and ground cooling conditions, an adjustable inlet should be provided. The stagnation point on a wing shifts with lift coefficient and for this reason an optimum wing duct for both the high-speed and climb conditions should have an adjustable opening. (See reference 11.) It may sometimes be possible to arrive at a compromise arrangement which will be satisfactory in climb and have almost optimum high-speed efficiency. The effects of the slipstream in shifting the stagnation points on the wing may, however, be the critical factor in the design of wing duct inlets. The effects are discussed in reference 12, and satisfactory solution of the problem may lead to the necessity for adjustable inlets.

Although scoops are not the best type of inlet openings, they have been widely used on the airplanes that were tested in the full-scale tunnel. External carburetor scoops were particularly popular since the carburetor ram pressure can be obtained most readily in this manner. In most cases it was found that the airplane drag was substantially reduced by refairing of the scoops.

Refairing the carburetor scoop of airplane 2 and the cowlings ahead of it as shown in figure 21(a) reduced the airplane drag coefficient by 0.0010. This further helped to maintain the carburetor pressure up to high angles of attack. The addition of the carburetor scoop to airplane 8 (fig. 21(b)) increased the drag coefficient of the airplane by 0.0006. This scoop could have been improved by increasing the leading-edge radius and lengthening the afterbody. Small sharp-edge scoops (fig. 21(c)) were used in the wing-fuselage fillets of airplane 9 which added 0.0019 to the drag coefficient of the airplane. In figure 21(c) the tufts show the large extent of the flow disturbance on the airplane caused by these scoops.

Tuft operation in airplane 10 showed that a satisfactory flow existed over the carburetor scoop, which was located in the nose of the cowlings (fig. 21(d)) for the power-off condition; however, with the propeller operating,

a distinct flow separation was observed on the downstream side of the scoop owing to the slipstream rotation. To eliminate this undesirable flow, the sides of the carburetor scoop were faired out more gradually into the cowl- ing line, as indicated by the section line on figure 21(d). This fairing decreased the drag coefficient by 0.0006.

Three different types of carburetor scoops were tested on airplane 11. (See fig. 21(e).) The most satisfactory scoop from the standpoint of both drag and ram pressure was the one designated as revised forward inlet. The characteristics of the three types of carburetor scoops are given in table II. The superiority of the revised forward inlet is due to the improved shape of the nose, which is more nearly parallel to the streamlines and to the elimination of the lower lip on the original inlet. It may be desirable to widen the revised forward inlet and fair it more gradually into the fuselage, as was done in the case of airplane 10 to avoid losses due to rotation of the slipstream.

The airplanes have been most severely penalized by the oil-cooler installations, since in most cases the oil coolers appear to have been added to the airplanes as an afterthought. The air for the oil cooler of airplane 2 (fig. 22(a)) was taken in by means of a scoop on the under surface of the wing, was passed through a cross-flow wing duct in which the cooler was located and discharged through louvers on the upper surface of the wing. The duct was at an angle of approximately  $45^\circ$  to the wing chord and the air was discharged at about this angle to the upper surface. The tufts in figure 22(a) show the flow interference due to the inefficient discharge, and a drag increment of 0.0020 was measured for this installation. The drag increment for a satisfactory oil cooler installation on this airplane should not exceed 0.0004. On airplane 3 the oil-cooler scoop was located on the bottom of the fuselage at the rear of the NACA cowl (fig. 22(c)). For this installation a drag increment of 0.0007 was measured, which is not considered excessive for the external installation. It will be noted that this scoop has a well-formed streamline shape.

The oil-cooler scoop on airplane 4 was placed on the top side of the NACA cowl, as shown in figure 22(b). The over-all drag coefficient of the installation obtained by removing the scoop and sealing the outlet was 0.0007. This was reduced to 0.0003 by refairing the scoop, as shown

by the section lines in the figure. An extremely inefficient oil-cooler installation was used in airplane 8 (fig. 22(d)). It consisted of a sharp-edge scoop located on the bottom of the fuselage which diverted air at a rather sharp angle up into the oil-cooler ducts located in the fuselage. The air then was discharged at an angle of about  $60^\circ$  to the fuselage axis. This oil-cooler installation failed to supply sufficient air flow for oil cooling and in addition increased the airplane drag coefficient by an increment of 0.0017. Since it was impossible to modify this installation without major changes to the airplane structure, an underslung radiator installation was designed to be attached to the bottom of the NACA cowling (fig. 10). When the required quantity of air flow passed through the cooler the drag coefficient was 0.0009. To determine what part of the drag was due to the protuberance and what part due to the air flow, the oil-cooler duct was faired over at the nose and tail so as to prevent air flow, and an increment in drag coefficient of 0.0004 was measured.

As an example of an extremely poor installation and an illustration of its harmful effects on the airplane drag, results are presented for the temporary oil-cooler installation which was installed on airplane 9, as shown in figure 22(e). This large scoop increased the airplane drag coefficient by an increment of 0.0040, which corresponded to approximately 25 percent of the entire airplane drag. This installation was later changed into a relatively inefficient wing duct in which location it increased the drag coefficient by 0.0011. A wing duct oil-cooler installation was also used in airplane 11, as shown in figure 22(g). The duct passages through both wings were bent sharply to avoid interference with the landing-gear struts and a considerable loss in internal efficiency resulted. The drag coefficient of the airplane was increased by 0.0006 because of the wing ducts. It is believed that with an efficient internal duct the drag coefficient would have been increased by no more than 0.0004 for this installation. The oil coolers for airplane 10 were located in streamline ducts on the lower surfaces of the wings outboard of the fuselage. The oil coolers were approximately half submerged into the wings (fig. 22(f)). These oil-cooler installations increased the airplane drag coefficient by an increment of 0.0008. As a check on the added external skin friction drag due to these ducts, streamline noses and tails were added to the units and a drag coefficient increment of only 0.0001

measured. This substantiates other data showing that streamline blisters located at noncritical positions on the airplane do not add large increments.

The largest scoops added to the airplanes were those provided for the Prestone radiator installations on airplanes 7 and 11. On airplane 7 in its original condition the Prestone radiator was located under the Allison engine and below the normal fuselage line. The air was taken into the radiator by means of a large scoop which is sketched on figure 23(a). This installation increased the drag coefficient of the airplane by an increment of 0.0034. In an attempt to reduce the drag of the Prestone radiator installation, the radiator was raised so as to place it within the original lines of the fuselage nose, as shown in figures 23(b) and (c). For this arrangement it will be noted that the inlet did not protrude below the normal fuselage line. The drag coefficient of the modified installation was 0.0017 or approximately one-half that of the original installation for the same air flow quantity. Other scoop arrangements similar to the modified scoops used on airplane 7 were investigated on airplane 11. Again the Prestone radiators were installed within the original faired contour of the fuselage; however, the scoop inlet protruded slightly below the original fuselage line (fig. 13). Owing to the efficient internal flow made possible through the gradual expansion of its internal duct, a drag coefficient increment of only 0.0011 was measured for this airplane. A similar underslung scoop arrangement was tested in which the radiator was located within the fuselage near the trailing edge of the wing (fig. 14). For this case with the cooling air flow as for the forward underslung arrangement, the drag coefficient increment was 0.0010. Attention is called in both of these cases to the fact that, with a well-designed scoop even of large size such as those just described, excessive drags were not obtained.

Rules for the design of scoops based on the experience gained with the airplanes are as follows:

1. Provide a nose radius on the lips of the scoop similar to that at the nose of an airfoil.  
Never use a sharp-edge scoop.
2. Provide sufficient camber in the scoop contour so as to match the streamlines of the flow.  
Scoops with low inlet velocities require more



camber. (See fig. 24.) When possible, measure the pressure distribution over the scoop with correct air flow through the opening.

3. Until more detailed data are available, design the scoop inlet area to provide an inlet velocity of from one-half to two-thirds of the stream velocity at the high-speed condition. If the scoop inlet is not made adjustable, the inlet velocity ratio will necessarily be required to be lower and the camber in the scoop greater. (See rule 2.)
4. Provide a well-shaped afterbody behind the maximum scoop section with sufficient length to avoid flow separation. Four times the scoop height will generally suffice, although an afterbody too short will be much more harmful than one too long.
5. When the scoop is located in a cross flow such as a propeller slipstream, fair the sides of the scoop gradually and smoothly into the body adjacent to it (fig. 24). The sides of the scoop for this case correspond to the afterbody in a straight flow.
6. If a scoop is located in a thick boundary layer, considerable difficulty will be experienced in obtaining high efficiency. The inlet area should be exactly proportioned to avoid flow separation in the boundary layer ahead of the inlet, and vanes used in the duct to obtain a more uniform velocity distribution.

Exhaust stacks and turbosupercharger.— The requirements for the recovery of thrust from exhaust stacks by rearward discharge of the heated gases have already been discussed. However, it is desirable to further consider the external drag due to protruding exhaust stacks on the fuselage. Tabulated results on the drag due to the various exhaust stacks are given in table III.

The exhaust stacks listed are for air-cooled engines with the exception of those for airplanes 7 and 11. The twin stacks on the air-cooled engines protruded from the engine cowlings at right angles except those for airplane 5 which were directed to rear at an angle of approximately

45°. The drag of all these installations is comparatively large and their form drag may be reduced by the elimination of sharp edges at large angles to the direction of flight, by discharging the stacks to the rear and by recessing them into the forward section of the fuselage. The advantages of individual stacks are discussed in another section of the paper.

It will be noted that the stacks as used on the liquid-cooled engines of airplanes 7 and 11 have much lower drag than those for air-cooled engines.

The drag of external turbosupercharger installations is high, as demonstrated by the 25.5-pound drag measured for the complete installation on airplane 9 (fig. 16(d)). A drag break-down for this installation showed that 2.7 pounds drag was due to the cooling system for the exhaust lines from engine to supercharger which had inlets in the leading edge of the wing, 7.6 pounds to the bypass stacks (fig. 16(d)), and 15.2 pounds to the supercharger. The high drag of this installation indicates that for a high-speed airplane, it is imperative to enclose the supercharger within the airplane with an efficient duct system for cooling the rotor and discharging the cooling air and exhaust gases.

TABLE III

Airplane	Exhaust Stacks	
	Figure	Drag at 100 mph (lb)
1	25(a)	8.6*
5	25(b)	8.2
6	1(f)	4.6*
7	1(g)	1.8
8	36(d)	3.4
11	25(c)	1.3

\*Drag measurement made by placing streamline blisters over stacks instead of removing them.

### Wings

The profile-drag coefficients of wings were measured for all of the airplanes by means of a wake rake (reference 2). Numerous surveys were made along the span of the wing so as to obtain an average value of the drag coefficient and the mean values are given in table IV.

The drag values were measured at a tunnel speed of 85 miles per hour, and values have been estimated for the drag of a smooth wing with the same sections and plan form to serve as a basis for comparison. The smooth-wing data were obtained from full-scale-tunnel data on smooth airfoils tested at the same Reynolds number. The drag coefficient increment  $\Delta C_D$  represents the drag due to roughness, rivets, laps, etc.

Since it may be of considerable interest to predict the drag of service wing from the full-scale-tunnel tests, or at least to determine whether drag increments due to wing protuberance and roughness measured at the tunnel speed apply at flight speeds, a brief review of present concepts on skin friction is presented. The drag results must be strictly interpreted to avoid inaccurate estimates of wing drag at high speeds and high Reynolds numbers owing to the widely varying effects of roughness and compressibility.

In attempting to compare the effect of roughness, such as rivets, laps, etc., at several different Reynolds numbers, it is necessary to know the extent of the laminar and turbulent flow regions on the rough wing for the speeds at which the comparison is to be made. It is characteristic of a row of rivets or other protuberance on a wing to fix the transition from laminar to turbulent flow at the location of the rivets. That is, a row of rivets on the 20-percent  $c$  location of a wing will definitely fix the transition point at this position regardless of the Reynolds number. For example, a smooth wing at low Reynolds numbers may have its transition occurring at the 0.50  $c$  position; the addition of a row of rivets at 0.20  $c$  would add a large drag increment made up of two parts, namely the form drag of the rivets and the drag due to the more extensive region of turbulent flow on the rough wing (fig. 26). With increasing Reynolds numbers, the transition point moves forward along the chord (reference 3), and it may be that at  $R$  equals thirty million even on a smooth wing, the transition point would normally occur at 0.20  $c$ . In

L-489  
this case, the addition of the row of rivets at this location would add a considerably lower drag increment equal to the rivet form drag, and no extra drag would be caused by a shift of the transition point. The drag increment obtained in the low Reynolds number tests is therefore not applicable at higher Reynolds number unless correction is made for the shift in the transition point. (See reference 13.)

In contrast to the effects of protuberances added in the laminar-flow region, the drags of roughness or protuberances added in the turbulent region of a smooth wing increase with increasing Reynolds number (fig. 27) so that the effect of wing irregularities measured in low-scale wind-tunnel tests do not conservatively predict their drag at flight speeds. This effect is probably due to the thinning of the boundary layer at the higher speeds, which may cause the irregularity in some cases to protrude through the boundary layer. Whether the drag increment measured in the full-scale tunnel should be increased or decreased at flight Reynolds numbers, therefore, depends upon the location of the wing irregularities with reference to the transition point on a comparable smooth wing. If the roughness begins ahead of the nominal smooth wing transition point, the drag increment will decrease with increasing scale, and vice versa.

With existing conventional airfoils, such as the NACA 23000 series, the transition at high Reynolds numbers (say 30 million) occurs close to the minimum pressure point, which at a lift coefficient of 0.15 is near the 0.15 c position. Owing to the initial turbulence in the full-scale tunnel, the transition point on a smooth wing at the test Reynolds number of 5 million also occurs near the same chord position, so that in the extrapolation of the smooth wing drag to higher Reynolds number, no increment is needed to take into account the difference in the transition point. The smooth wing drag can be extrapolated along a modified turbulent skin-friction curve defined as follows:

$$C_{D\text{Flight}} = C_{D\text{Test}} \left( \frac{R_{\text{Test}}}{R_{\text{Flight}}} \right)^{0.11} \quad (6)$$

Owing to the forward location of the transition point in the tunnel tests (see table IV) and the relatively smooth leading edges on most of the wings tested, their irregularities were largely located in the turbulent region.

From the previous discussion, this would indicate that the drag increments measured in the tunnel tests are conservative and that, at flight speeds, the effects of the surface irregularities will be even greater. The extent of the drag increase with speed for some types of irregularities is shown in reference 13. (See fig. 27.)

In extrapolating the drag coefficients to higher Mach numbers, it is necessary to correct the usual Reynolds number extrapolation for the increased drag due to compressibility. As a first approximation, at speeds well below the critical, the drag coefficient should be increased as follows:

$$C_{D_c} = C_{D_1} \left( 1 + \frac{M^2}{4} \right) \quad (7)$$

in which  $M$  is the Mach number and equal to the ratio of the speed of flight to the speed of sound. The effects of compressibility on the drag due to wing irregularities depend intimately on the types of irregularity. High-speed tunnel tests on rivets and laps (reference 13) show that up to speeds of 500 miles per hour their form drag is not greatly dependent on the Mach number since the local velocities over the wing are not appreciably changed. In the case of one wing, however, in which a local surface irregularity existed that caused a change in the surface contour, the critical speed was greatly decreased.

Based on the foregoing discussion, the extrapolation of the wind-tunnel results to flight speeds may be made as follows:

1. Extrapolate the smooth wing drag by equation (6).
2. Correct for compressibility by equation (7).
3. Add the drag increments due to surface irregularities as shown in figure 28. In general, it will not be conservative to use the roughness increments measured at tunnel speeds.
4. Ascertain whether any of the wing irregularities modify the velocity field over the wing and correct the critical velocity accordingly.

A review of the wing drag results reveals several interesting facts. Fabric-covered wings with flush stitching such as used on airplane 4 (fig. 29(c)), have drags as low as the best flush-riveted metal wings.

The use of perforated trailing-edge flaps added drag increments of 0.0013 and 0.0016, respectively, for airplanes 5 (fig. 29(d)) and 6. The increments were measured by testing with the perforations covered and open.

A typical example of the way in which small wing protuberances, gaps, and roughness increase the drag is shown by the momentum measurements on the wing of airplane 9 (fig. 30). This wing is flush-riveted and has butt joints on the lateral seams and lap joints on the longitudinal seams. The estimated smooth-wing drag coefficient is 0.0060 and the measured service wing drag coefficient 0.0073. The sources of the increment of 0.0013 in  $C_D$  are estimated from figure 30 to be as follows:

Walkway and landing-gear fairing bumps	0.00015
Gaps around ailerons	.00020
Pitot head	.00015
Manufacturing irregularities	<u>.00080</u>
Total	0.00130

Similar increments have been measured on other airplanes for the same items. On airplane 8 two sanded walkways protruding about 1/8 inch above the wing surface increased the wing drag coefficient by 0.0007. The item labeled "manufacturing irregularities" includes small surface discontinuities, waves, roughness, etc. The drag of one section of the wing on airplane 8 was reduced about 0.0006 by filling it carefully with paint and sanding with No. 400 water sandpaper. This drag increment was verified in a flight test. The gaps in conventional ailerons add an increment of from 0.0001 to 0.0002.

#### Cockpit Canopies

Modifications of a number of the cockpit canopies were investigated, but only in the case of airplane 9 was it practicable to remove the canopy to measure its entire drag. Photographs of the original and three modified cano-

pies for this airplane are given in figure 31(b) and their principal dimensions are shown in figure 32. The low coefficients for these canopies demonstrate their excellent design and confirm one of the conclusions from the canopy investigation in the 8-foot high-speed tunnel (reference 14) that the drag of a well-designed canopy represents a small part of the over-all airplane drag. The canopy drag coefficients given in the table are from one-half to two-thirds as large as would be expected from reference 14. This is believed to be due to a difference in the boundary-layer flow conditions existing on the aerodynamically smooth model on which the investigation of reference 14 was conducted and the actual airplane.

The first modification of the canopy, that of reducing its height  $3\frac{5}{8}$  inches, reduced the drag to one-half of the original amount. As the reduction in the cross-sectional area of the canopy was less than 20 percent, the drag reduction is attributed largely to the improvement in the longitudinal section. Decreasing the length of the tail section of the lowered canopy slightly increased the drag, indicating that for the boundary-layer flow conditions on the airplane the canopy tail section should be greater than four times the height recommended in reference 14. The flat-sided windshield offering improved vision slightly increased the canopy drag and would not be recommended for a high-speed airplane because of the low critical speed that would result from the sharp corners.

A modification of the flat-sided windshield was tested on airplane 11 (fig. 31(e)). It will be noted that rounded sections were placed between the flat surfaces to eliminate early compressibility effects. This windshield when tested on the model without carburetor scoop in place gave a reduction in the airplane drag coefficient of 0.0002, which was due principally to increasing its length. A repeat test with the modified forward carburetor scoop in place, however, showed no reduction in drag, further demonstrating that the drag of the canopy is critically affected by flow conditions. Static pressure measurements on this windshield indicated that its critical speed would be as high as for the original rounded windshield.

On airplane 10 (fig. 31(a)) a comparatively large drag reduction was obtained by increasing the radius of the windshield at its juncture with the hood and slightly

reducing its angle. The modified canopy of airplane 5, although of greater height and cross-sectional area than the original canopy, did not increase the drag, owing to its improved shape.

The largest drag reductions were obtained on airplane 6 (fig. 31(d)). Inasmuch as the unflapped engine cowling on this airplane allowed a far greater amount of air to flow than would be optimum for the high-speed condition, the tests were made with the cowling gap sealed. Rounding the windshield and eliminating the sharp edge at its juncture with the forward hood reduced the airplane coefficient by 0.0011. The elimination of the quarter-spherical tail section by one of greater length brought the total reduction to 0.0019. Fairing out the joints at the ends of the movable hoods did not produce a measurable drag reduction; however, on an airplane with smooth surfaces, this change would undoubtedly be beneficial.

### Landing Gears

There were four general types of retractable landing gears on the airplanes tested: (1) wheel retracting into the sides of the fuselage; (2) wheels on struts attached to bottom of front spars which swing to the rear and rotate through  $90^\circ$  to place them in wing wells; (3) wheel struts pivoted above the lower surface of the wing and swinging inboard so as to place the entire gear within the wing; and (4) tricycle gear with front wheel retracting into nose of fuselage and rear wheels retraction similar to type 3. The drags of the landing gears as given in table VI were determined from the differences in the drag at 100 miles per hour of the airplanes with the original retracted gears and the airplanes in a smooth condition with all landing-gear openings and protruding parts eliminated.

The results obtained for the landing gears of type 1 showed that the use of flush cover plates over the wheel wells would produce appreciable drag reductions. The landing gear of type 2 on airplane 6 gave the highest drag of all of those tested. As indicated in the table, several modifications of the gear were investigated. Extending and improving the fairing of the oleo struts (fig. 33(c)) together with rounding the edges of the rear halves of the wells by inserting a half round section 1-1/8 inches wide did not produce a large reduction in drag. The use of



wheel-well cover plates proved effective and with the addition of the faired oleo struts reduced the gear drag from 14.8 to 3.9 pounds, the latter quantity representing the drag of the faired oleo struts. A similar type gear was used on airplane 7 (fig. 33(b)). The sealing of gaps and improving the oleo strut fairing (item 1, fig. 33(c)) reduced the drag 4.2 pounds while the extension of the wheel covers to include the entire wheels (item 2) brought the total drag reduction to 5.3 pounds.

The lowest landing gear drag for the airplanes was measured for the type 3 gear on airplane 8 (fig. 33(f)). The entire elimination of this drag would be possible by sealing the cover plates against leakage and improving the fairings of the joint with the wing surface. This type of gear has the advantage over preceding types in that the oleo strut may be readily retracted into the wing.

The tricycle gear on airplane 9 (fig. 33(e)) proved to be one of the higher drag arrangements. This is attributed largely to the fact that the main wheels protruded about one-third of their thickness as shown in the photograph. On a later series of tests on this airplane after the landing gear had been modified to entirely retract the nose wheel into a fuselage compartment with cover plate and to retract the rear main wheels to their full depth into wing wells without cover plates, it was found that the drag had only been reduced from 10.3 to 8.7 pounds. This drag was eliminated by a tight cover plate, which emphasizes its necessity.

#### Armament

The drags of gun installations measured at a speed of 100 miles per hour are given in table VII. It will be noted that the drag of all the installations is of about the same order except for airplane 3 (fig. 34(c)), which is over five times as large. The value given for this airplane does not represent the total drag for the guns, as in all other cases, but is the drag reduction obtained by sealing the openings in the nose of the engine cowlings around the blast tubes and the filleting and the fairing of the tubes. Measurements were made for both the power-off and propeller-operating conditions, and the lower value for the power-on condition is given in the table. The source of the high drag for the original installation is

obviously not due to the form drag of the blast tubes but to the large air leakage induced by the negative pressure over the nose of the cowlings. This installation is discussed in further detail under the heading of leakage.

The lowest drag installation for an airplane with a radial engine was obtained for airplane 10 (fig. 33(b)), in which there are no openings in the cowlings and the guns are placed in troughs with no protruding parts. On the model of airplane 11 (fig. 34(f)) with liquid-cooled engine, the blast tubes placed low on the fuselage nose also proved to be a low-drag arrangement. The installation of the eight wing guns represented by 2-inch holes in the leading edge showed a low drag. Although the effect of the openings on the maximum lift coefficient was not investigated, tests of inlets on the leading edge of wings indicate that if edges of the openings are not well rounded and located near the stagnation point, appreciable reductions in the maximum lift will result.

The drag of the external Navy gun sight was measured on airplanes 1, 6, and 10, and only on airplane 1 (fig. 34(a)) was there a measurable drag, which was 2.5 pounds at 100 miles per hour. It is believed, however, that, with the aerodynamic improvements in the fuselage and canopies, the elimination of the external gun sight will assume greater importance.

The bomb rack on airplane 5 (fig. 33(d)) and two bomb racks on airplane 6 (fig. 1(f)) gave large drags of 8.5 and 11.2 pounds, indicating the desirability of suitable fairings for reducing their drag.

### Aerials

The drags for the three types of aerial shown in figure 35 are given in table VIII. With the possible exception of the type 3 aerial, all aerials cause more drag than should be considered satisfactory for a modern high-speed airplane. If the angle between the wires and the direction of flight is large, as in the case of type 1 aerial (fig. 35(a)), the effects of compressibility on the drag at high speeds should be considered. For example, reference 15 shows that the critical speed of a circular cylinder inclined at an angle of  $45^\circ$  would be about 330 miles per hour at 16,000 feet altitude.

## LEAKAGE

Any air flows on the airplane other than those usefully employed for cooling, ventilation, etc., should be prevented by sealing all surfaces across which pressure differences exist. Air leakage through the airplane surfaces or between compartments within the airplane will ordinarily result in appreciable drag losses since the leakage air is usually discharged normal to the flight direction. The drag is due to the loss of the momentum of the leakage air and to the disturbance of the external flow over the airplane surfaces. The first of these losses can be computed if the pressure drop across the leak and the leak area are known. Assuming leakage from a large reservoir, such as a cowl or fuselage, then the approximate quantity of air flow through the leak is

$$Q = 0.65 A \sqrt{\frac{2}{\rho} p} \quad (8)$$

and the drag

$$D = \rho Q V \quad (9)$$

in which  $Q$  is the quantity of leakage flow,  $A$  the area of the leak, and  $p$  the pressure difference across the leak. The drag due to the effect of the leakage on the disturbance of the external flow cannot readily be computed, since it depends on the location of the leak, its magnitude, external boundary-layer conditions, etc.

The large adverse effects of leakage are amply demonstrated in the full-scale tunnel tests. The results are summarized in table IX. Isolation of the drag increments in some cases is impossible, since several items were changed at the same time.

Openings in NACA cowl noses are particularly disadvantageous, since the pressure difference may be as much as 2  $q$ . In cases in which armament installations pass through the cowl nose, such as airplanes 1 and 3, extreme care must be taken to prevent outflow through the opening. The effect of the opening and the outflow is shown by photographs of the tufts on the cowl for airplane 3 (fig. 36(a)). The region behind the opening is completely stalled, as shown by the reversal of the direction in which the tufts point, and the large drag increment

of 0.0029 measured for this case is explained. Other common errors to be avoided are unsealed holes through the fire wall, random flow from the engine cowlings compartment into the accessory compartment, gaps in cockpit enclosures, leaks in cooling ducts, particularly ahead of the cooling unit, flow circulation through incompletely sealed landing-gear wells, leaks around cowlings flaps, etc. For cases in which leakage is desirable, that is, for ventilation air, the outlet should be carefully shaped and directed along the contour of the surface at the point of discharge. (See fig. 7.)

Compressibility.- Discussions of drag results on airplanes from test data obtained at 100 miles per hour are obviously incomplete without consideration of the possible effects of compressibility on the drag at the actual flight speeds. Numerous fundamental investigations have shown that, if the speed of an aerodynamic body is increased, a critical value is finally reached at which the drag of the body rapidly increases. This corresponds to the occurrence of sonic velocity at some point on the body and investigations have shown (reference 16) that if the pressure distribution over the body in low-speed flight is known, then it is possible to estimate the flight speed at which this critical sonic speed will occur. Bumps, canopies, scoops, cowlings, etc., that increase the local air speed at any point lead to the occurrence of local sonic speeds at lower flight speeds than on a perfect streamline body.

The method of estimating the critical speed from pressure measurements made at low air speeds is described in reference 16 and the agreement between theory and experiment shown in references 15 and 16. The theory does not conservatively predict the critical speed and the value may be 15 miles per hour lower than estimated. Values of  $P_{cr}$ , critical pressure, corresponding to various Mach numbers are calculated from the Bernoulli equation for compressible flow (fig. 37). The pressures measured at low air speed are extrapolated by the method of Ackeret to take into account the variations of the pressures on the body with changes in Mach number; that is,

$$P_c = \frac{P_i}{\sqrt{1 - M^2}}$$

in which  $P_c$  and  $P_i$  refer to the pressure in compres-

sible and incompressible fluids and  $M$  is the Mach number. If  $P_c$  and  $P_{cr}$  are plotted against  $M$ , the intersection of the two curves defines the critical Mach number.

Measurements were made of the pressure distribution at numerous critical points on the airplanes tested in the full-scale tunnel to aid in estimation of their critical speeds. Typical results are presented in figure 37 for four of the airplanes.

The lowest critical velocity will usually occur for single-engine airplanes in the wing-fuselage juncture, since here the thicker wing roots and combined wing-fuselage flows lead to high local velocities. This point was critical for airplanes 9 and 11 (figs. 37(b) and 37(d)) and will be critical for airplanes 7 and 10 (figs. 37(a) and 37(c)) when their windshields are correctly modified. The use of wing and fuselage sections expressly designed to avoid high negative pressures is a mandatory requirement on airplanes designed for the 450 to 500 miles per hour speed class. The data in references 5, 15, and 17 will be useful in designing the wing and fuselage shapes to avoid low critical speeds.

A well-rounded juncture should also be provided between the top of the windshield and the cockpit hood. The sharp radius of curvature at this point was found to be responsible for a critical speed of 390 miles per hour in the case of airplane 7 (fig. 37(a)). Tests on canopies in the high-speed tunnel (reference 14) are valuable in defining the relation between the radius of curvature at the windshield juncture and the critical speed.

The nose of the cowl of an air-cooled-engine airplane is a further point of high local velocities and should be designed for high-speed airplanes entirely from the consideration of obtaining a high critical speed. Design data on the subject are given in reference 10.

As a further caution in the use of scoops on high-speed airplanes, it should be recognized that, although their drag may not be large at low speeds, their effect in reducing the critical speed may be serious. Sharp-edged scoops designed for low inlet velocities may become critical at speeds from 350 to 450 miles per hour. If scoops are used on any high-speed airplanes, pressure-distribution measurements should be made to check on their critical speeds.

## REFERENCES

1. DeFrance, Smith J.: The N.A.C.A. Full-Scale Wind Tunnel. NACA Rep. No. 459, 1933.
2. Goett, Harry J.: Experimental Investigation of the Momentum Method for Determining Profile Drag. NACA Rep. No. 660, 1939.
3. Silverstein, Abe, and Becker, John V.: Determination of Boundary-Layer Transition on Three Symmetrical Airfoils in the N.A.C.A. Full-Scale Wind Tunnel. NACA Rep. No. 637, 1939.
4. Brevoort, M. J., and Leifer, M.: Radiator Design and Installation. NACA ACR, May 1939.
5. Biermann, David, and McLellan, Charles H.: Wind-Tunnel Investigation of Rectangular Air-Duct Entrances in the Leading Edge of an NACA 23018 Wing. NACA ACR, Sept. 1940.
6. Silverstein, Abe: Experiments on the Recovery of Waste Heat in Cooling Ducts. NACA ACR, May 1939.
7. Pinkel, Benjamin, and Turner, L. Richard: Flight Tests of Exhaust Gas Jet Propulsion. NACA ACR, Nov. 1940.
8. Meredith, F. W.: Note on the Cooling of Aircraft Engines with Special Reference to Ethylene Glycol Radiators Enclosed in Ducts. R. & M. No. 1683, British A.R.C., 1936.
9. Sherman, Albert: Interference of Tail Surfaces and Wing and Fuselage from Tests of 17 Combinations in the N.A.C.A. Variable-Density Tunnel. NACA Rep. No. 678, 1939.
10. Robinson, Russell G., and Becker, John V.: High-Speed Tests of Radial-Engine Cowlings. NACA Rep. No. 745, 1942.
11. Nickle, F. R., and Freeman, Arthur B.: Full-Scale Wind-Tunnel Investigation of Wing Cooling Ducts. NACA ACR, Oct. 1938.

## CONCLUSION

Results show that the drag of many of the airplanes was decreased 30 to 40 percent by removal or refairing of inefficiently designed components. In one case the drag was halved by this process. Emphasis on correct detail design appears at present to provide greater immediate possibilities for increased high speeds than improved design of the basic elements.

Langley Memorial Aeronautical Laboratory,  
National Advisory Committee for Aeronautics,  
Langley Field, Va.

1-489

12. Nickle, F. R., and Freeman, Arthur B.: Full-Scale Wind-Tunnel Investigation of Wing-Cooling Ducts - Effects of Propeller Slipstream. NACA ACR, March 1939.
13. Hood, Manley J.: The Effects of Some Common Surface Irregularities on Wing Drag. NACA TN No. 695, 1939.
14. Robinson, Russell G., and Delano, James B.: An Investigation of the Drag of Windshields in the 8-Foot High-Speed Wind Tunnel. NACA Rep. No. 730, 1942.
15. Robinson, Russell G., and Wright, Ray H.: Estimation of Critical Speeds of Airfoils and Streamline Bodies. NACA ACR, March 1940.
16. Stack, John, Lindsey, W. F., and Littell, Robert E.: The Compressibility Burble and the Effect of Compressibility on Pressures and Forces Acting on an Airfoil. NACA Rep. No. 646, 1938.
17. Stack, John: Tests of Airfoils Designed to Delay the Compressibility Burble. NACA TN No. 976, 1944. (Reprint of ACR, June 1939.)



TABLE I - Drag Analysis of Airplanes in Original Condition

$$C_L = 0.15$$

Item	Airplane										
	1	2	3	4	5	6	7	8	9	10	11
Original condition	0.0377	0.0328	0.0390	0.0267	0.0320	0.0362	0.0257	0.0275	0.0329	0.0269	0.0201
Excessive cooling drag			.0017 <sup>4</sup>			.0017			.0015		
Engine cowling (no cooling air)								.0020		.0013	
Fuselage shape					.0009	.0006					
Carburetor intake		.0010 <sup>2</sup>						.0006	.0019	.0006 <sup>3</sup>	.0001
Prestone radiator							.0034		.0024		.0011
Oil cooler		.0020	.0007	.0007			.0003	.0017	.0040	.0008	.0006
Intercooler								.0011	.0007	.0011	
Exhaust stacks	.0016 <sup>3</sup>				.0010	.0007 <sup>3</sup>	.0003	.0006	.0014		.0003
Supercharger									.0033		
Perforated flaps					.0020	.0012					
Seals on control surfaces							.0005			.0002	
Sanded walkway								.0007			
Cockpit canopy						.0019 <sup>3</sup>			.0004	.0004 <sup>3</sup>	
Landing gear	.0016	.0014	.0007	.0019	.0008	.0007	.0009 <sup>3</sup>	.0002	.0019	.0005	
Gun installations	.0069 <sup>1</sup>		.0029 <sup>3</sup>					.0003	.0006	.0002	.0005
Gun sight	.0003										
Bomb racks					.0008	.0017					
Ejector chute								.0003			
Aerial		.0005					.0005	.0008		.0007	
Air leakage					.0008		.0007	.0017	.0004	.0011	

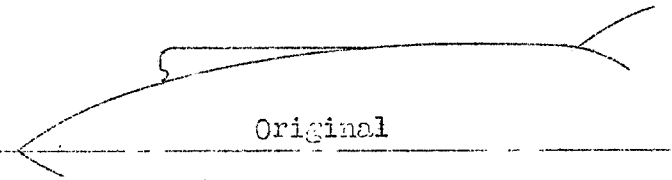
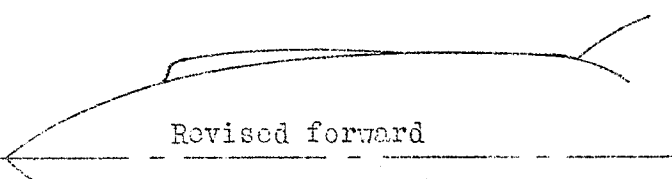
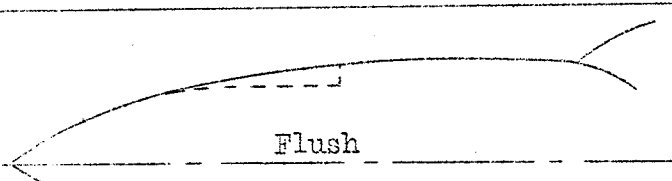
<sup>1</sup>Includes carburetor and oil cooler scoop drag (largely due to leakage).

<sup>2</sup>Plus cowling change.

<sup>3</sup>Faired, not removed.

<sup>4</sup>Includes fairing flame arrestor.

TABLE II.- Carburetor Intake Scoops

Duct characteristics			Flow characteristics				Drag data
Type	Inlet area (sq in.)	Outlet area (sq.in.)	$C_L = 0.48$ $V = 216 \text{ mph}$		$C_L = 0.15$ $V = 430 \text{ mph}$		$C_D$ $C_L=0.15$ $S=170 \text{ sq ft}$
			Ram (percent q)	Quantity (lb/hr)	Ram (percent q)	Quantity (lb/hr)	
 Original	37.1	22	---	---	95.0	13,820	0.0010
	37.1	15	---	---	97.0	10,390	.0007
	37.1	9	---	---	97.5	7,930	.0008
 Revised forward	26.9	22	94.5	7,960	97.0	14,940	.0005
	26.9	15	94.5	6,170	98.0	12,420	.0003
	26.9	9	95.5	5,260	97.8	8,310	.0001
	26.9	0	---	---	88.0	0	.0000
 Flush	27.8	22	---	---	70.5	12,100	- .0002
	27.8	15	63.0	5,580	73.5	9,810	.0000
	27.8	9	57.4	3,720	61.6	7,200	.0000

Flow characteristics are corrected to 12,000 feet altitude.  
 Military rating requires 8100 pounds of air per hour.

TABLE IV.-- Wing Profile Drags and Transition Points

Airplane	Description	Figure	Transition point location on upper surface of wing		$C_{D_0}$ measured	$C_{D_0}$ smooth wing (est.)	$\Delta C_{D_0}$
			s/c *	Remarks			
1	Metal covered, brazier-head rivets; larger rivets on forward portion of wing; laps facing back	---	---	---	0.0090	0.0058	0.0032
2	Metal covered, brazier-head rivets; row of larger rivets on upper surface about 15% c behind l.e.; laps facing back	29a	---	---	.0083	.0062	.0021
3	Fabric covered, raised stitching; drag measured on lower wing	29b	---	---	.0084	.0070	.0014
4	Front portion of wing metal covered, flush rivets; rear portion fabric covered, flush stitching	29c	---	---	.0070	.0063	.0007
5	Metal covered, flush rivets to about 18% c behind l.e., remainder brazier-head rivets; perforated dive and landing flaps	29d	---	---	.0109	.0072	.0037
6	Metal covered, flush rivets on front half of wing, laps facing back; fabric covering on rear half; perforated dive and landing flaps	---	---	---	.0106	.0065	.0041
7	Metal covered, flush rivets, laps facing forward	---	0.176	9.0 ft from $\frac{c}{2}$ airplane $t/c^* = 0.126$	.0079	.0060	.0017
8	Metal covered, flush rivets, joggled laps	29e	.198	7.3 ft from $\frac{c}{2}$ airplane $t/c^* = 0.134$	.0070	.0059	.0011
9	Metal covered, flush rivets, filled joints	---	.180	7.2 ft from $\frac{c}{2}$ airplane $t/c^* = 0.135$	.0071	.0060	.0011
10	Metal covered, flush rivets, filled joints	---			.0077	.0061	.0016
11	Wood, filled and polished	---	.180	5.7 ft from $\frac{c}{2}$ airplane $t/c^* = 0.130$	.0074	.0061	.0013

- \* distance along surface behind stagnation point  
 c length of chord  
 t section thickness

TABLE V.- Cockpit Canopies and Windshields

Airplane	Modification	Figure	Drag of canopy		Reduction of drag by modifications		Cross-section area of windshield
			$\Delta C_D$	$\Delta C_{D_{FW}}$	$\Delta C_D$	$\Delta C_{D_{FW}}$	
5	Longitudinal section of canopy modified to increase height 3.2 in.	31c			0	--	1.76 (mod.) 1.24 (orig.)
6	Modified windshield	31d			.0011	0.13	2.17
	Modified tail				.0009	.11	2.17
	Modified windshield and tail				.0019	.22	2.17
9	Original canopy	31b	0.0004	0.04	--		2.64
	Lowered enclosure		.0002	.02	.0002	.02	2.19
	Lowered enclosure - short tail		.0003	.03	.0001	.01	2.19
	Lowered enclosure - flat sided windshield and short tail		.0004	.04	0	0	2.19
10	Modified windshield	31a			.0004	.05	2.00
11	Flat side windshield	31e			0	0	1.14
					.0002*	.03	

\*Obtained for condition with carburetor scoop removed.

The subscript FW designates frontal area of canopy.

TABLE VI.- Drag of Landing Gears

1-489	Air-plane	Fig-ure	Type of gear	Tire size (in.)	Drag 100 mph (lb)	Reduction in drag for modifications, 100 mph	
						lb	Modification
	1	1a	1	26 x 6	8.5		
	2	1b	1	26 x 6	8.3		
	3	1c	1	26 x 6	4.7		
	4	33c	2	30 x 7	14.8		
						3.1	Oleo strut faired and sharp edge at rear half wells rounded
						7.0	Wheel well cover plates
						10.9	Wheel well cover plates and faired oleo struts
	5	33d	3	30 x 7	6.5		
	6	1f	1	27 streamline	5.3		
	7	33b	2	30 smooth contour		4.2	Fairing no. 1.
						5.3	Fairings no. 1 and no. 2
	8	33f	3	27 smooth contour	1.1		
	9	33e	4	Front 19 streamline --- Rear 27 smooth contour	10.3		
	10	33a	1	26 x 6	3.3		
	11	1k	3	27 smooth contour	0		

TABLE VII.- Gun Installations

Airplane	Figure	Number and size of guns	Drag at 100 mph (lb)	$\Delta C_D$
3	34c	one 30-cal. one 50-cal.	19.6	0.0029
8	34e	two 50-cal.	2.3	.0004
9	34d	one 37-mm cannon two 50-cal. guns	3.8	.0007
10	34b	two 50-cal.	1.3	.0002
11	34f	two 50-cal. (fuselage) eight 30-cal. (wing)	1.3 .9	.0003 .0002

TABLE VIII.- Drag of Aerials

Airplane	Type of aerial (fig. 3c)	Drag at 100 mph (lb)
2	2	2.9*
7	1	3.0
8	1	4.6
10	3	1.3
10	2	4.7

\*Drag only for wires - mast in place

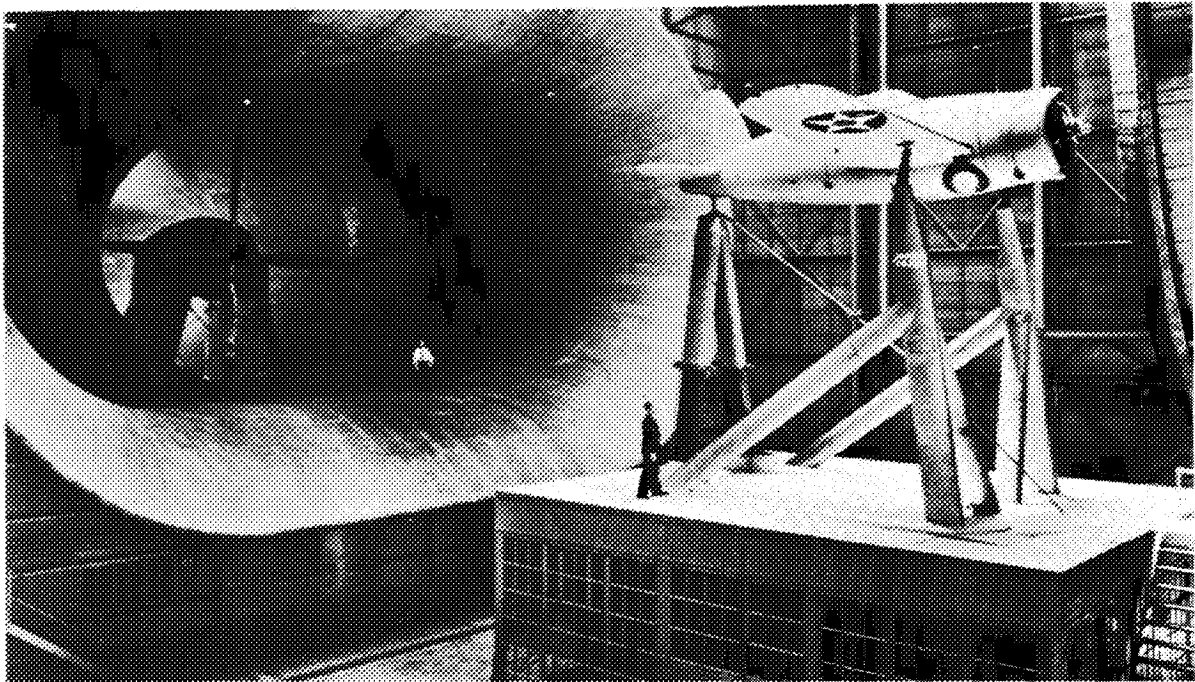
TABLE IX.- Leakage Drag Increments

Airplane	Source of Leak	Figure	$\Delta C_D$	D at 100 mph (lb)
1	Gun blast tube openings in nose of cowl (similar to fig. 35a) <sup>x</sup>	--	0.0069	36.8
3	Gun blast tube openings*	36a	.0029	28.7
5	Openings between cowl sections and at flaps	36b	.0008	6.5
7	Hole in the nose of the propeller spinner and openings around the blades	36c	.0007	4.2
8	Openings between cowl sections and at flaps	36d	.0009	5.1
	Accessory exit slot		.0005	2.9
9	Fuselage louver openings	22c	.0004	2.2
10	Openings between cowl sections, at flaps	36e	.0003	2.0
	Fuselage openings	--	.0008	5.3

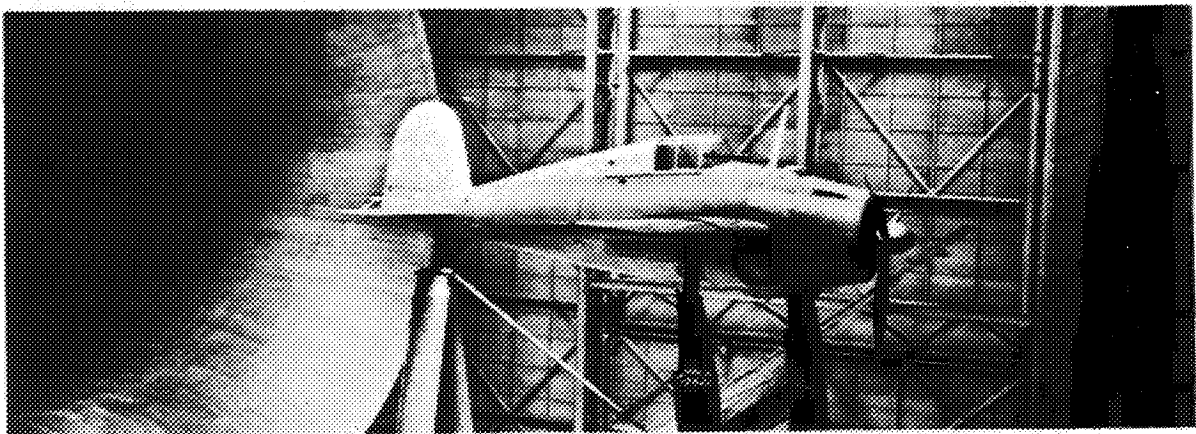
<sup>x</sup>This item includes drag reduction due to modification of oil and carburetor scoops.

\*This item was measured with propeller operating.

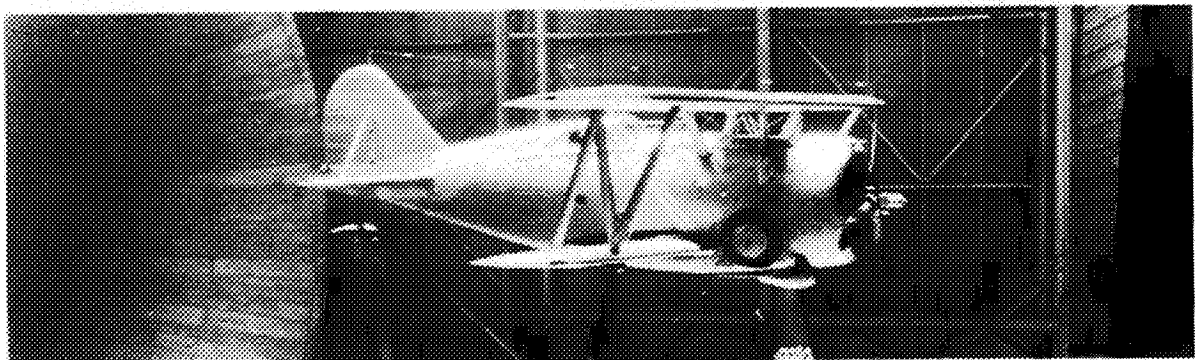
I-489



(a) Airplane 1.



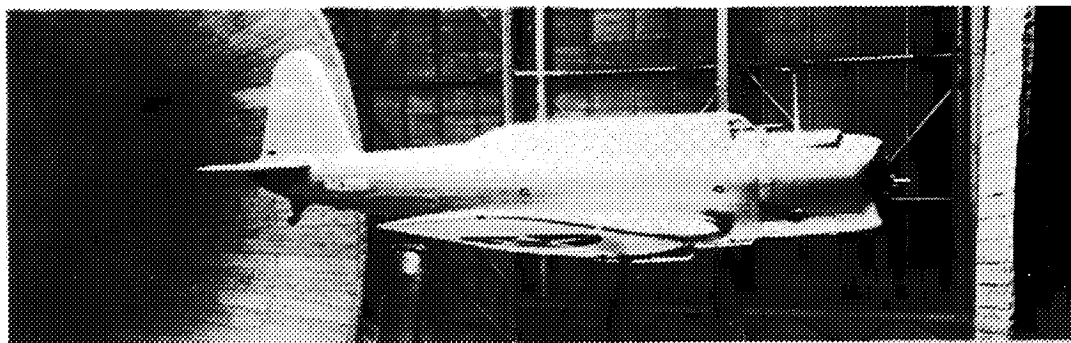
(b) Airplane 2.



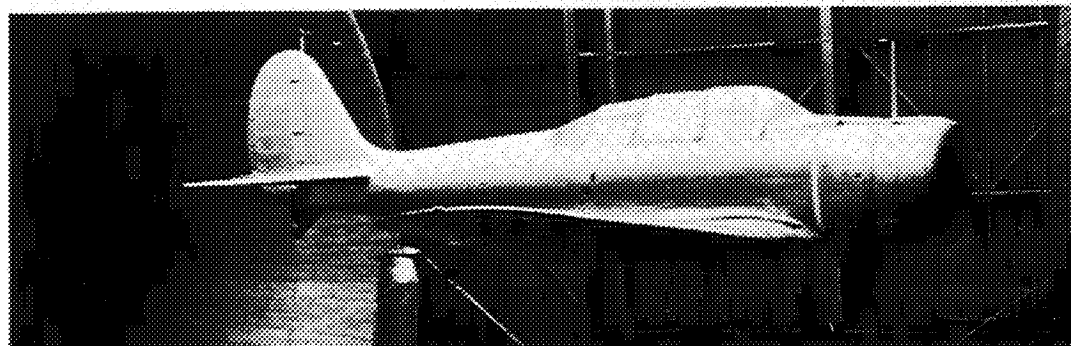
(c) Airplane 3.

Figure 1.—Airplanes mounted for tests in the NACA full-scale wind tunnel.





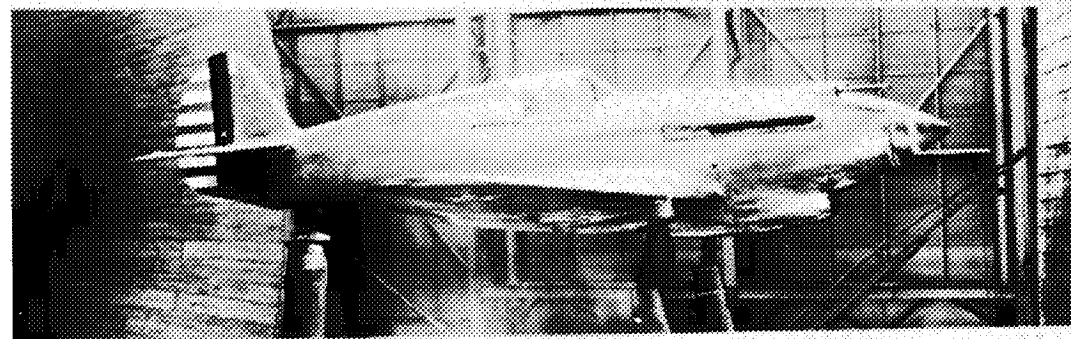
(d) Airplane 4.



(e) Airplane 5 with modified cockpit canopy.

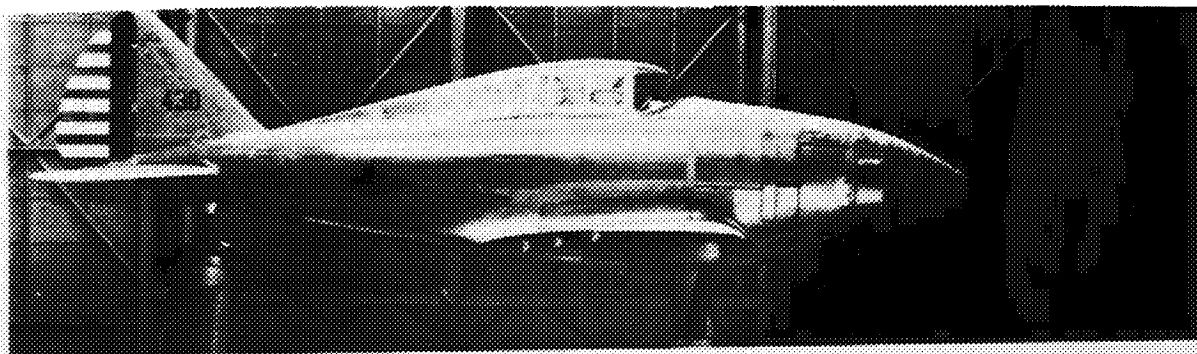


(f) Airplane 6.

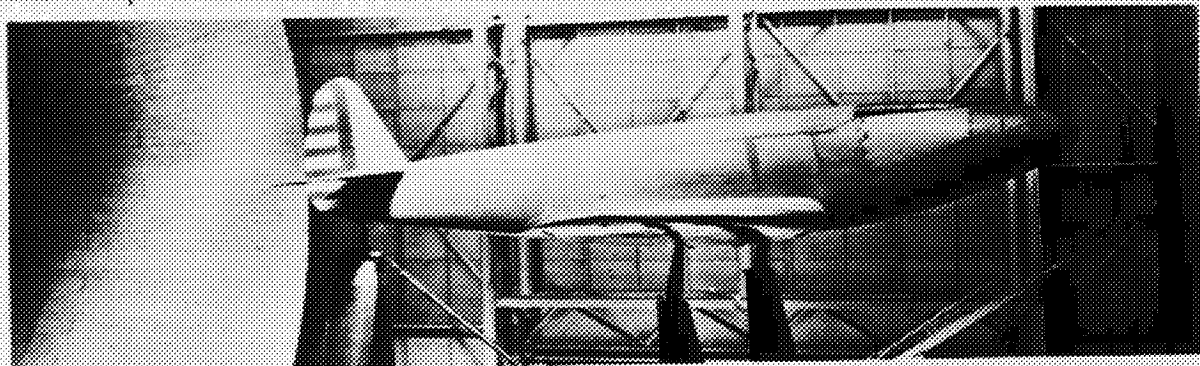


(g) Airplane 7.

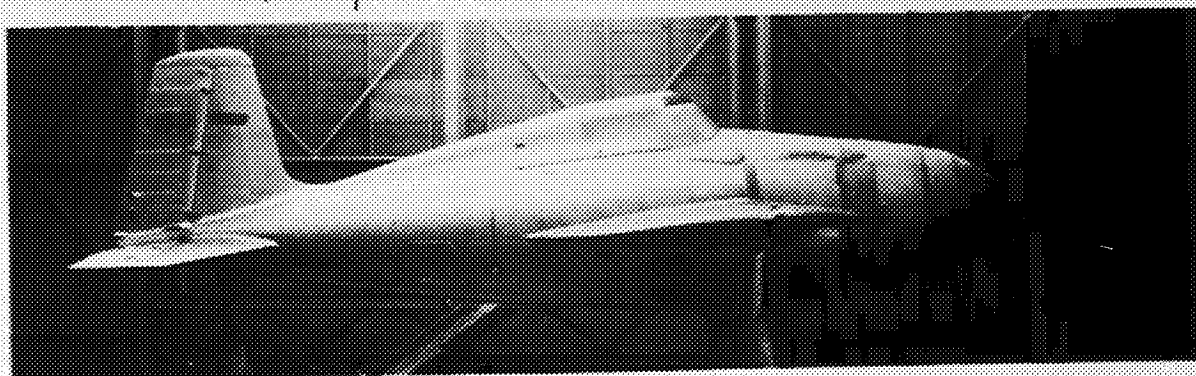
Figure 1.—continued. Airplanes mounted for tests in the NACA full-scale wind tunnel.



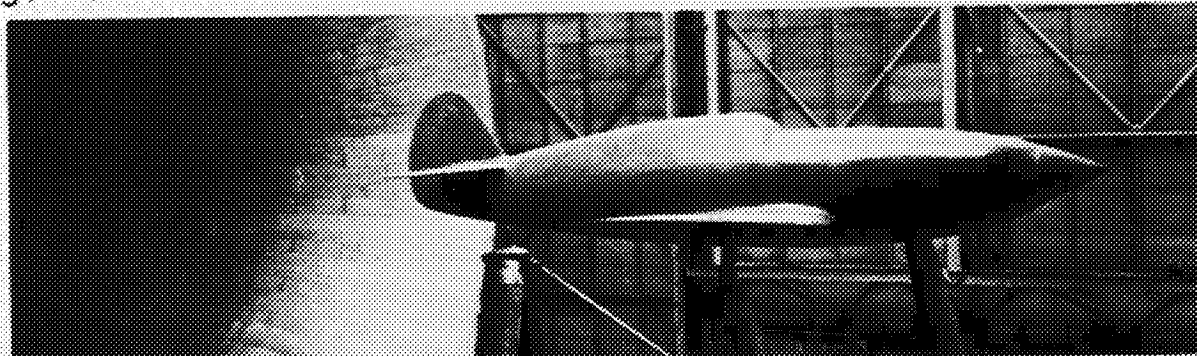
(h) Airplane 8 in smooth condition except for cockpit canopy.



(i) Airplane 9 in smooth condition.

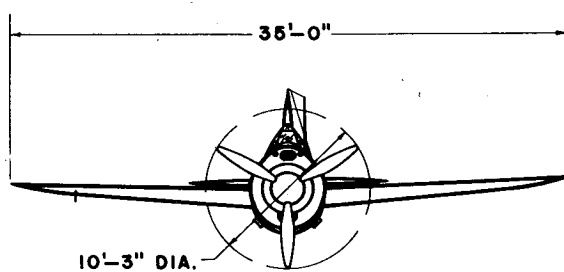
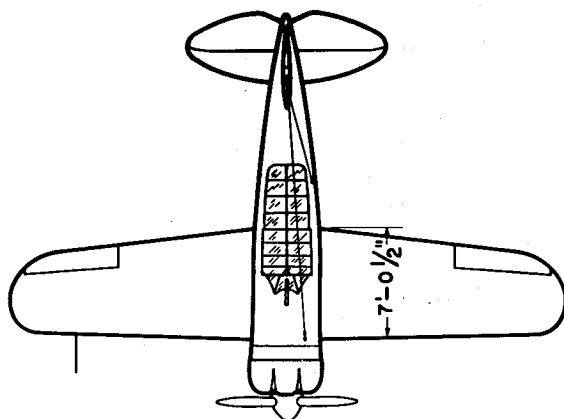


(j) Airplane 10 in smooth condition except for modified cockpit canopy.



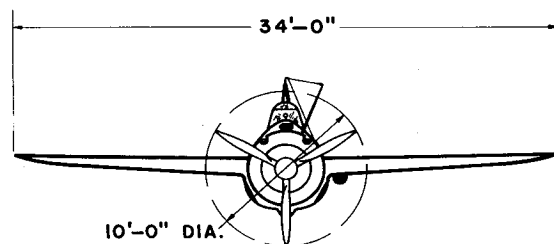
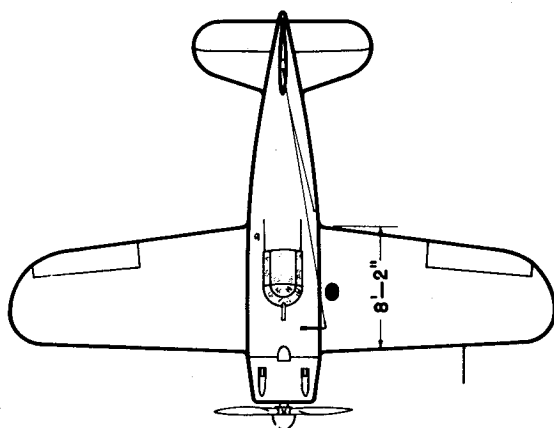
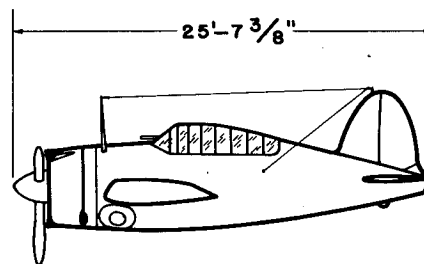
(k) Full-scale model of airplane 11 in smooth condition except for cockpit canopy.

Figure 1.—continued. Airplanes mounted for tests in the NACA full-scale wind tunnel.



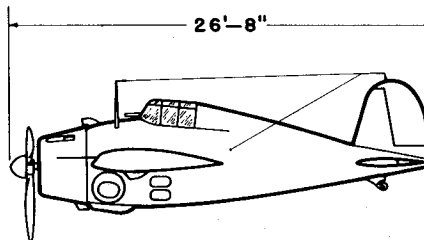
AIRPLANE 1

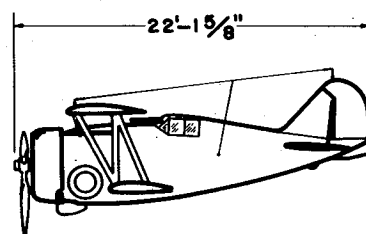
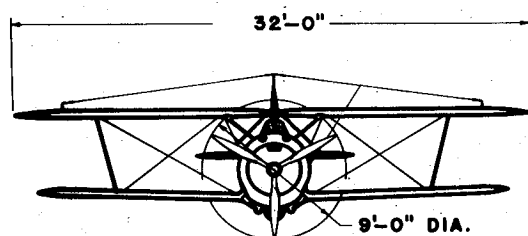
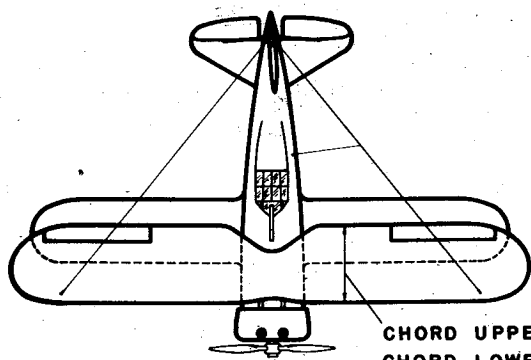
WEIGHT ..... 4,932 LBS.  
 WING SECTION ..... N.A.C.A. 23018-09  
 WING AREA ..... 209.0 SQ. FT.  
 SINGLE-ROW AIR-COOLED ENGINE.  
 750 H.P. 2,100 R.P.M. 15,200 FT.  
 ALTITUDE. DIRECT DRIVE.



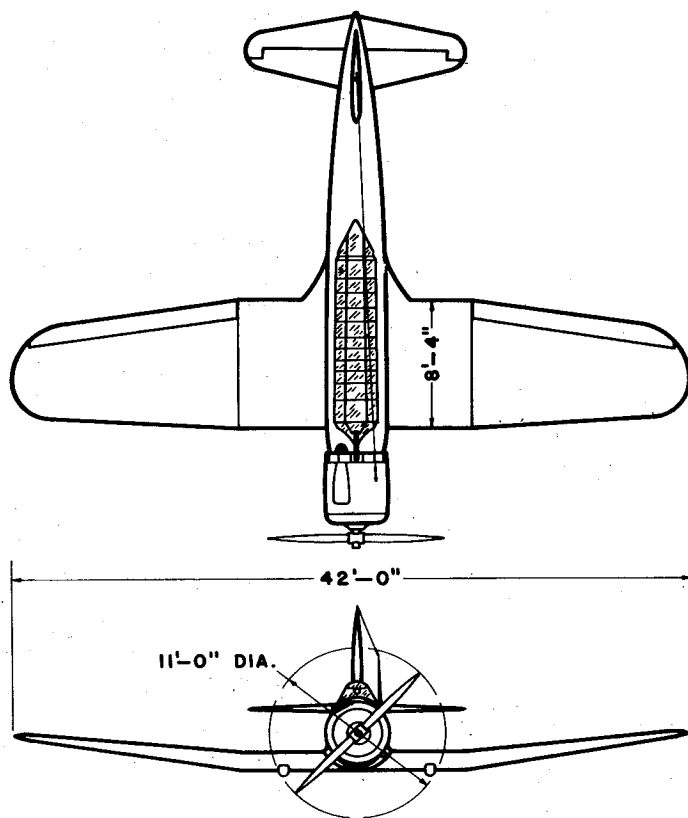
AIRPLANE 2

WEIGHT ..... 5,448 LBS.  
 WING SECTION ..... N.A.C.A. 23015-09  
 WING AREA ..... 233.2 SQ. FT.  
 TWO-ROW AIR-COOLED ENGINE.  
 900 H.P. @ 2,550 R.P.M. @ 10,000 FT.  
 ALTITUDE. PROPELLER GEAR RATIO, 3:2

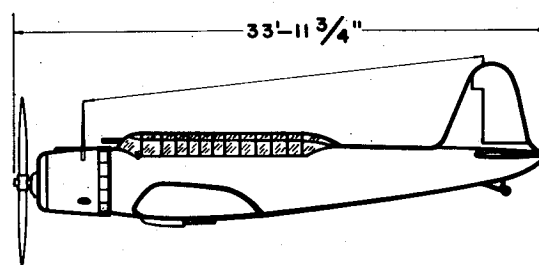




AIRPLANE 3



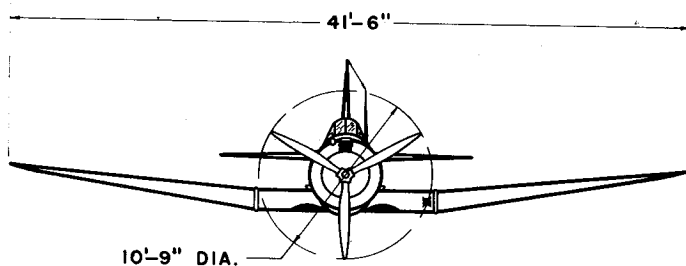
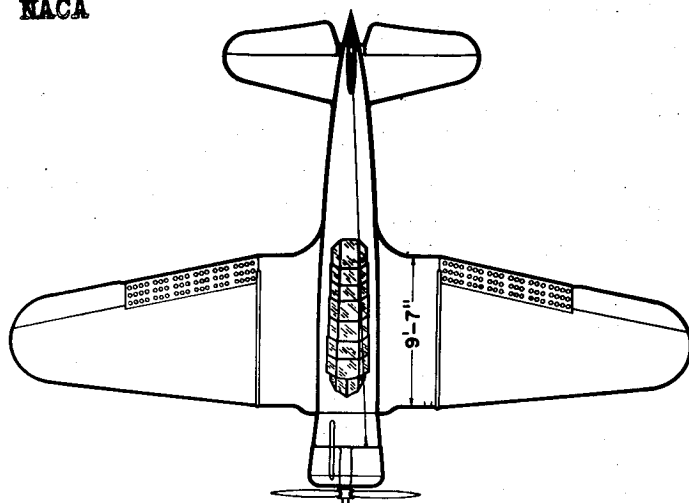
WEIGHT ..... 6,270 LBS.  
WING SECTION ..... N.A.C.A. 23015-09  
WING AREA ..... 305.3 SQ. FT.  
TWO-ROW AIR-COOLED ENGINE.  
750 H.P. @ 2,550 R.P.M. @ 14,200 FT.  
ALTITUDE. PROPELLER GEAR RATIO. 3:2



AIRPLANE 4

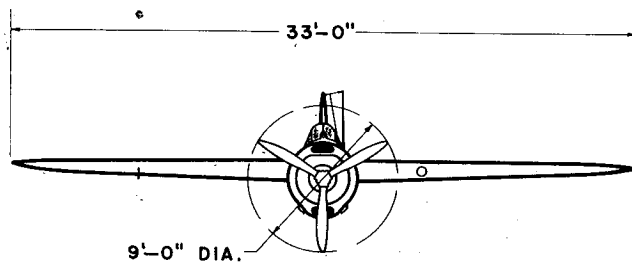
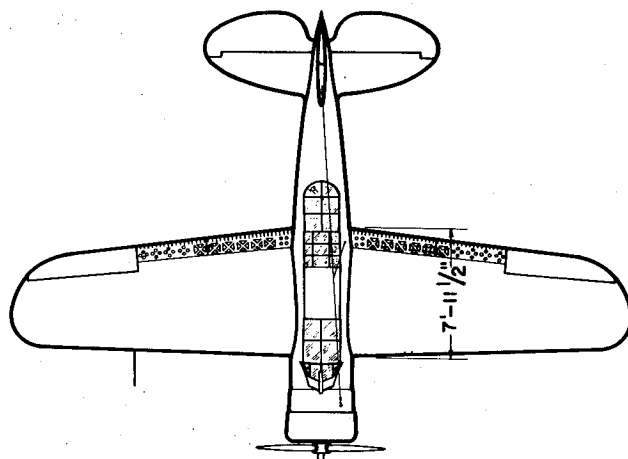
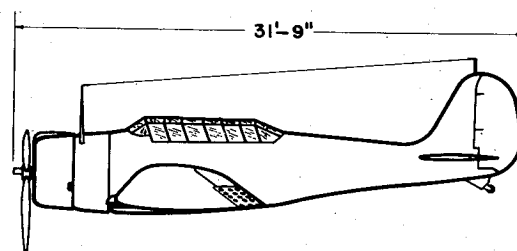
NACA

Fig. 2 (5-6)



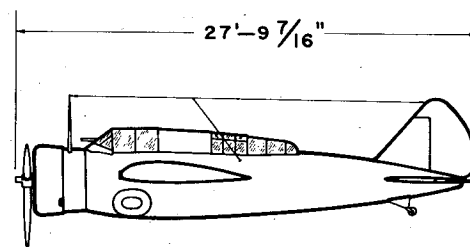
AIRPLANE 5

WEIGHT ..... 7,253 LBS.  
 WING SECTION ..... N.A.C.A. 2415-09.  
 WING AREA ..... 318.6 SQ. FT.  
 SINGLE-ROW AIR-COOLED ENGINE.  
 800 H.P. @ 2,300 R.P.M. @ 16,000 FT.  
 ALTITUDE. PROPELLER GEAR RATIO, 16:11



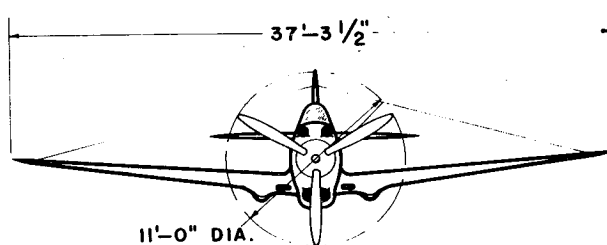
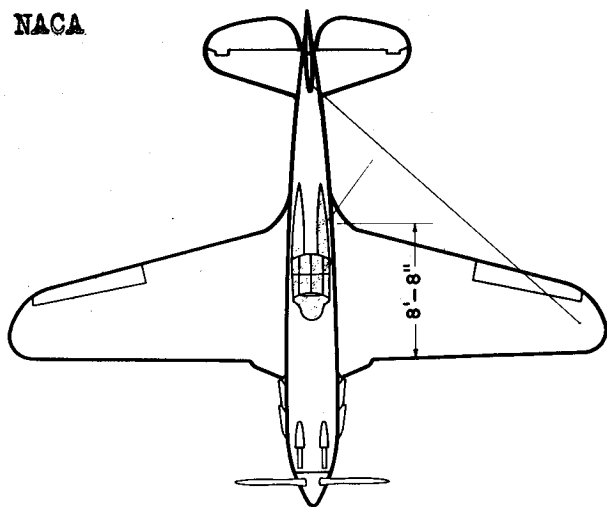
AIRPLANE 6

WEIGHT ..... 5,921 LBS.  
 WING SECTION ..... CLARK Y.H. 18-11.8 %  
 WING AREA ..... 258.0 SQ. FT.  
 SINGLE-ROW AIR-COOLED ENGINE.  
 750 H.P. @ 2,100 R.P.M. @ 15,000 FT.  
 ALTITUDE. DIRECT DRIVE.



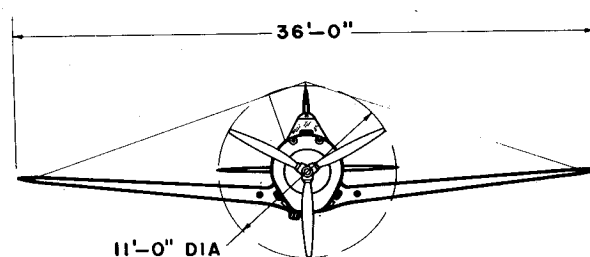
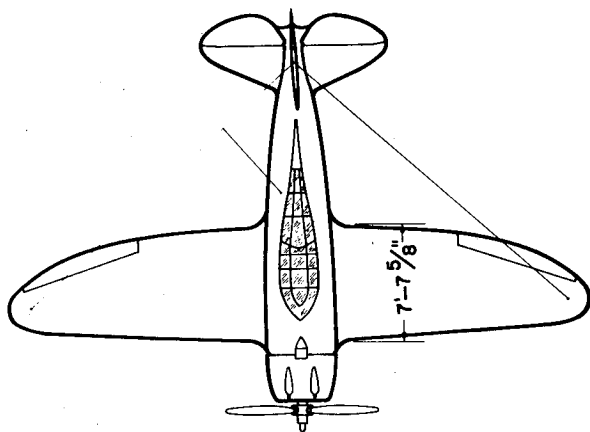
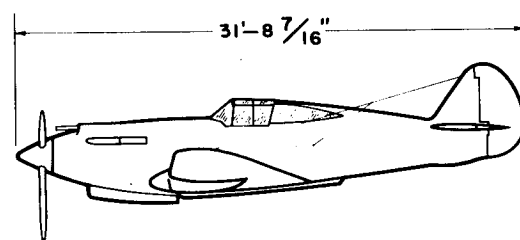
NACA

Fig. 2 (7-8)



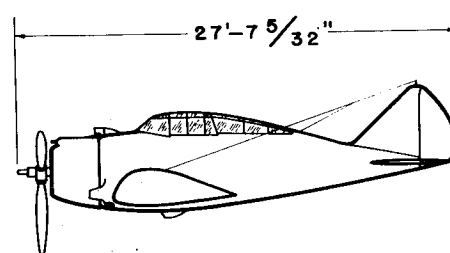
AIRPLANE 7

WEIGHT ..... 6,783 LBS.  
 WING SECTION ..... N.A.C.A. 2215-09  
 WING AREA ..... 236.0 SQ. FT.  
 PRESTONE-COOLED ENGINE.  
 1,000 H.P. @ 2,600 R.P.M. @ 16,000 FT.  
 ALTITUDE. PROPELLER GEAR RATIO, 2:1



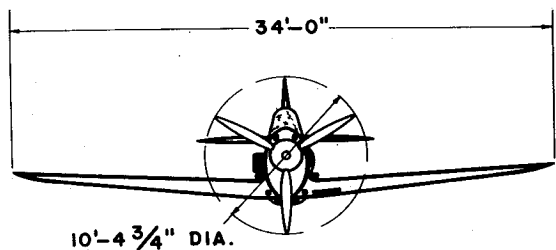
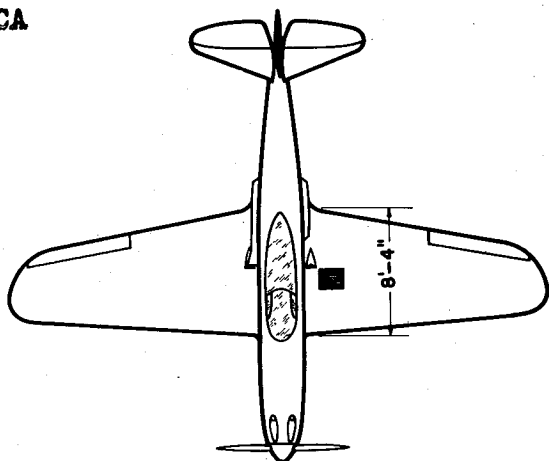
AIRPLANE 8

WEIGHT ..... 6,755 LBS.  
 WING SECTION ..... S3-AIRFOIL, 16.7-8.2%  
 WING AREA ..... 223.7 SQ. FT.  
 TWO-ROW AIR-COOLED RADIAL ENGINE  
 WITH GEAR-DRIVEN SUPERCHARGER.  
 1,100 H.P. @ 2,700 R.P.M. @ 15,000 FT.  
 ALTITUDE. PROPELLER GEAR RATIO, 16:9



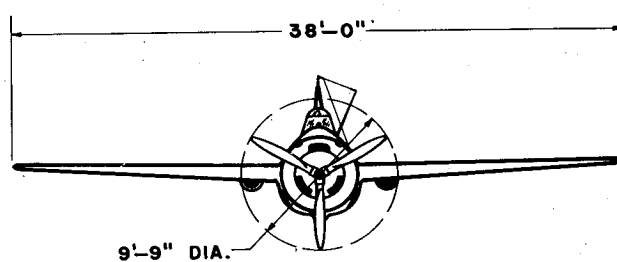
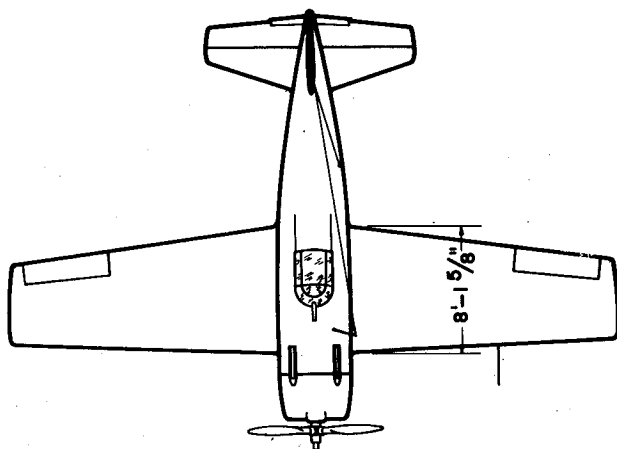
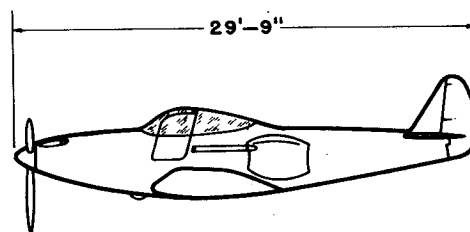
NACA

Fig. 2 (9-10)



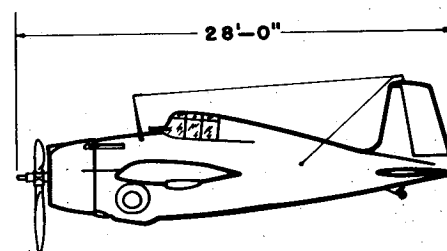
AIRPLANE 9

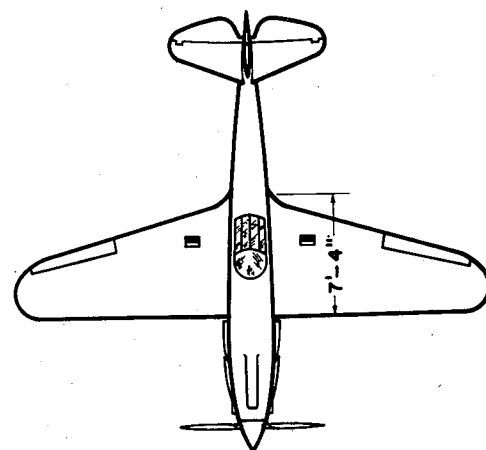
WEIGHT ..... 6,150 LBS.  
 WING SECTION ..... N.A.C.A. 0015-23009  
 WING AREA ..... 213.0 SQ. FT.  
 PRESTONE-COOLED ENGINE WITH TURBO-  
 SUPERCHARGER. 1,150 H.P. @ 2,950 R.P.M.  
 @ 20,000 FT. ALTITUDE.  
 PROPELLER GEAR RATIO, 9:5



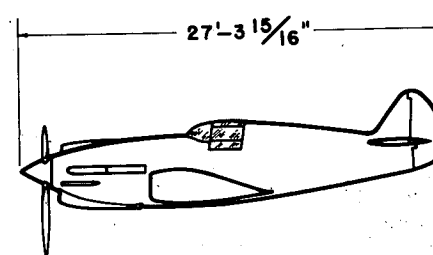
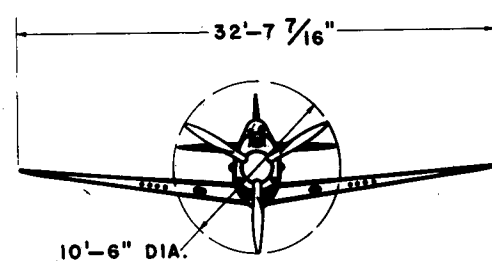
AIRPLANE 10

WEIGHT ..... 5,825 LBS.  
 WING SECTION ..... N.A.C.A. 23015-09  
 WING AREA ..... 260.0 SQ. FT.  
 TWO-ROW AIR-COOLED ENGINE WITH TWO-  
 STAGE GEAR-DRIVEN SUPERCHARGER.  
 1,000 H.P. @ 2,550 R.P.M. @ 20,000 FT.  
 ALTITUDE. PROPELLER GEAR RATIO, 3:2





WEIGHT ..... 6,600 LBS.  
 WING SECTION ..... N.A.C.A. 23016.5-09  
 WING AREA ..... 170.0 SQ. FT.  
 PRESTONE-COOLED ENGINE.  
 1,150 H.P. @ 3,000 R.P.M. @ 12,000 FT.  
 ALTITUDE. PROPELLER GEAR RATIO, 2:1



AIRPLANE II



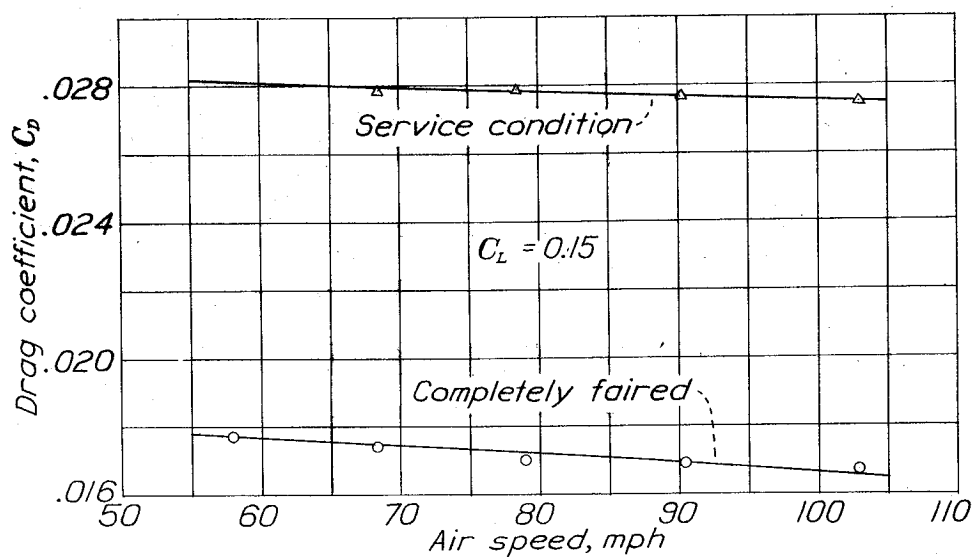


Figure 3.- Scale effect on drag coefficient at  $C_L = 0.15$  for airplane 8.

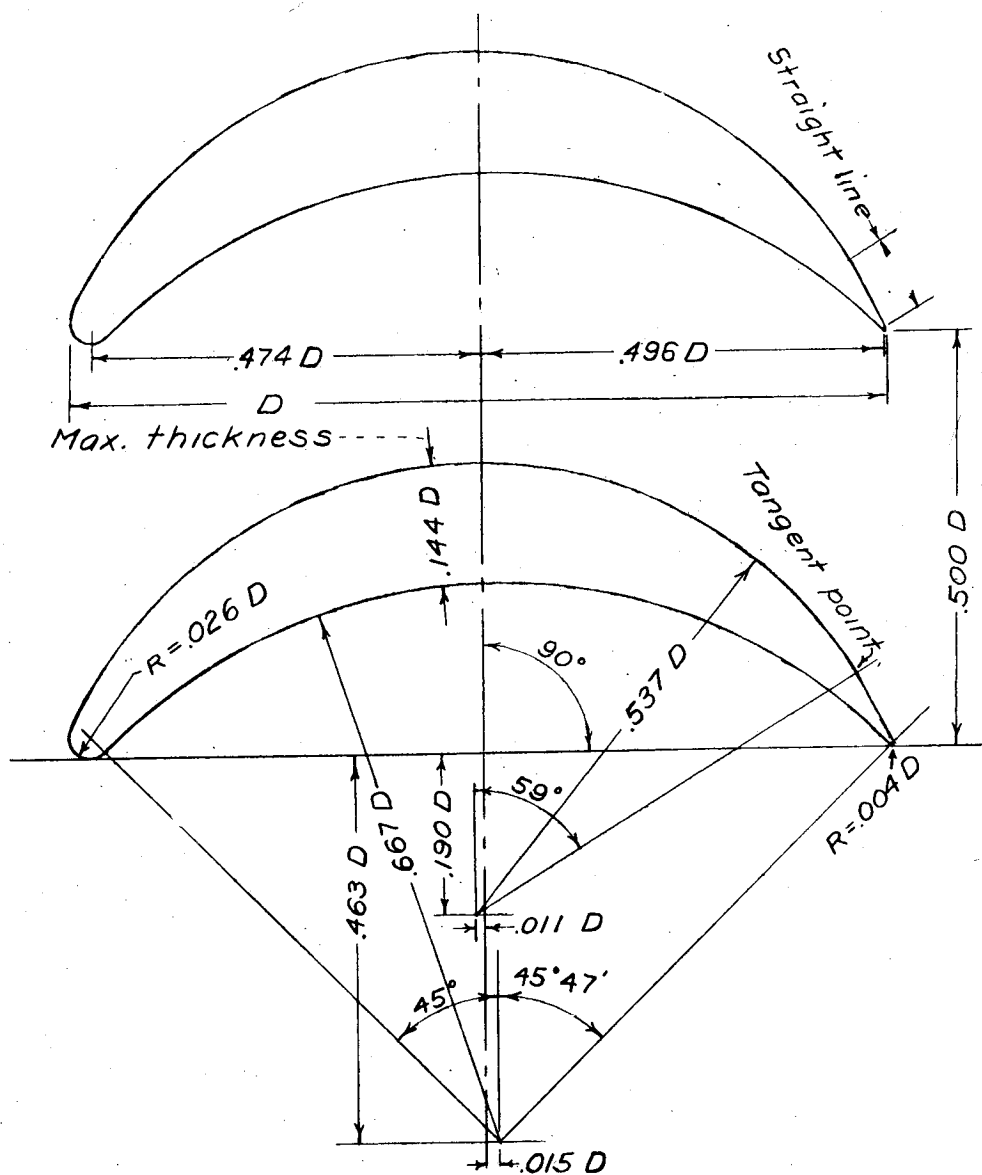
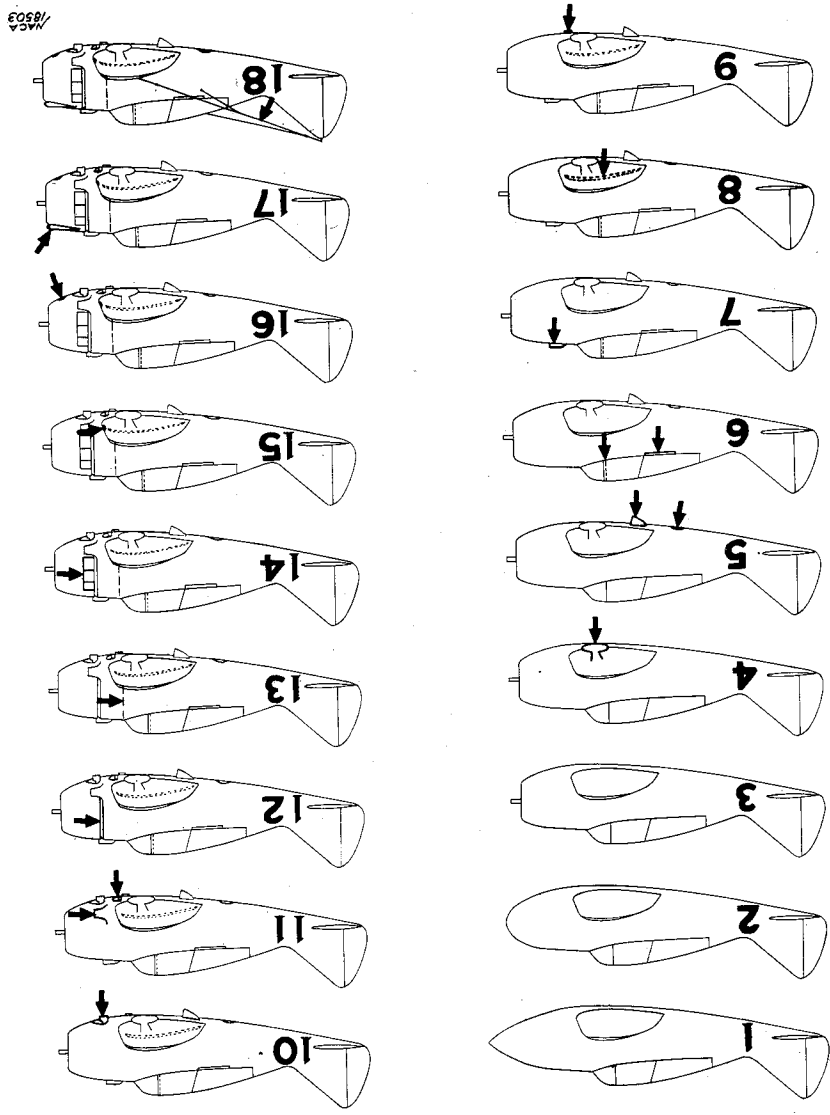


Figure 5.- Design of an efficient  $90^\circ$  turning vane.

NACA

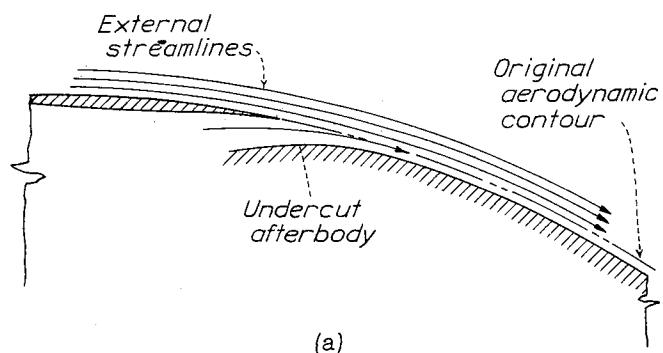
Fig. 4.

No.	Airplane conditions	$C_D$ ( $C_D=0.15$ )	$\Delta C_D$	$\Delta C_D^*$
1	Completely faired condition with long nose fairing	.0166	0	0
2	nose fairing with blunt	.0169	0	0
3	nose fairing original NACA	.0186	.0020	12.0
4	cowling: no air flowing through cowling Same as 3 except landing gear seals and fairing removed	.0188	.0002	1.2
5	" " " " original oil cooler installed	.0205	.0017	10.2
6	" " " " canopy fairing removed	.0203	.0002	-1.2
7	" " " " carburetor scoop added	.0209	.0006	3.6
8	" " " " sanded walkway added	.0216	.0007	4.2
9	" " " " ejector chute added	.0219	.0003	1.8
10	" " " " exhaust stacks added	.0225	.0005	3.6
11	" " " " intercoolers added	.0236	.0011	6.6
12	" " " " cowling exit opened	.0247	.0011	6.6
13	" " " " accessory exit opened	.0252	.0005	3.0
14	" " " " cowling fairing and seals removed	.0261	.0009	5.4
15	" " " " cockpit ventilator opened	.0262	.0001	.6
16	" " " " cowling vents installed	.0264	.0002	1.2
17	" " " " blast tubes added	.0267	.0003	1.8
18	" " " " radio aerial installed	.0275	.0008	4.8
Total drag change		.0111		66.9
* Percentages based on completely faired condition with long nose fairing				



Airplane Conditions

Figure 4.- Example illustrating test sequence as followed for airplane 8.



(a)

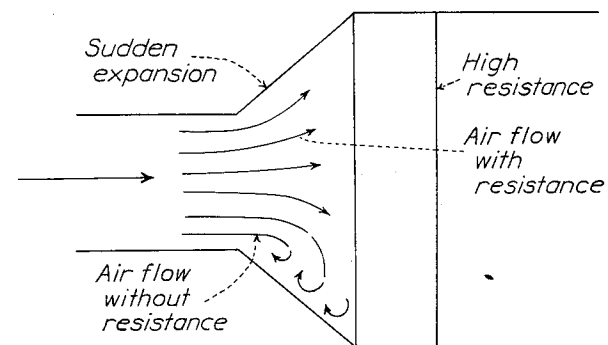
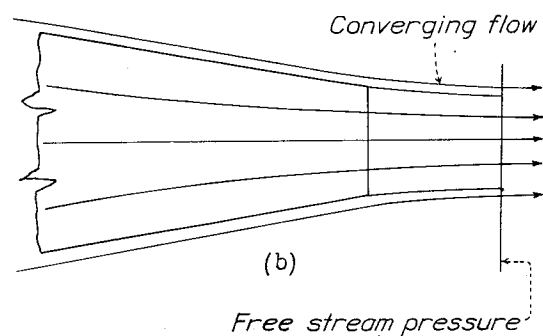
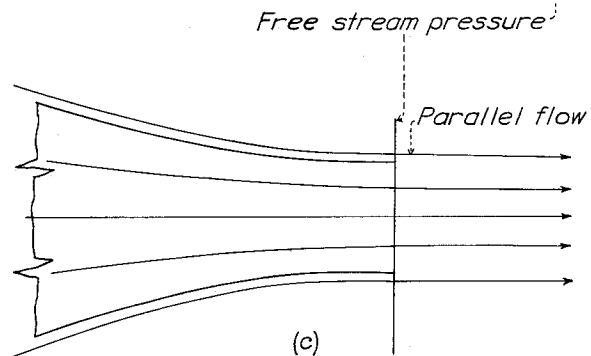


Figure 6.- Effect of high resistance in increasing allowable duct expansion.

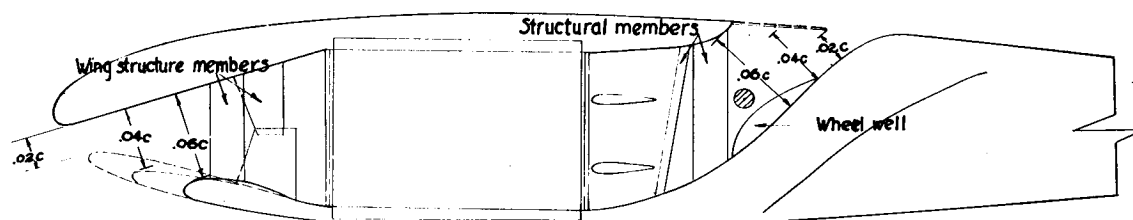
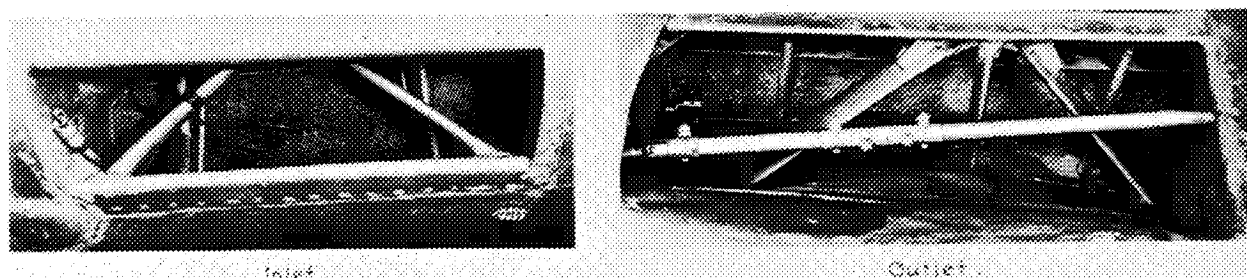


(b)



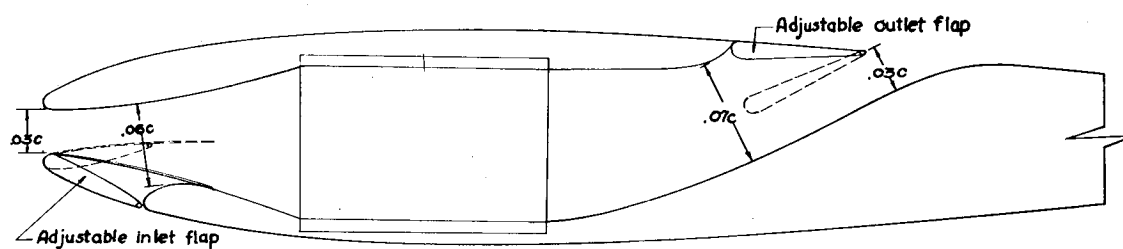
(c)

Figure 7.- Factors in outlet design.



Longitudinal section (including modifications)

(a) Original installation



(b) Proposed installation

Figure 8.—Prestone radiator installation on airplane 9.

NACA 27204

L-489

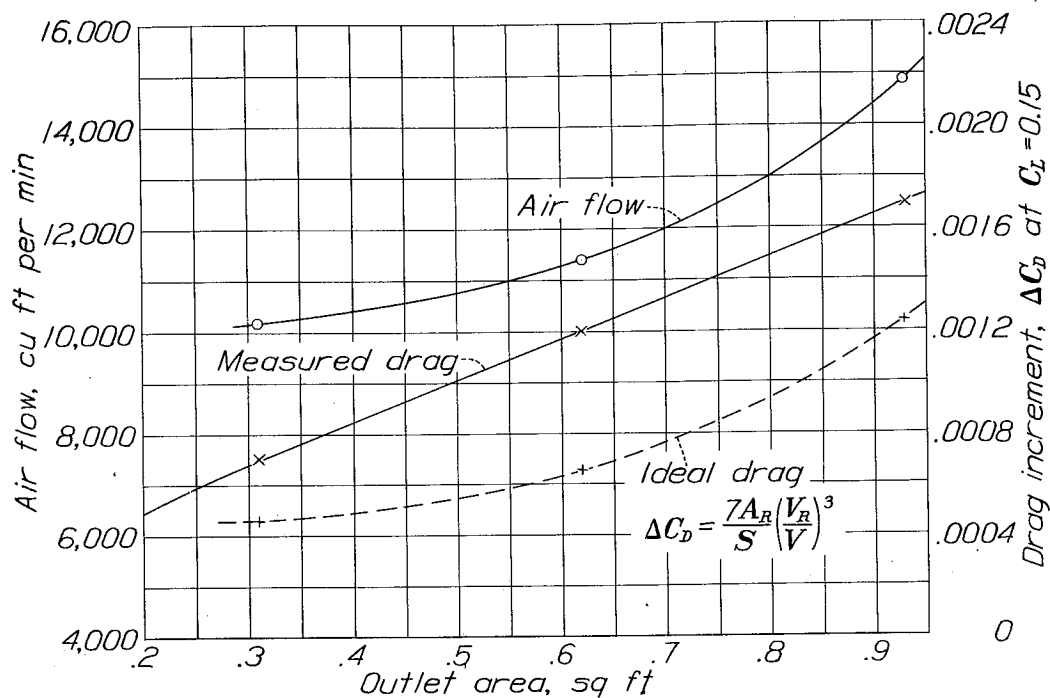


Figure 9.- Variation of cooling drag and air-flow quantity with outlet area for Prestone radiator installation on airplane 9.

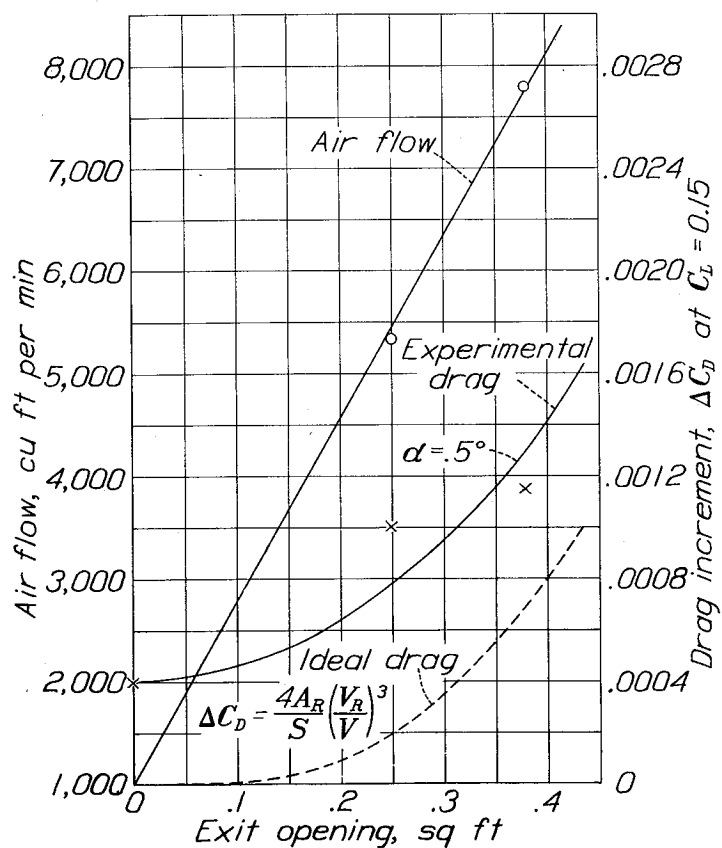
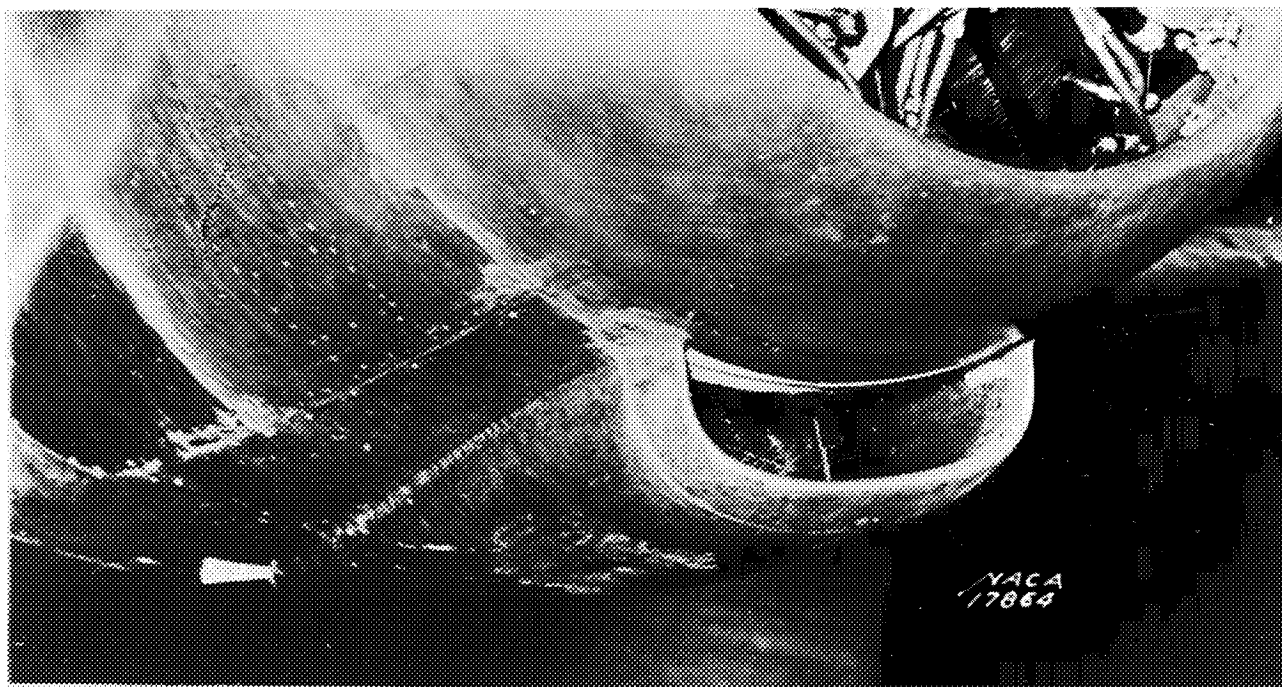
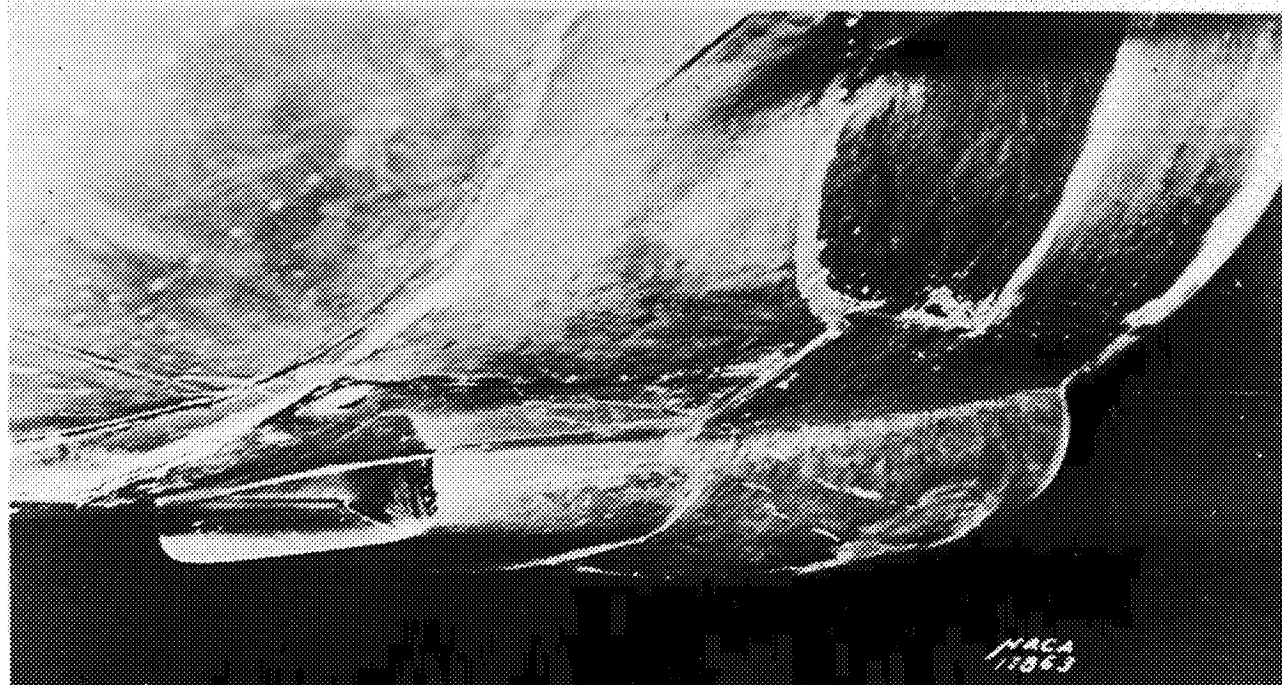


Figure 11.- Variation of cooling drag and air-flow quantity with outlet area for modified oil-cooler installation on airplane 8.



(a) Front view



(b) Rear view

Figure 10.—Modified oil cooler installation on airplane 8.

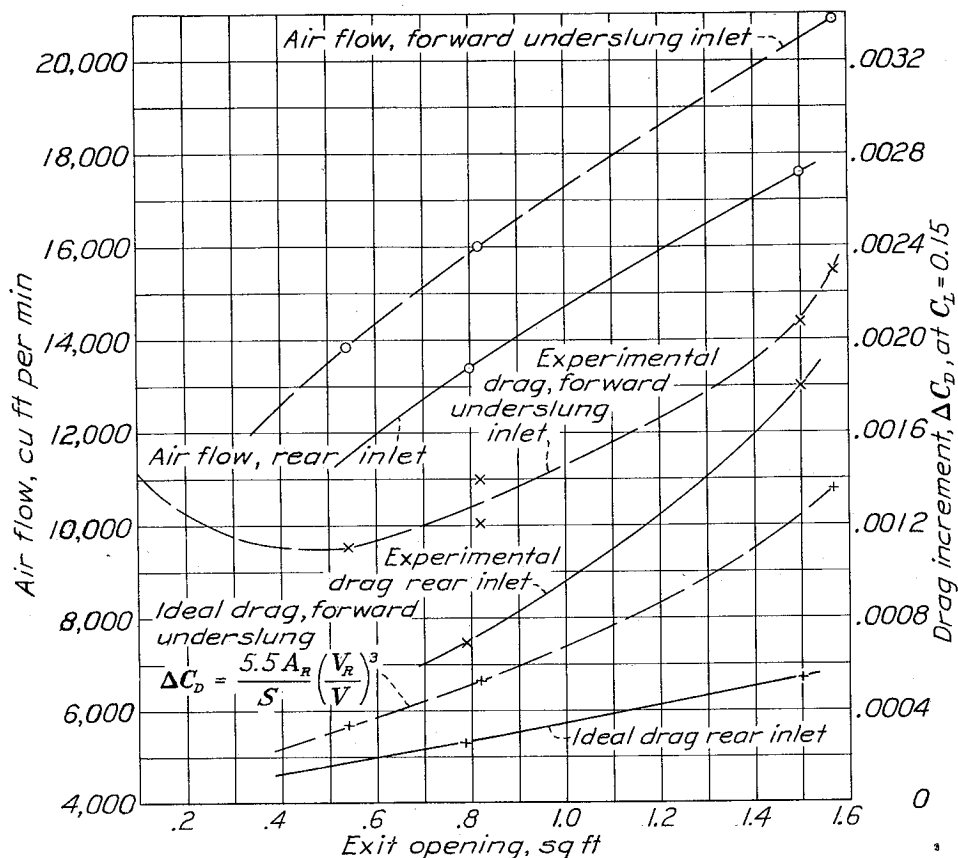


Figure 12.- variation of cooling drag and air-flow quantity with outlet area for Prestone radiator installation on airplane 11.

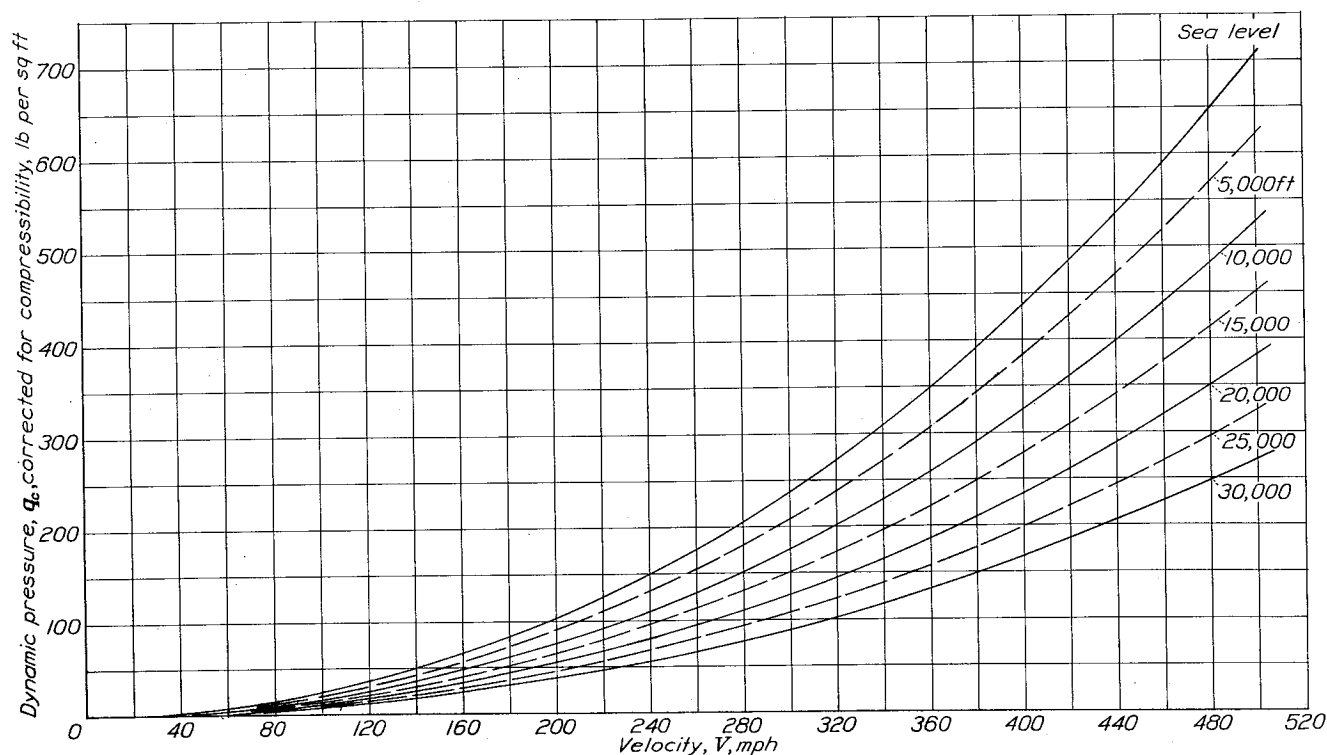


Figure 15.- Dynamic pressure available for ram at altitude.

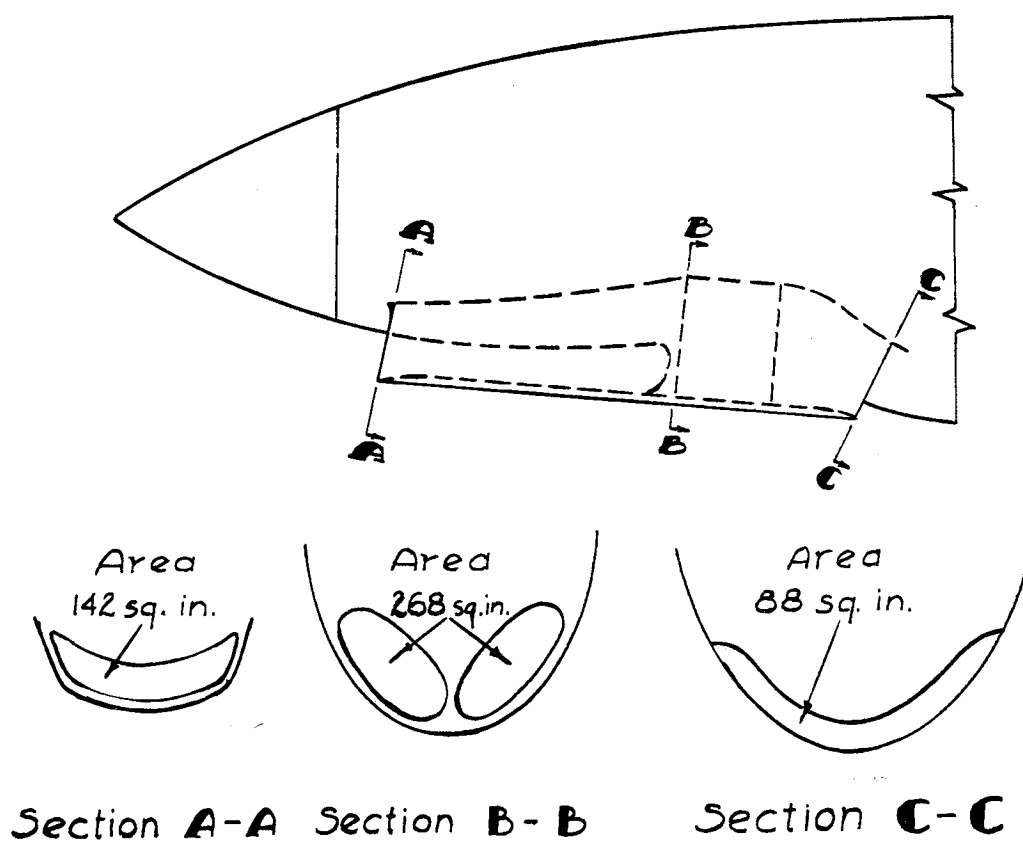
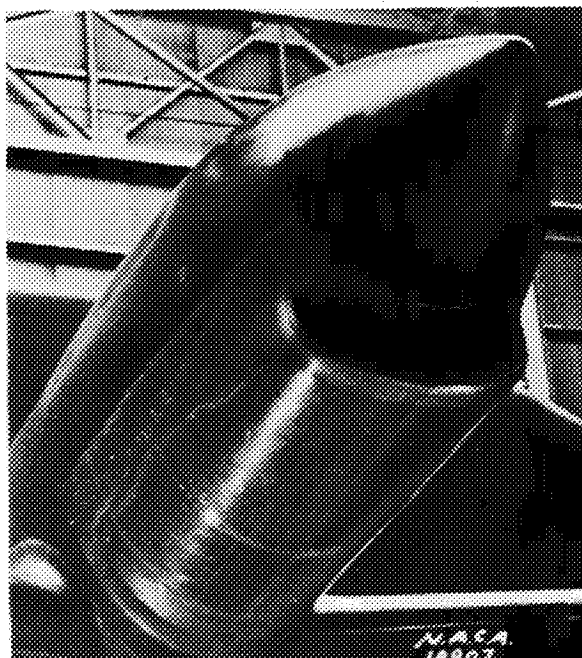
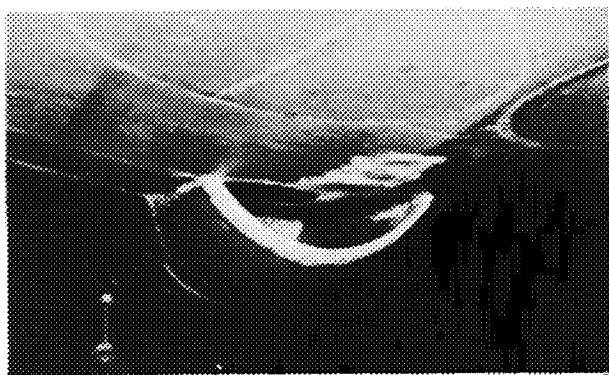


Figure 13.—Forward underslung prestone radiator installations for airplane 11.

NACA 20897.





Inlet



Outlet

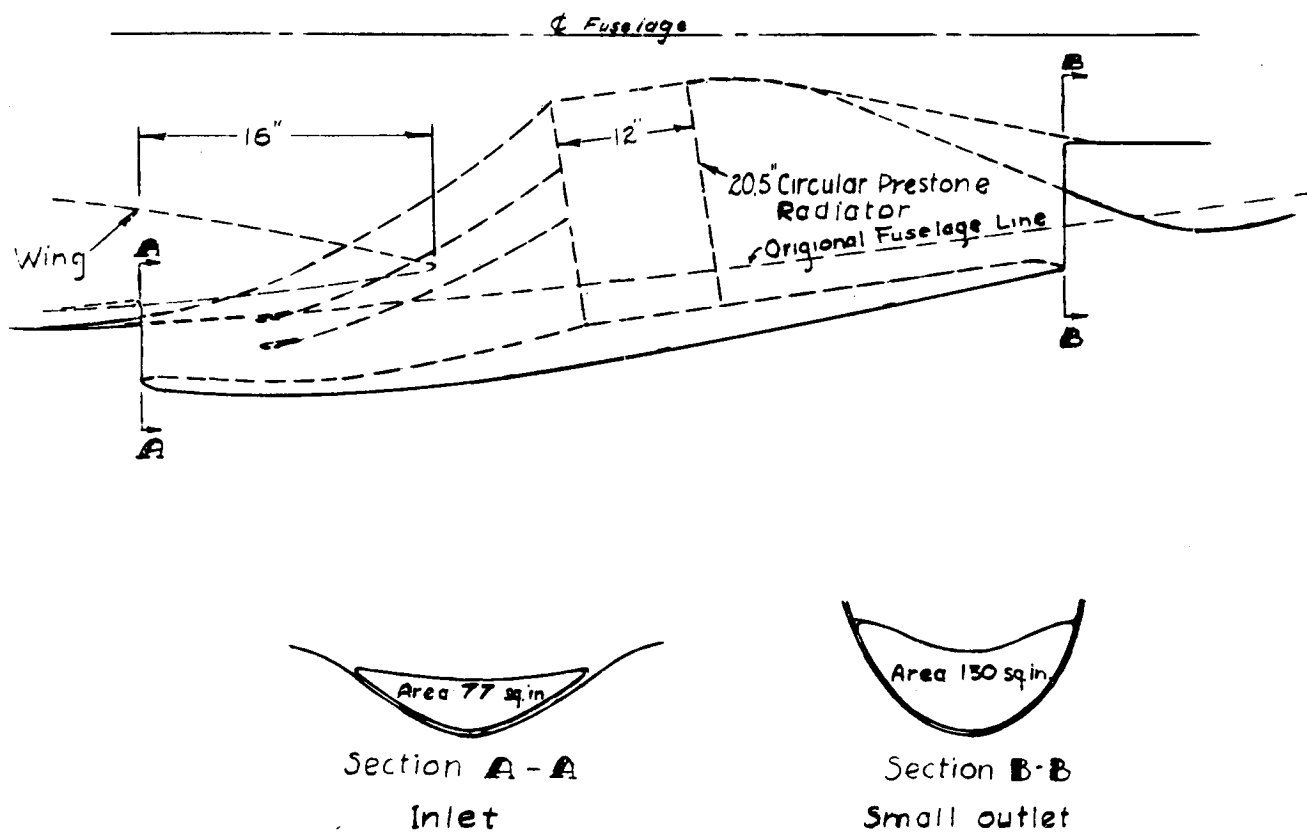
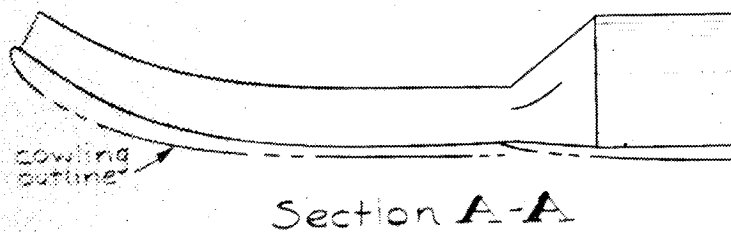
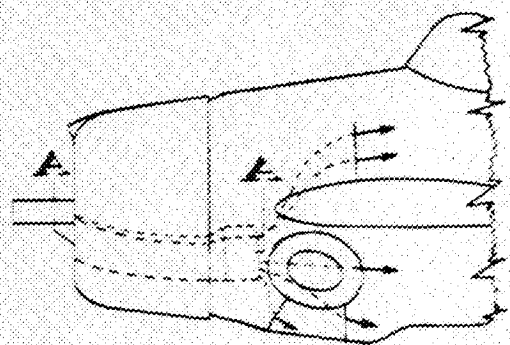
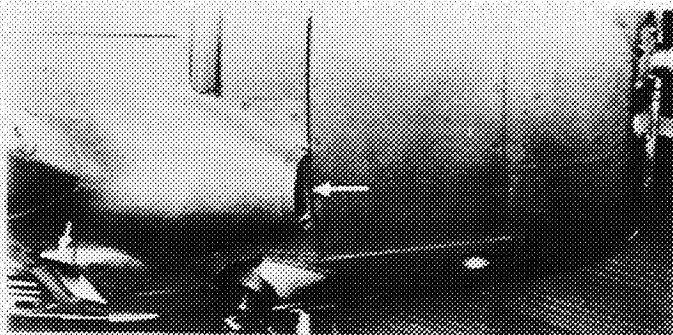


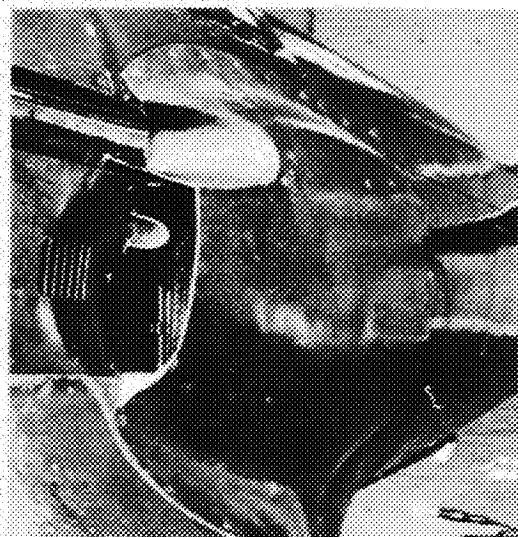
Figure 14.—Rear underslung prestone radiator installation for airplane 11.



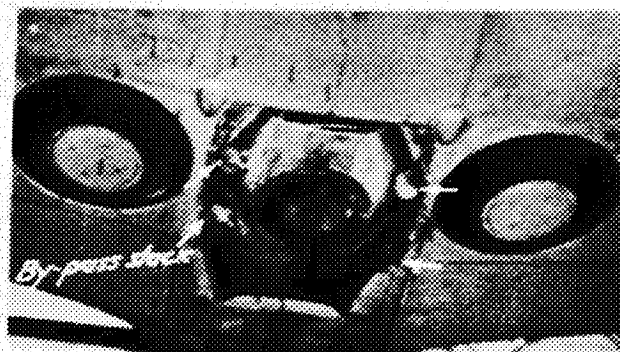
a) Intercooler on airplane 10.



b) Intercooler on airplane 8.



(c) Intercooler on airplane 9.



(d) Supercharger on airplane 9.

Figure 16. Air intercooler and supercharger installations.

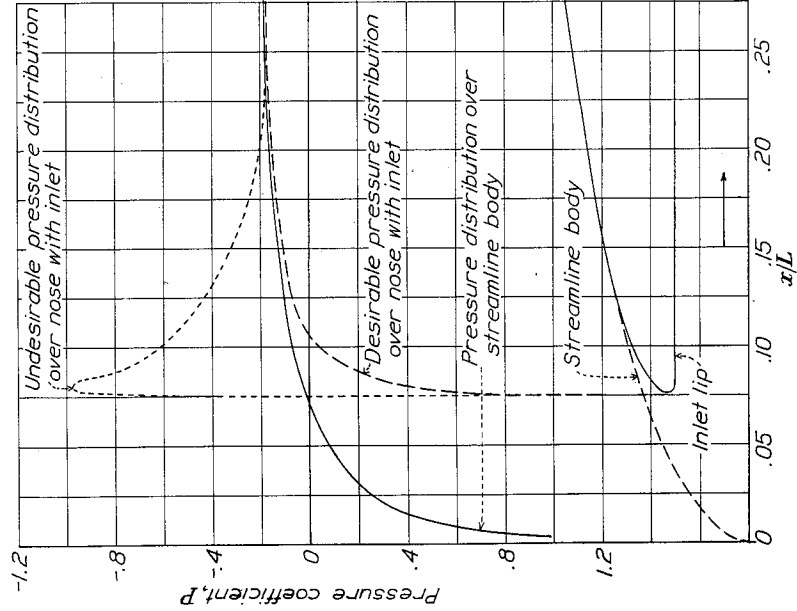


Figure 20.- Pressure distributions over air inlets.

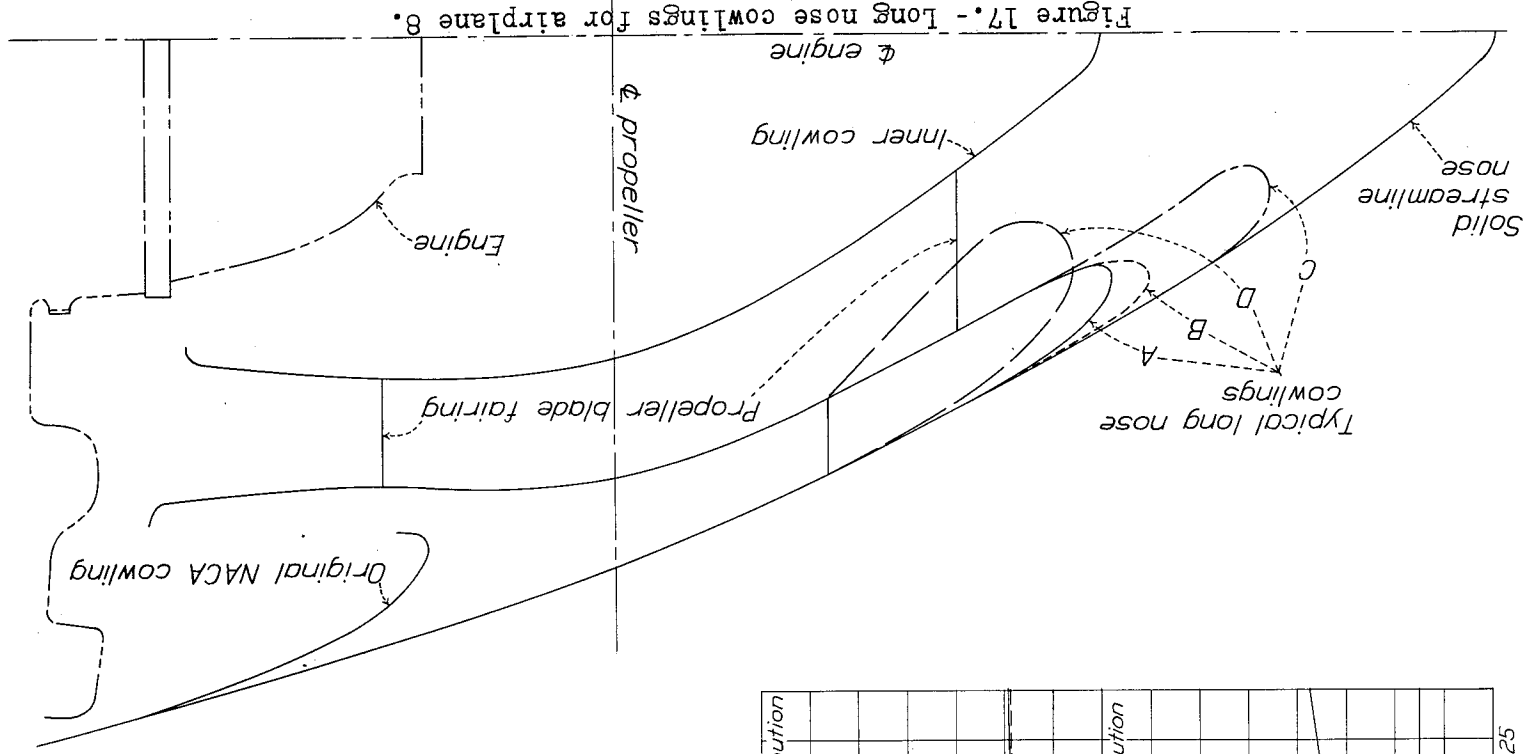


Figure 17.- Long nose cowlings for airplane 8.

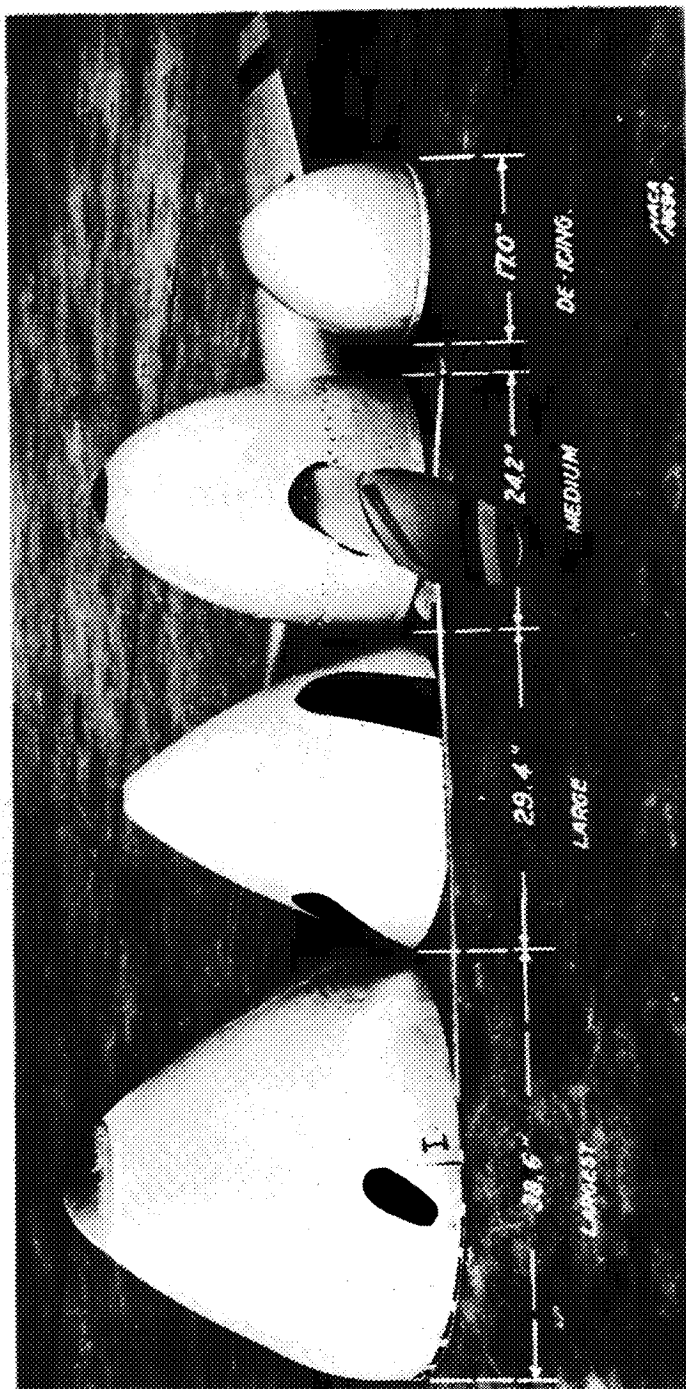
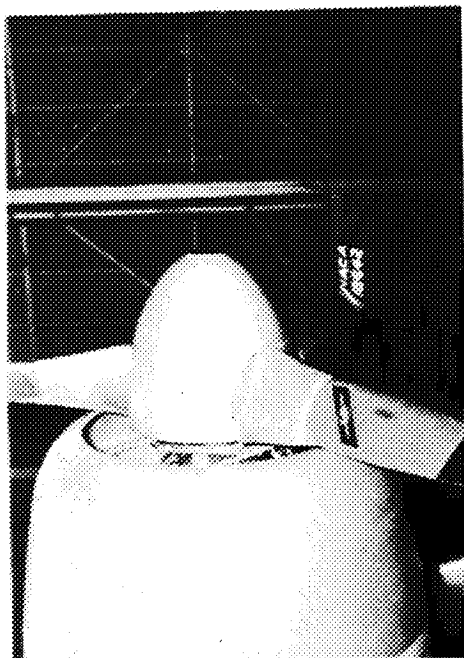
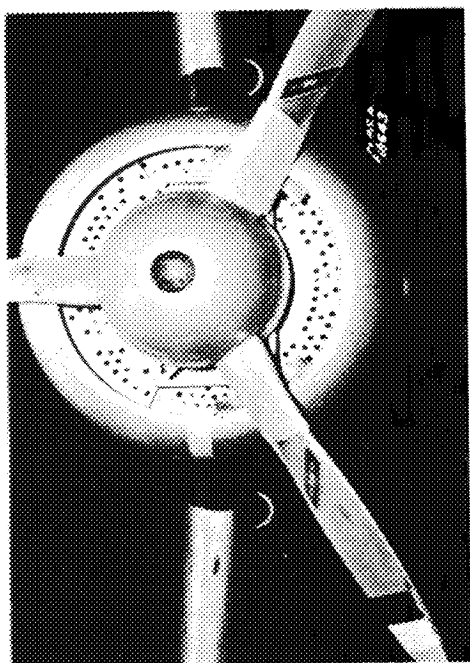
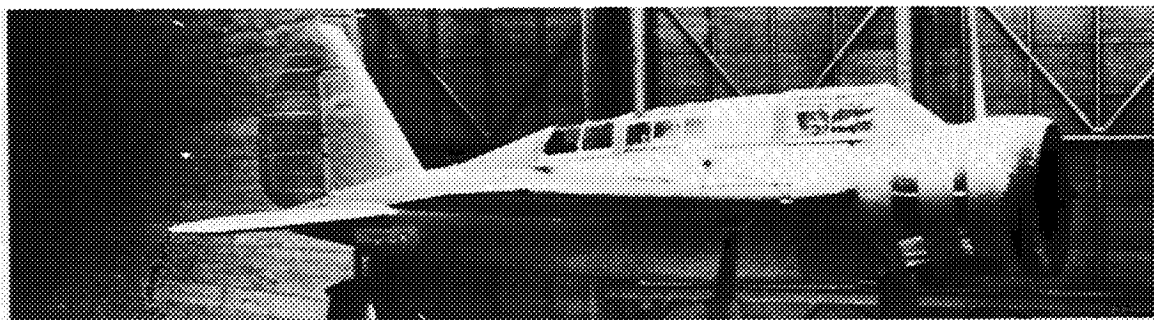
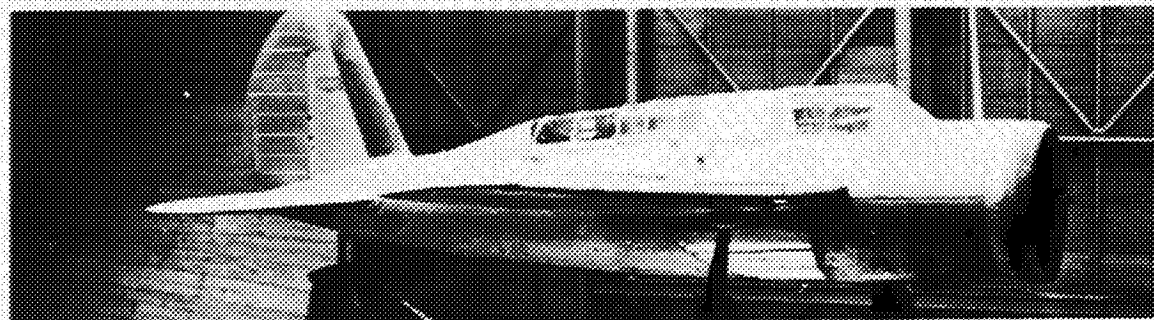


Figure 18.- Spinner arrangements for airplane 10.

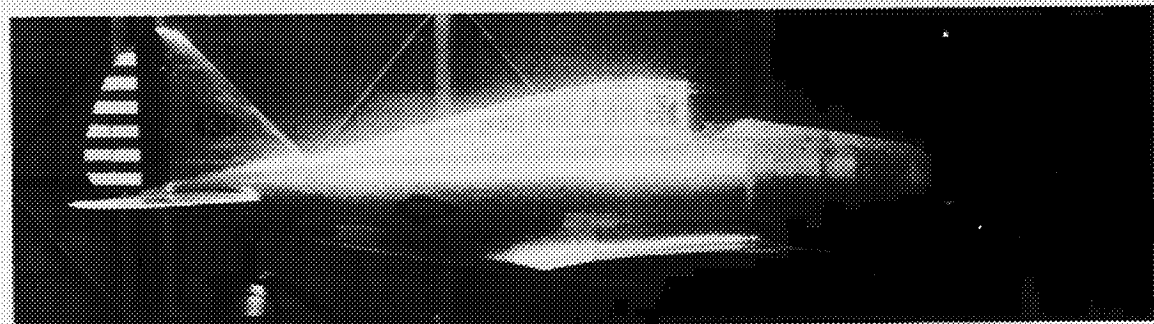


Original condition.

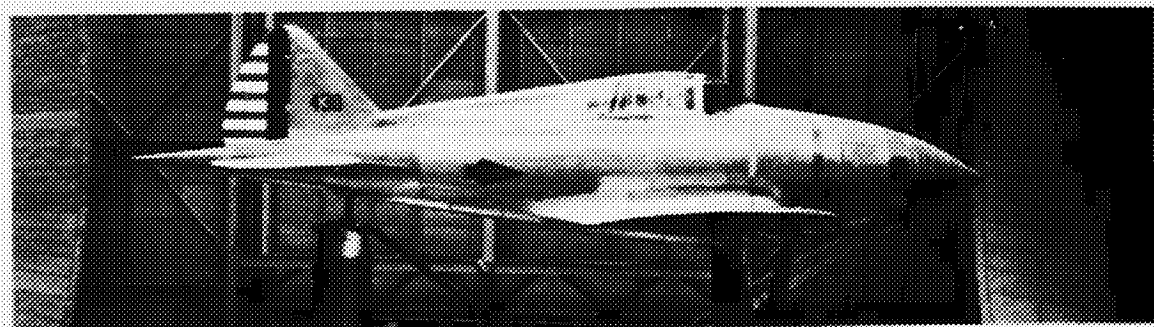


Refaired.

(a) Airplane 6.



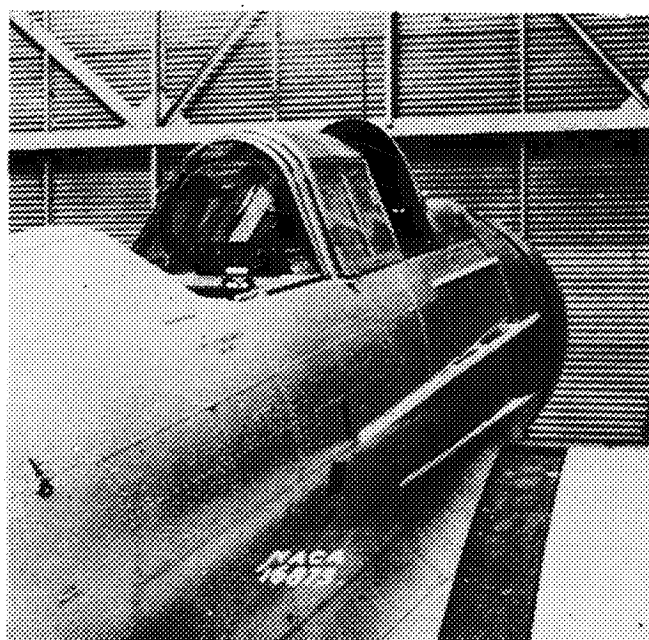
Original condition.



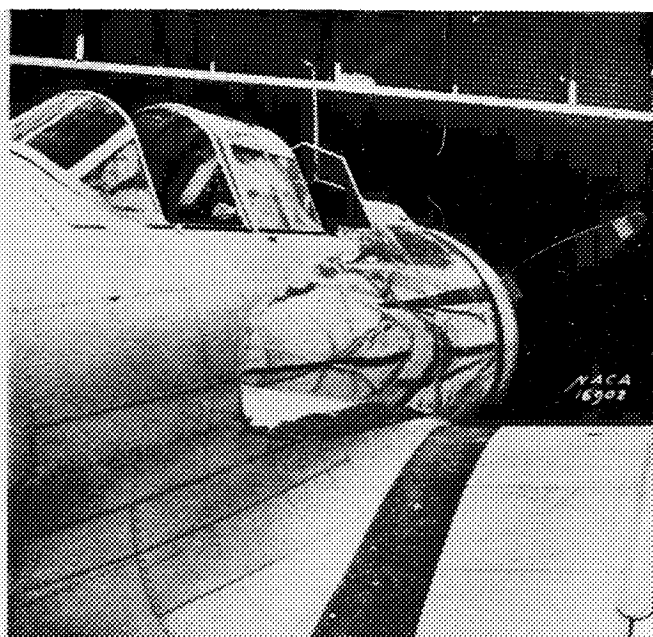
Refaired.

(b) Airplane 10.

Figure 19.—Refairing of fuselage.

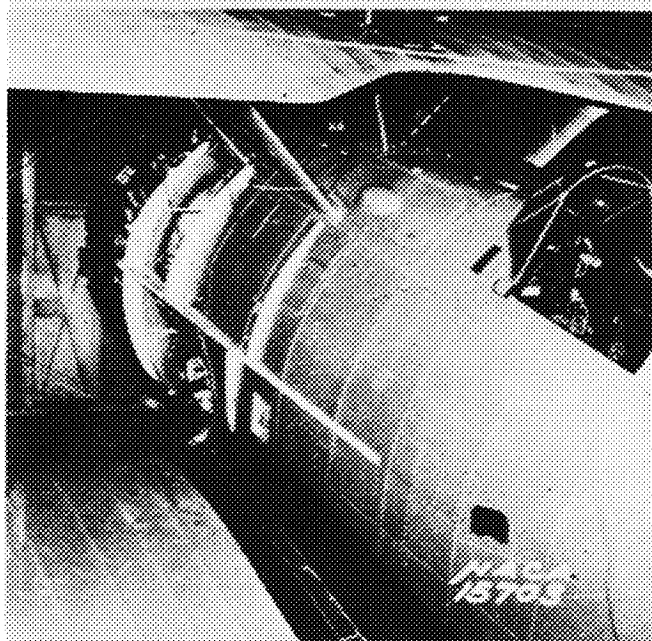


Original condition.



Refaired.

(c) Airplane 5.



Original condition.

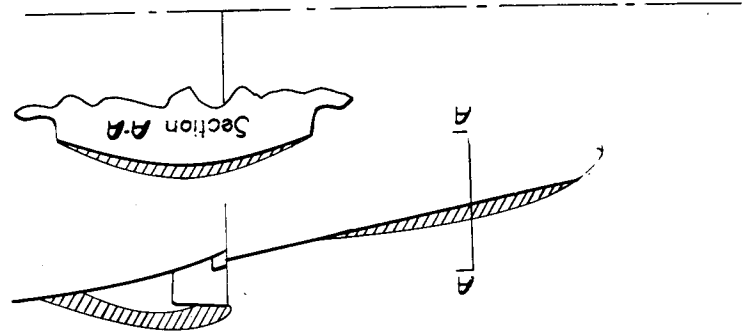


Refaired.

(d) Airplane 3.

Figure 19.— continued. Refairing of fuselage.

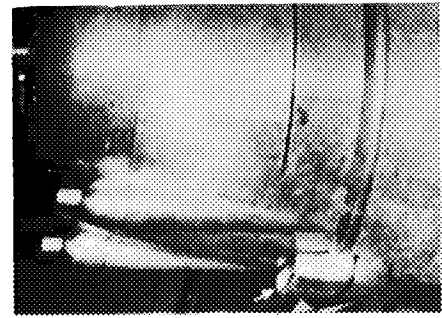




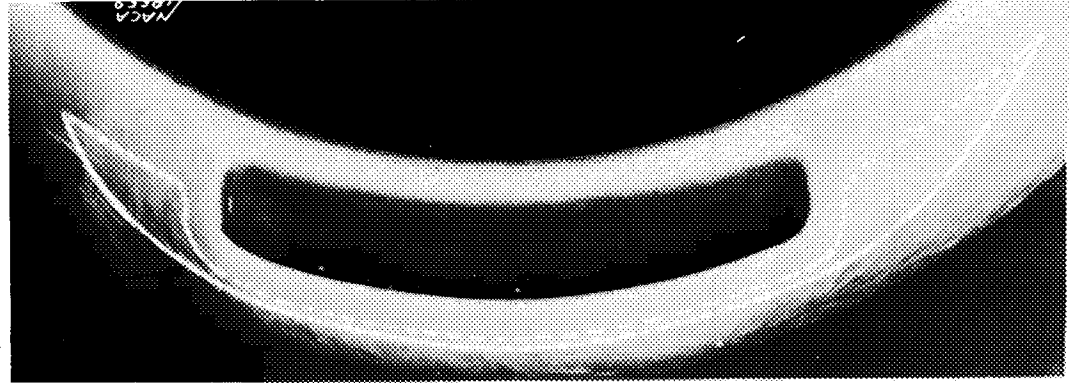
(a) Airplane 2.



(c) Airplane 9.



(b) Airplane 8.

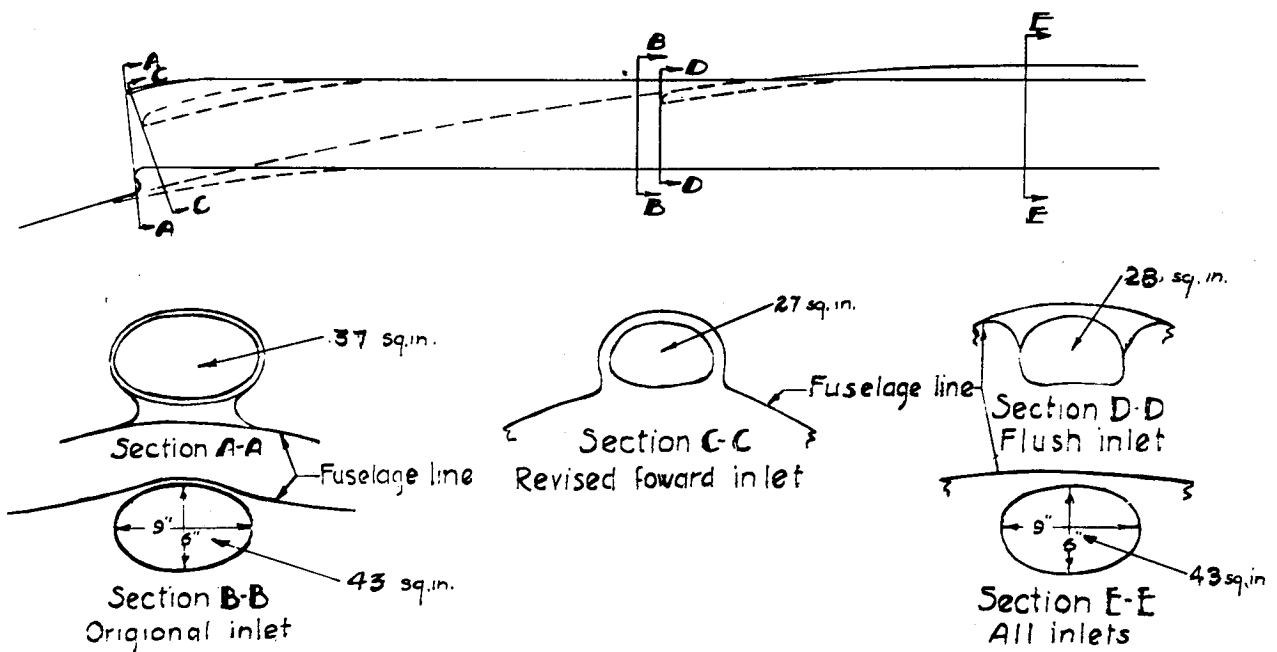
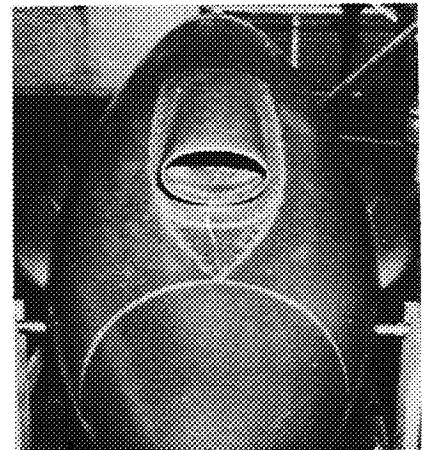
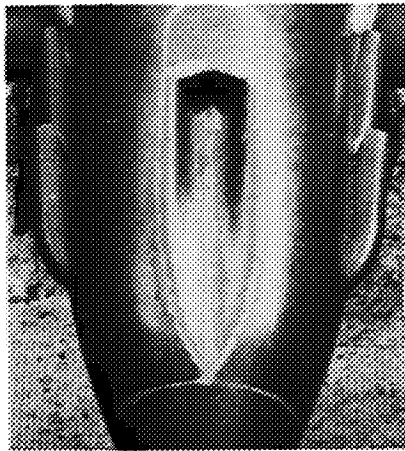
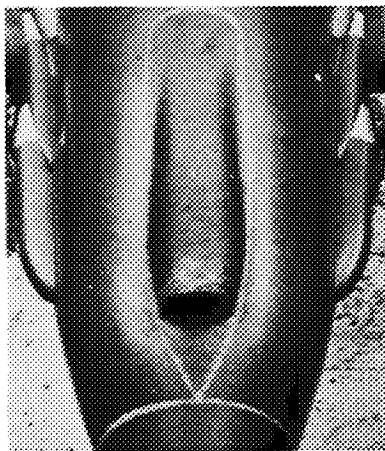


(d) Airplane 10.

Figure 21.-Carburetor air-intakes.

NACA-20905

Fig. 21 a,b,c,d

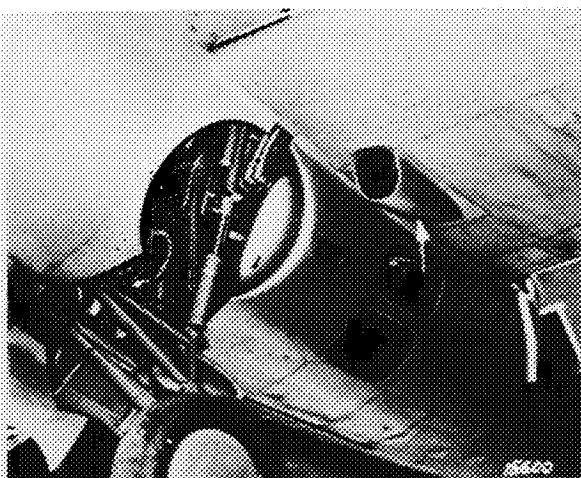


(e) Airplane 11.

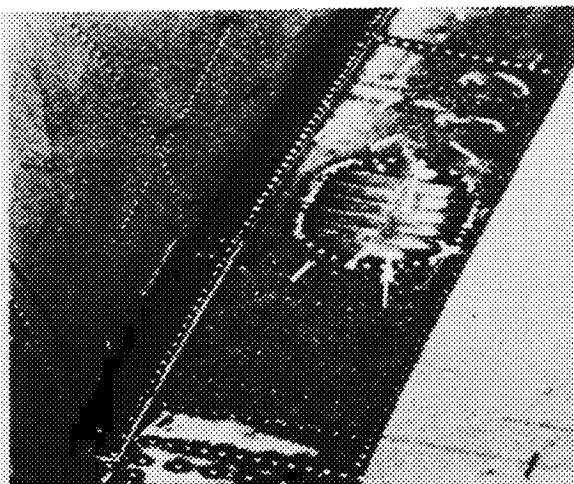
Figure 21.-continued. Carburetor air-intakes.

NACA-20908.



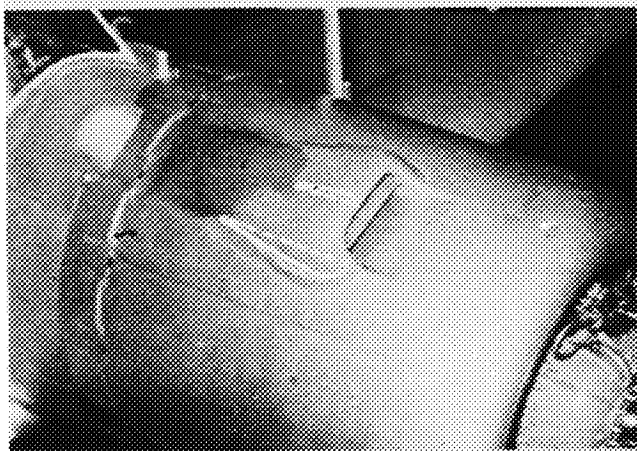


Inlet.

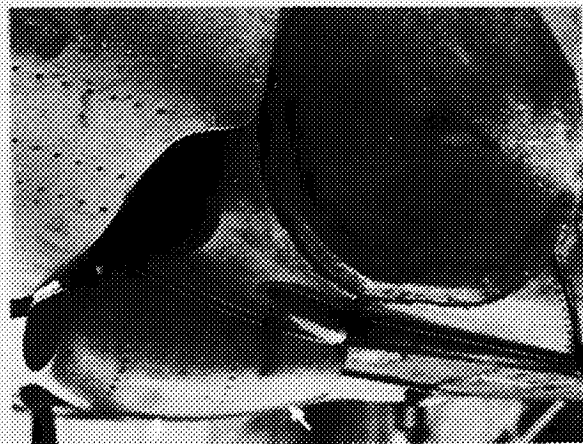


Outlet.

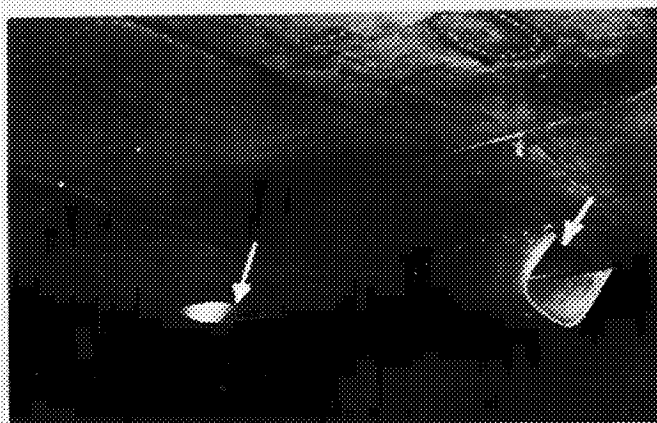
(a) Airplane 2.



(b) Airplane 4.

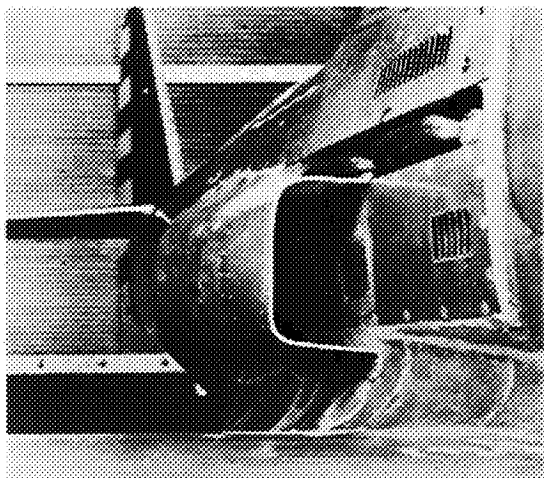


(c) Airplane 3.

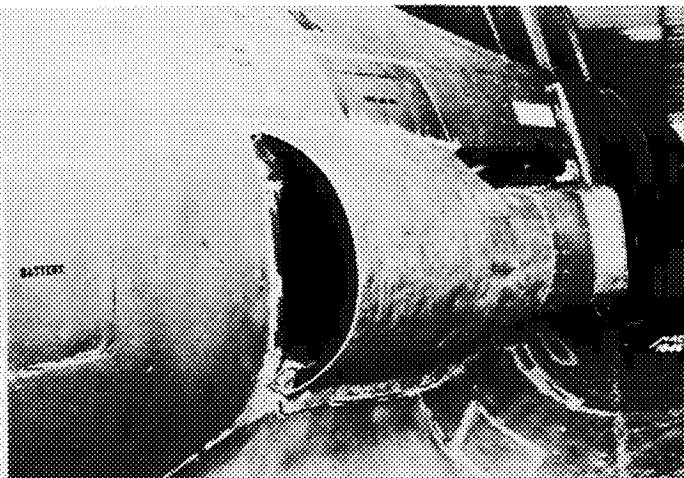


(d) Airplane 8.

Figure 22.— Oil cooler installations.

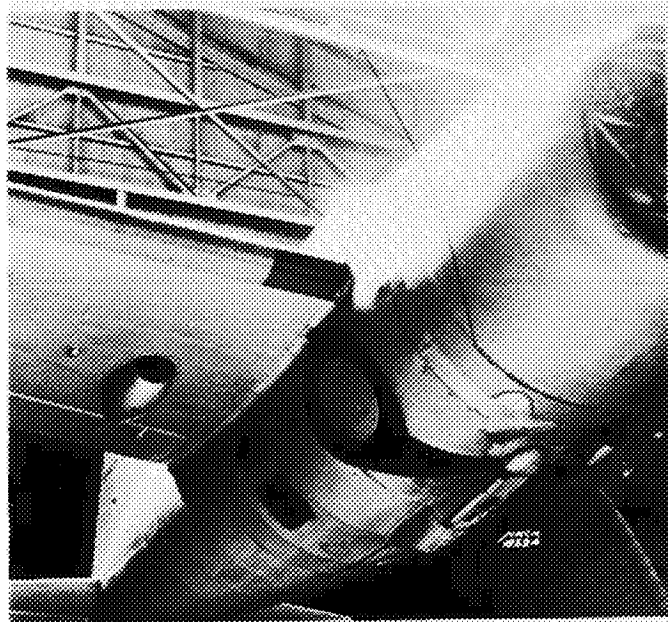


Inlet.

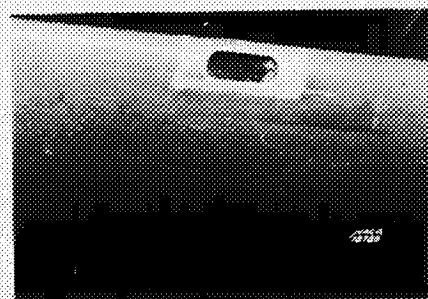


Outlet.

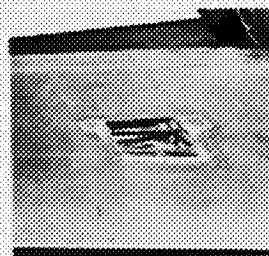
(e) Airplane 9.



(f) Airplane 10.

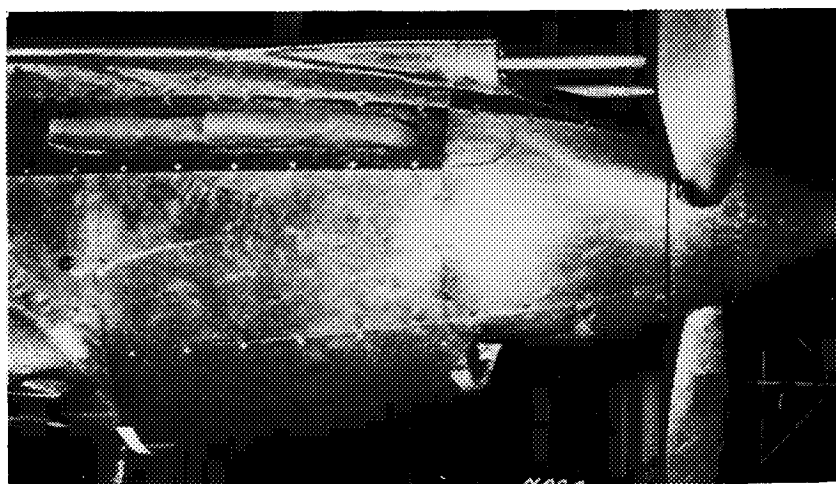
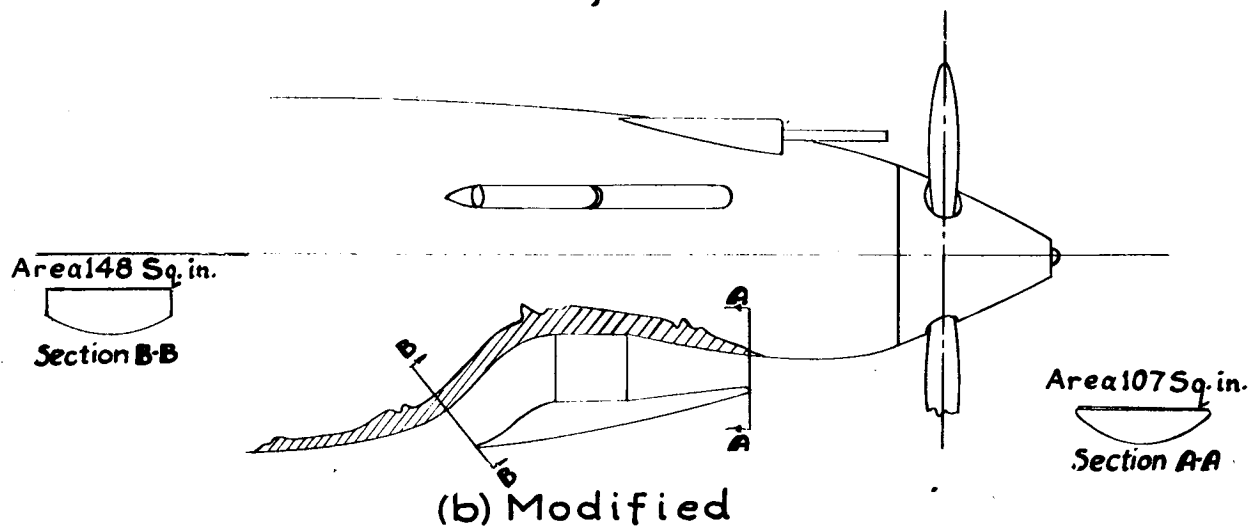
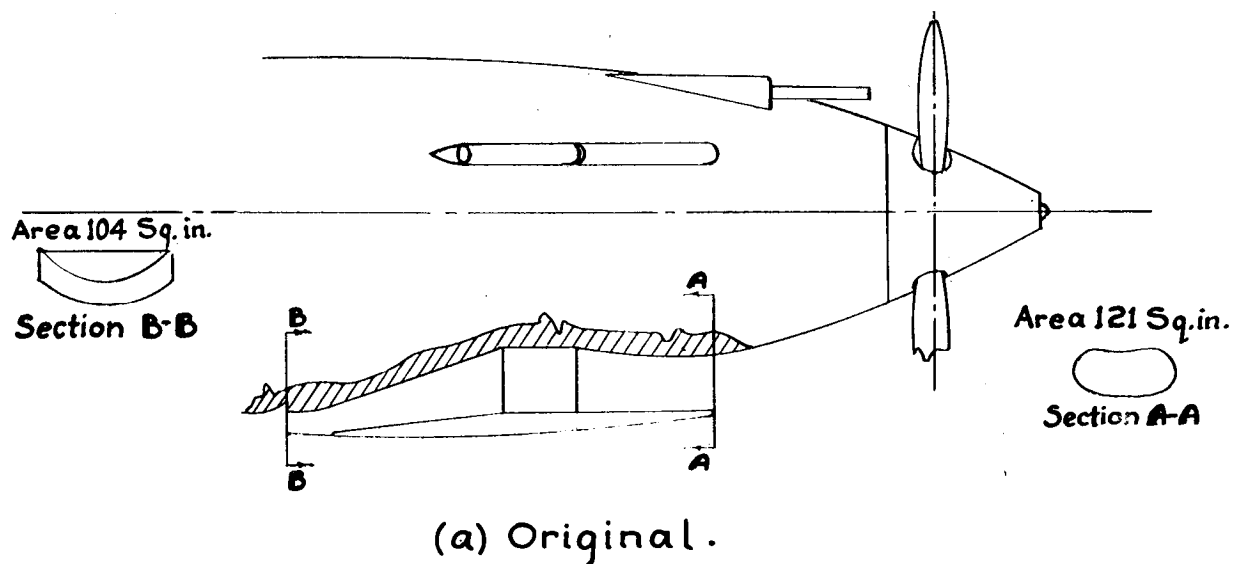


Inlet.

Hinge at l.e. Hinge at t.e.  
Outlet control flap.

(g) Airplane 11.

Figure 22.- continued. Oil cooler installations.



(c) Modified.

Figure 23.-Prestone radiator installation on airplane 7.

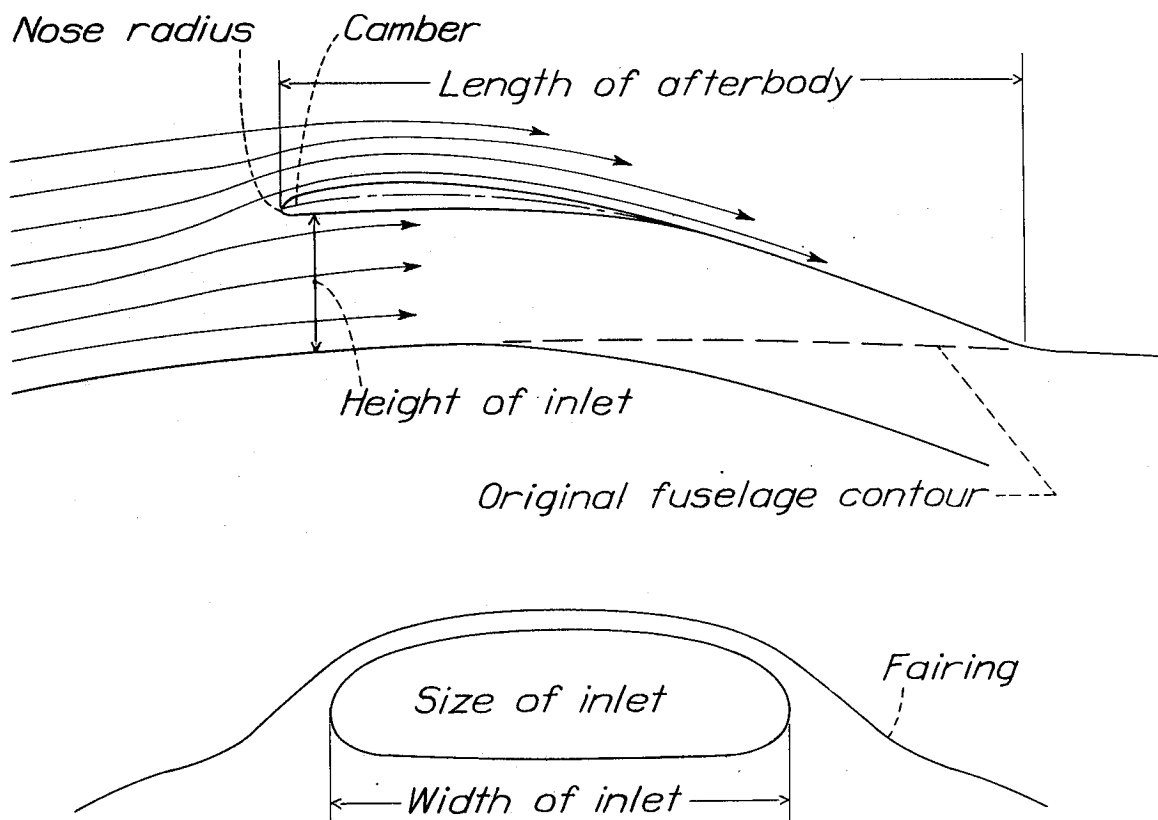


Figure 24.- Details of scoop design.

- 1 Turbulent skin friction curve,  $C_D \propto R^{0.11}$
- 2 Curve corrected for compressibility,  $C_{D_c} = C_D \left(1 + \frac{M^2}{4}\right)$
- 3 Curve corrected for surface roughness

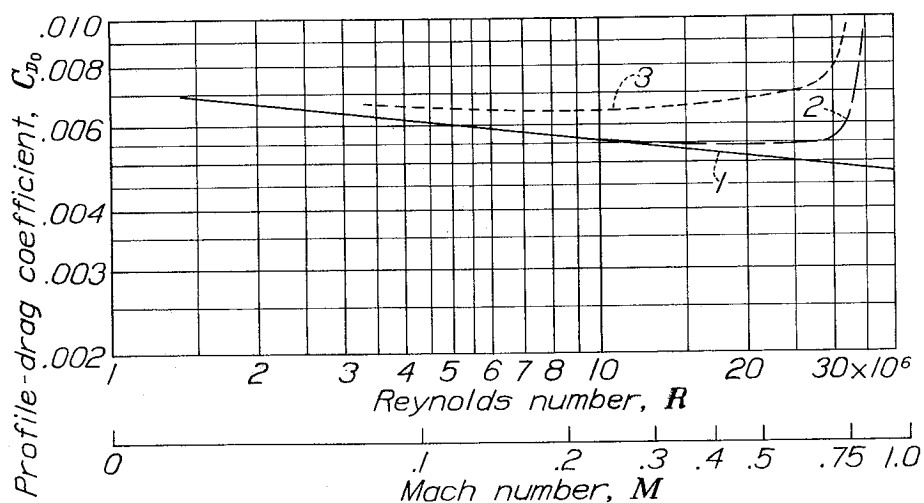
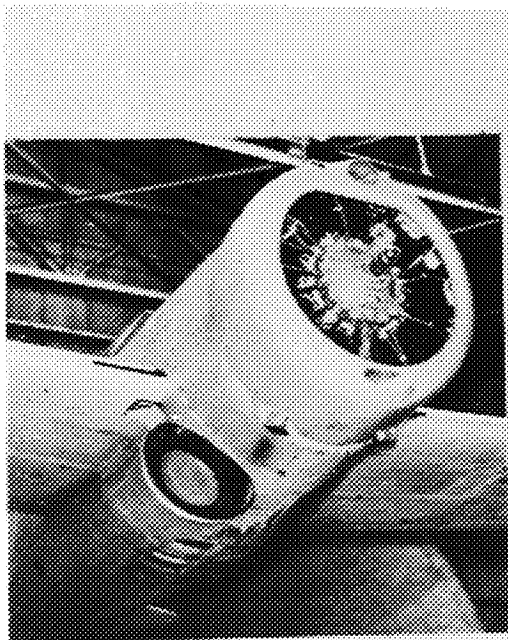
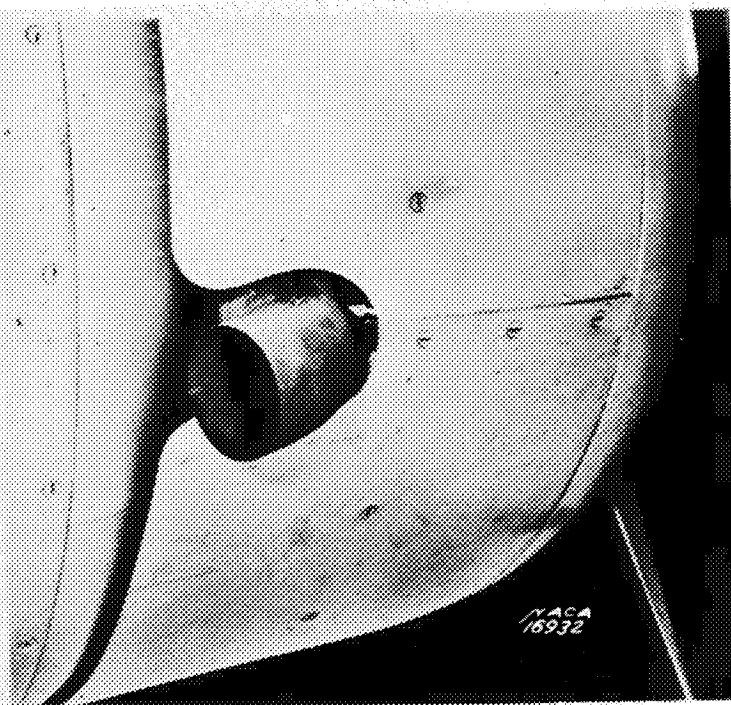


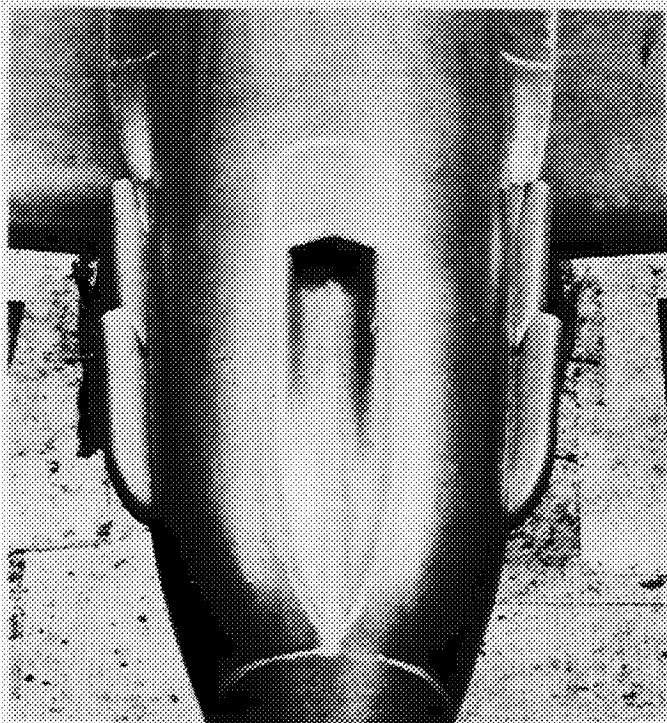
Figure 28.- Method of extrapolation of wing profile-drag coefficients to flight speeds-wing chord, 6 feet.



(a) Airplane 1 .



(b) Airplane 5 .



(c) Airplane 11 .

Figure 25.— Exhaust stacks.

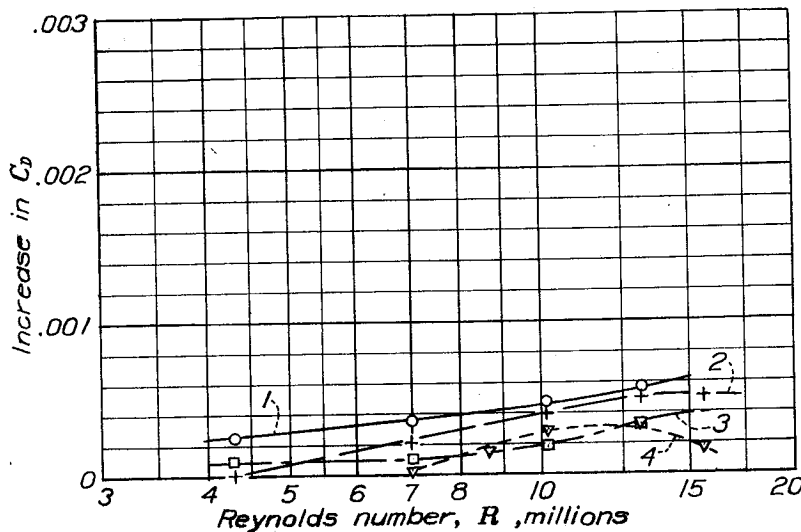


Figure 27.- Drag of surface irregularities added behind the normal smooth wing transition point.

- 1 6 rows of 3/32" brazier head rivets on each surface of 5-foot chord airfoil Pitch 3/4". Forward rows, 52 percent of the chord from leading edge.
- 2 13 rows of 3/32" countersunk rivets on each surface of 5-foot chord airfoil Pitch 3/4". Forward rows, 4 percent of the chord from leading edge.
- 3 8 rows on top and 6 rows on bottom surface of 5-foot chord airfoil. Pitch 3/4". Forward rows, 36 and 52 percent of the chord from leading edge.
- 4 6 joggled laps facing aft on each surface of 5-foot chord airfoil. Forward laps, 8 percent of the chord from leading edge.

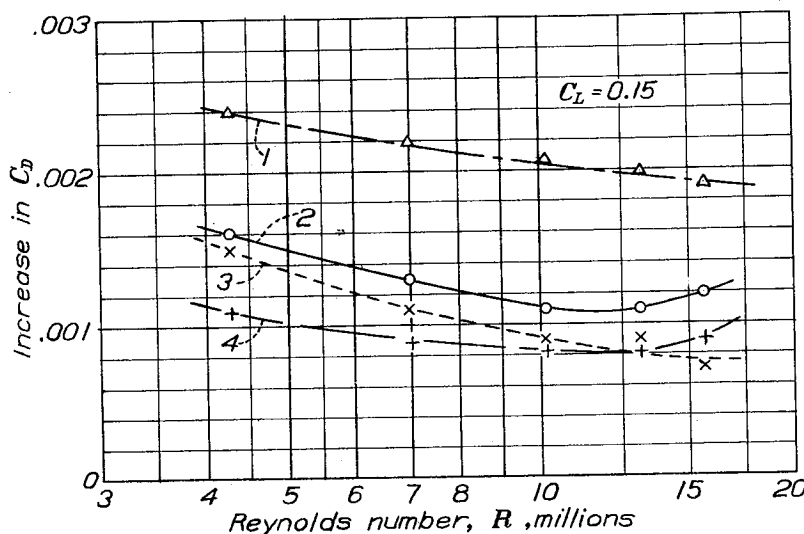
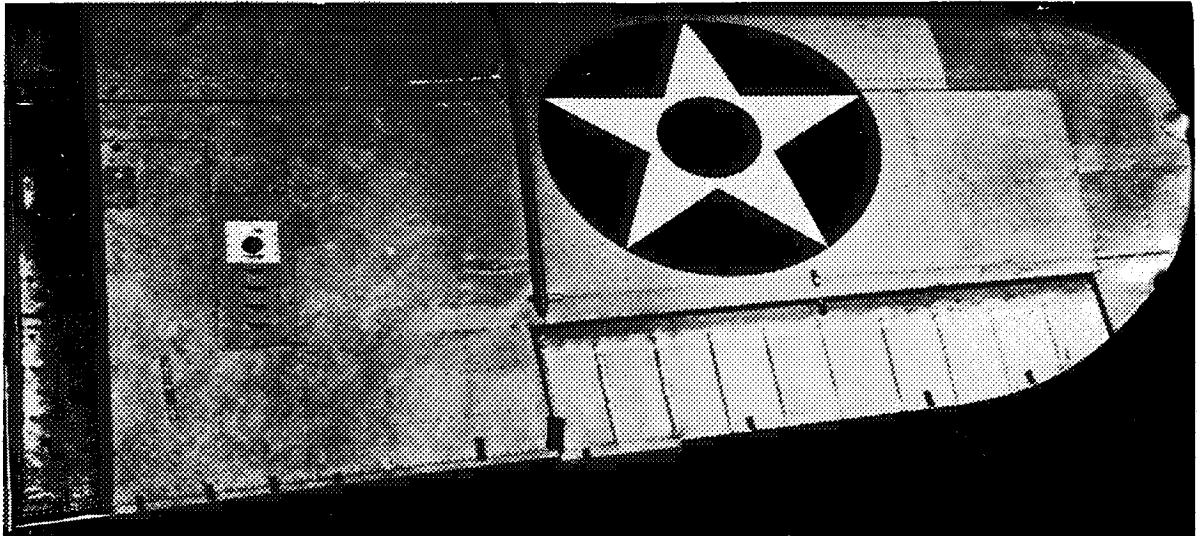


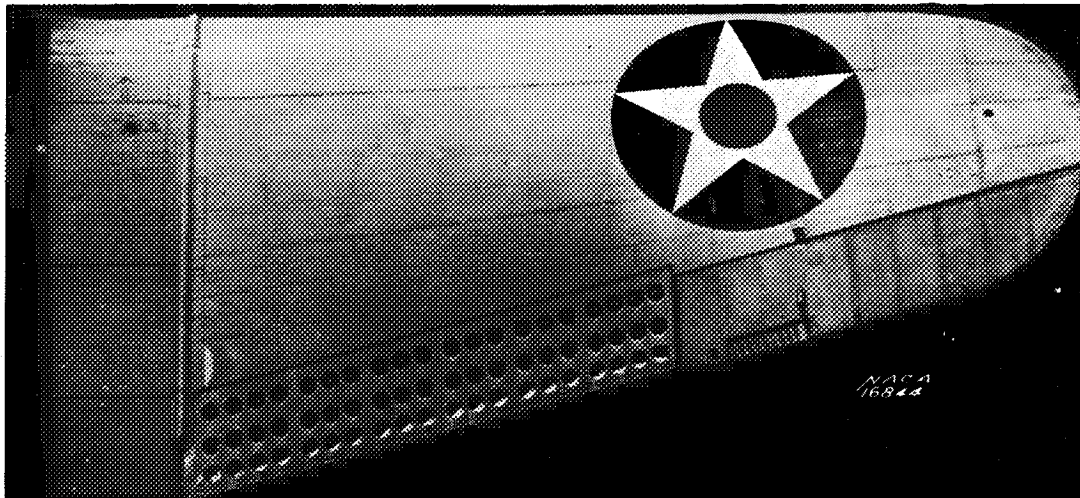
Figure 26.- Drag of surface irregularities added ahead of the normal smooth wing transition point.

- 1 6 joggled laps facing aft on each surface of 5-foot chord airfoil. Forward laps, 8 percent of the chord from leading edge.
- 2 13 rows of 3/32" thin brazier head rivets on each surface of 5-foot chord airfoil Pitch 3/4". Forward rows, 4 percent of the chord from leading edge.
- 3 13 rows of 1/16" brazier head rivets on each surface of 5-foot chord airfoil Pitch 3/4". Forward rows, 4 percent of the chord from leading edge.
- 4 6 plain laps facing aft on each surface of 5-foot chord airfoil. Forward laps, 8 percent of the chord from leading edge.





(a) Airplane 2.

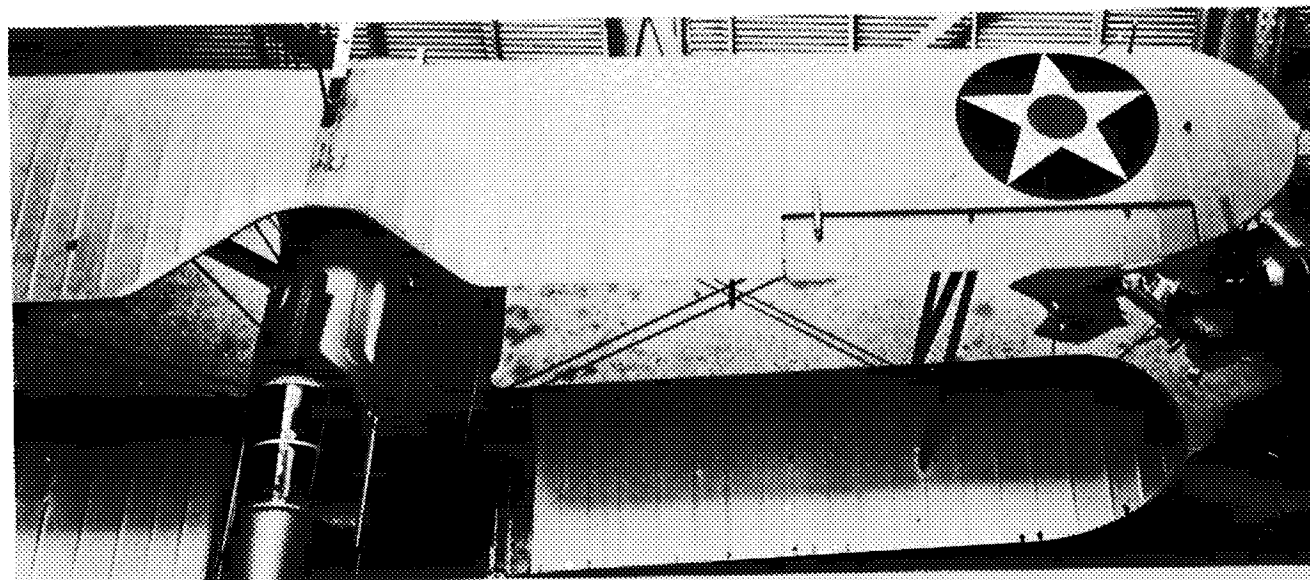


(d) Airplane 5.

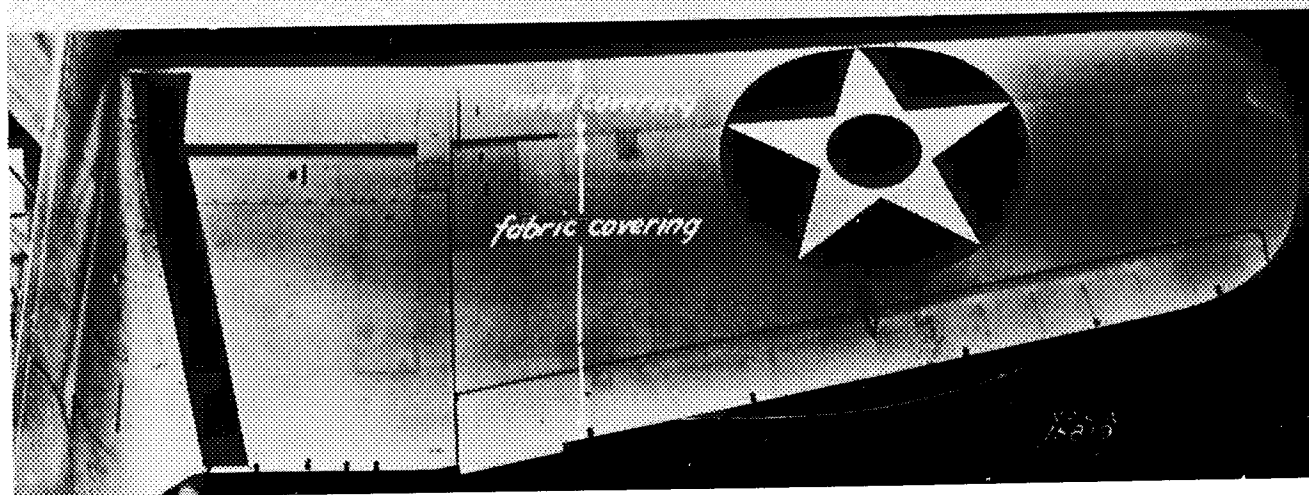


(e) Airplane 8.

Figure 29.- Wing surface conditions.



(b) Airplane 3.



(c) Airplane 4.

Figure 29.- Wing surface conditions.



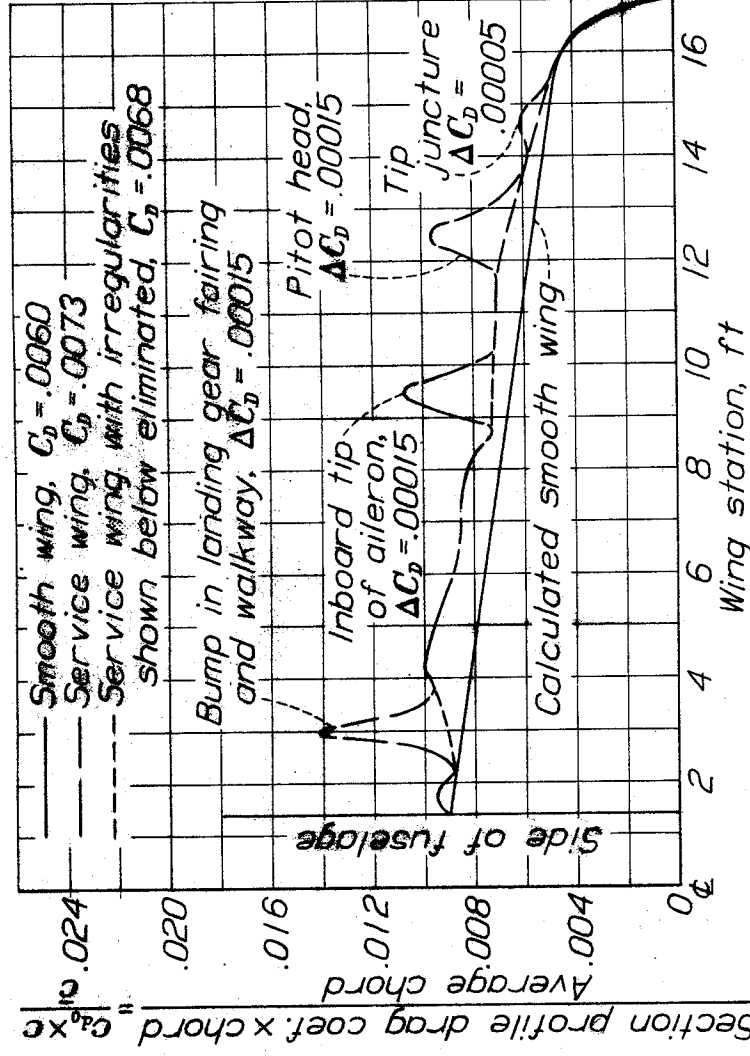


Figure 30.- Typical results obtained by momentum traverse along wing span and calculated smooth wing drag. Airplane 9.

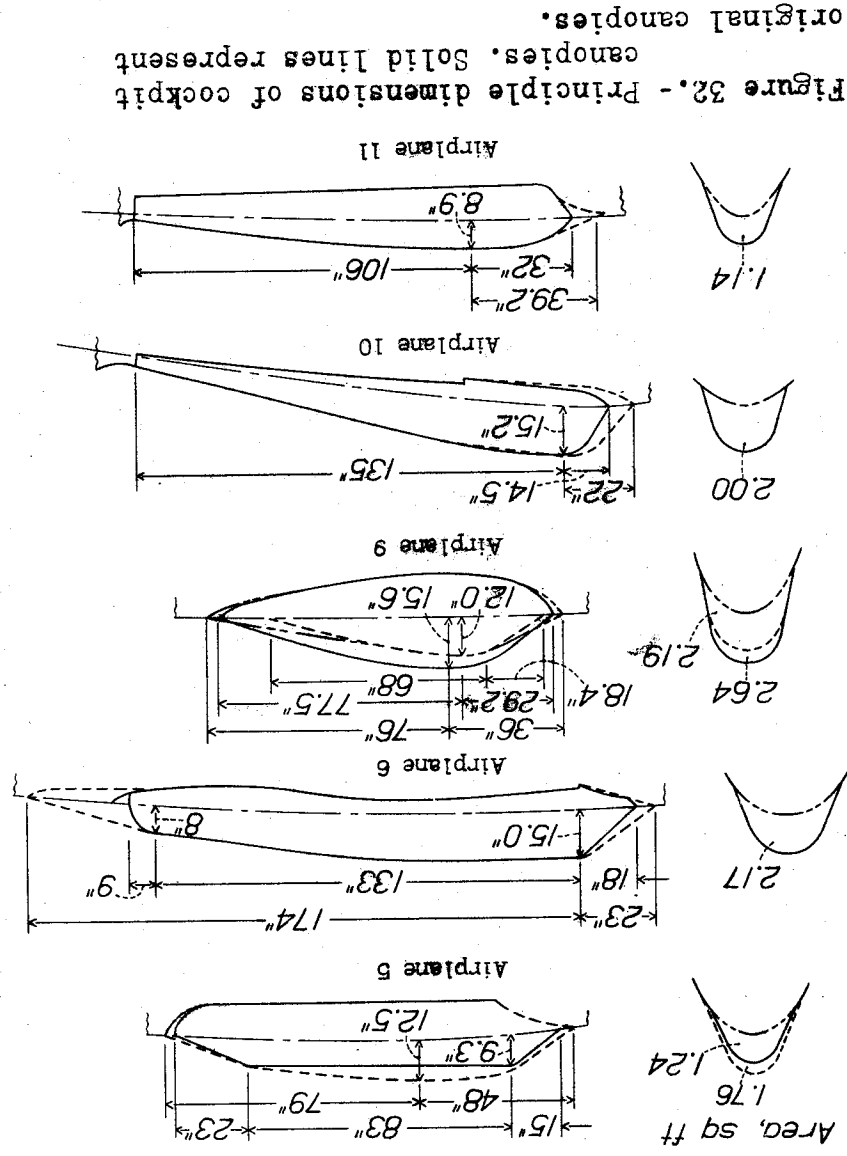
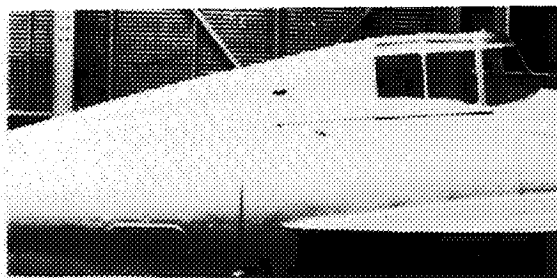
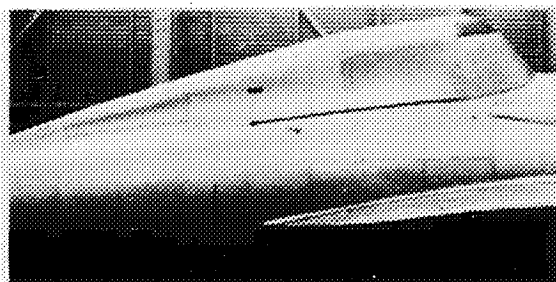


Figure 32.- Principle dimensions of cockpit canopies. Solid lines represent original canopies.

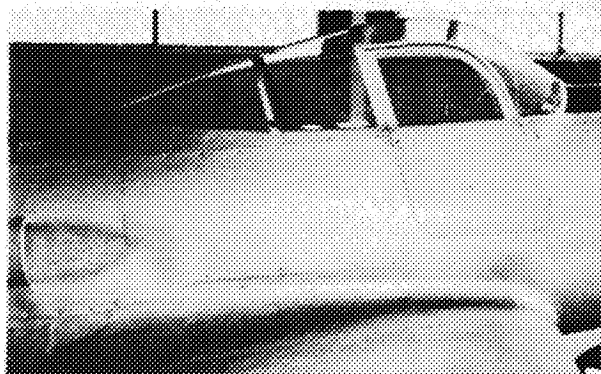


Original windshield

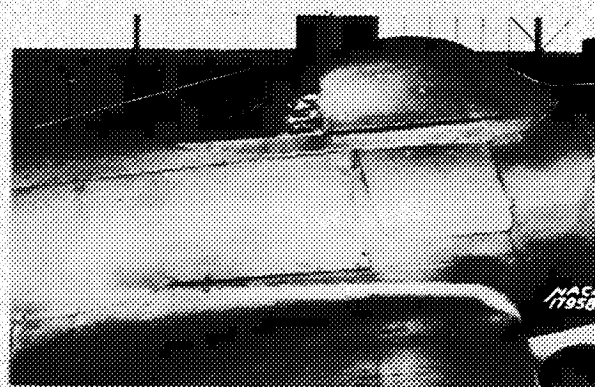


Modified windshield

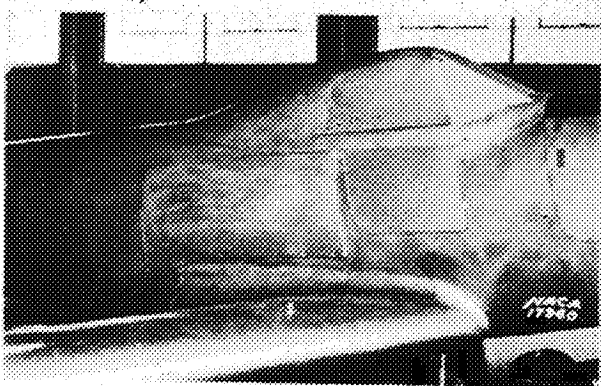
(a) Airplane 10.



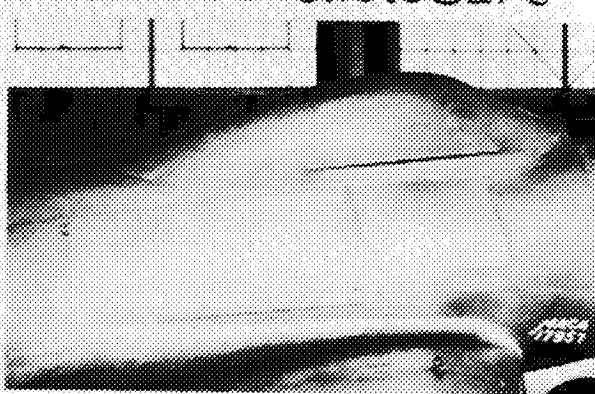
Original enclosure



Lowered enclosure



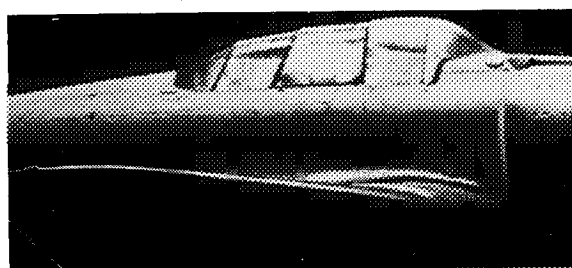
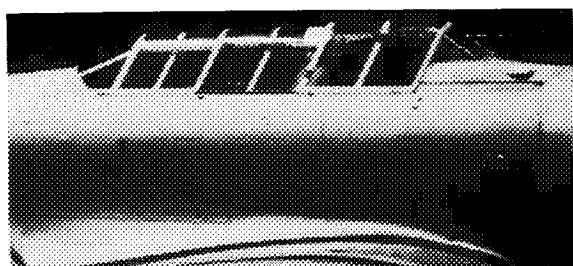
Lowered enclosure, short tail, flat-sided windshield.



Lowered enclosure, short tail.

(b) Airplane 9.

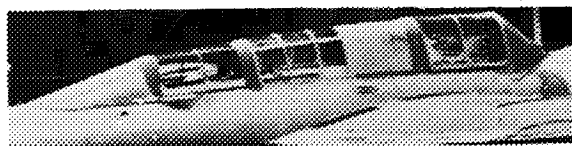
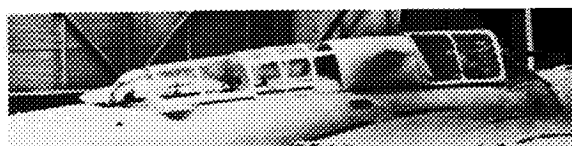
Figure 31.— Cockpit enclosures.



Original enclosure

Modified enclosure

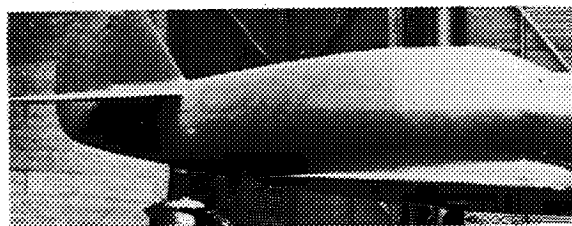
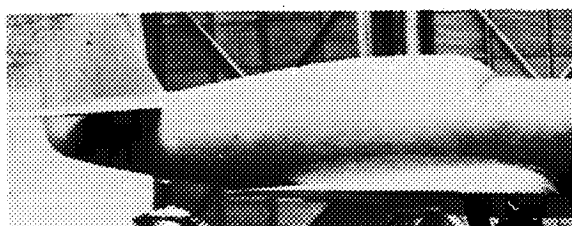
(c) Airplane 5.



Original enclosure

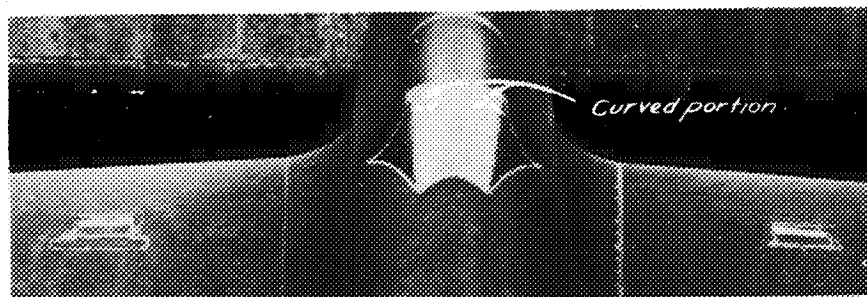
Modified enclosure

(d) Airplane 6.



Original windshield

Flat-sided windshield



Front view of flat-sided windshield

(e) Airplane 11.

Figure 31.- continued. Cockpit enclosures.

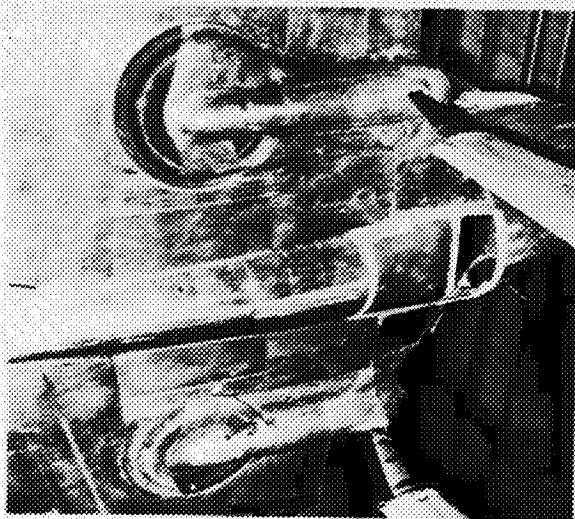


Original condition.

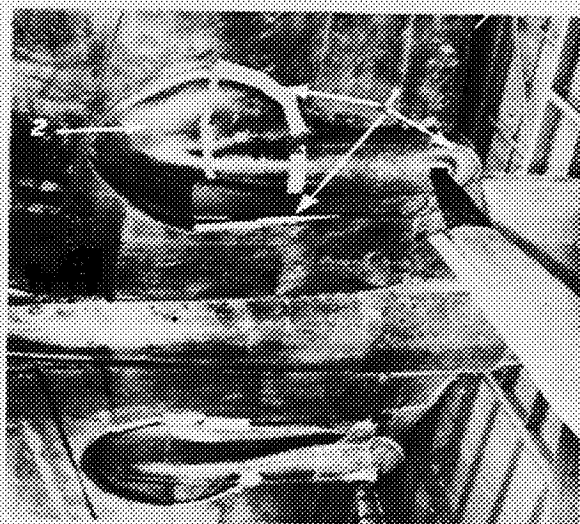


Faired.

(a) Airplane 10.



Original condition.

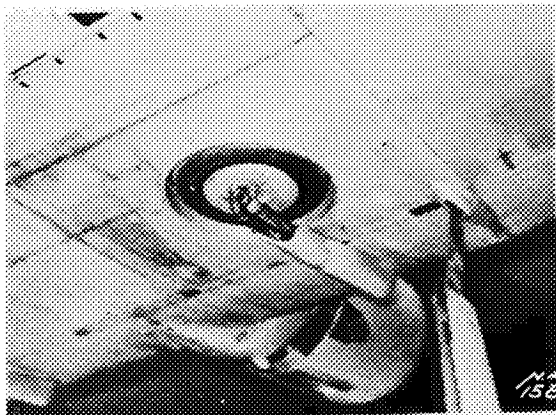


Faired.

(b) Airplane 7.

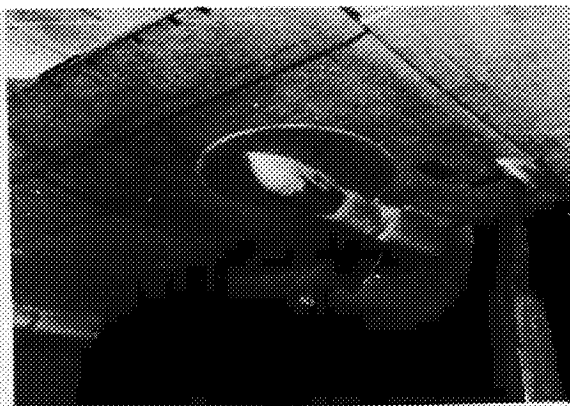
Figure 33.—Landing gears.

NACA 16834

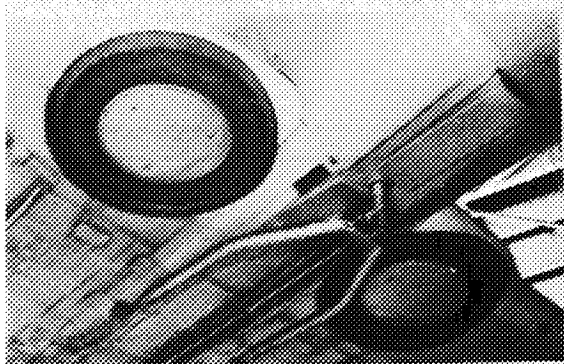


Original condition.

(c) Airplane 4.

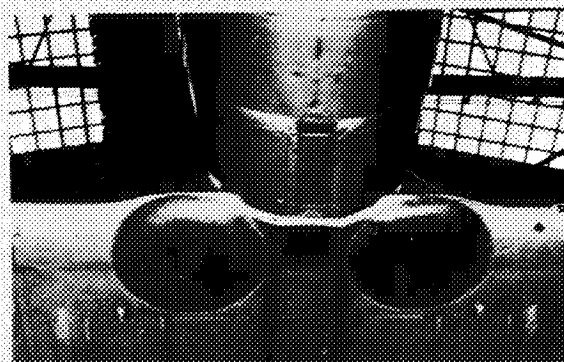


Faired.

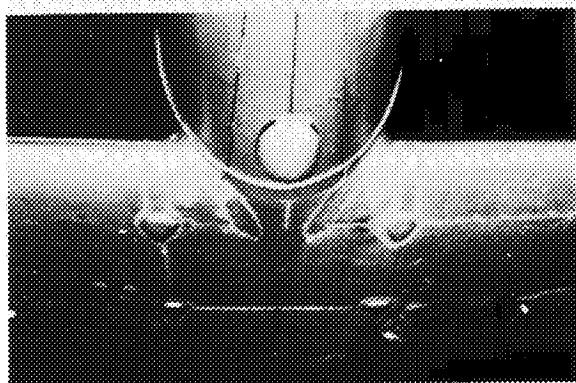


Original condition.

(d) Airplane 5.



Faired.



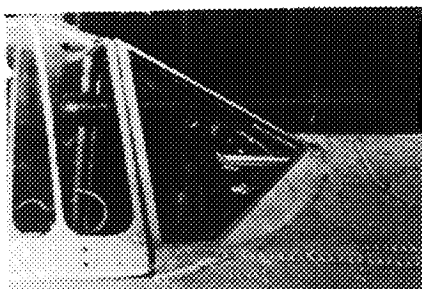
(e) Airplane 9.



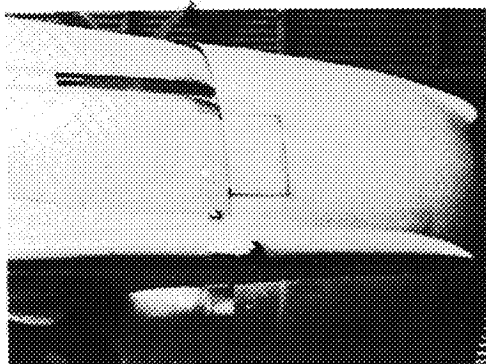
(f) Airplane 8.

Figure 33.-continued. Landing gears.

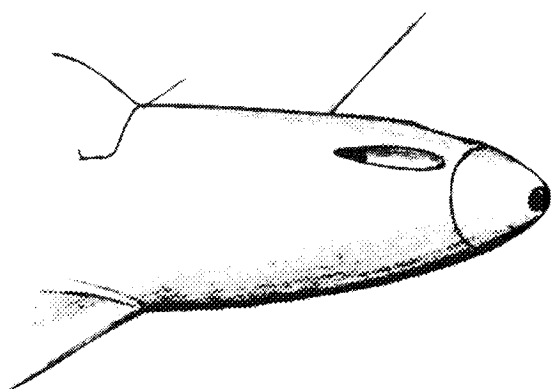




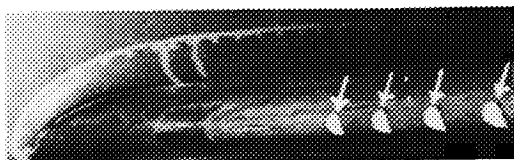
(a) Gun sight on airplane 1.



(b) Blast tube on airplane 10.



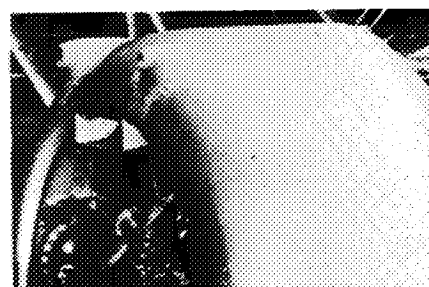
(d) Gun and cannon installation on airplane 9.



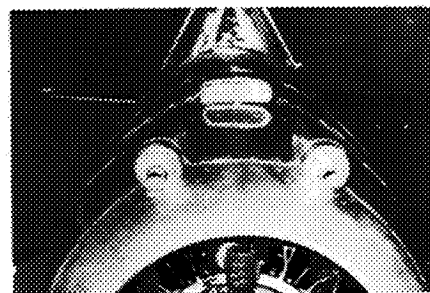
(f) Wing and fuselage guns on airplane 11.



Original condition.



Sealed and faired.  
(c) Blast tube installation on airplane 3.



(e) Blast tubes on airplane 8.

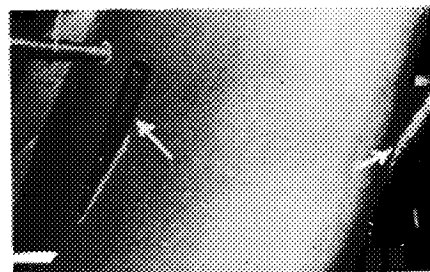


Figure 34.- Armament.

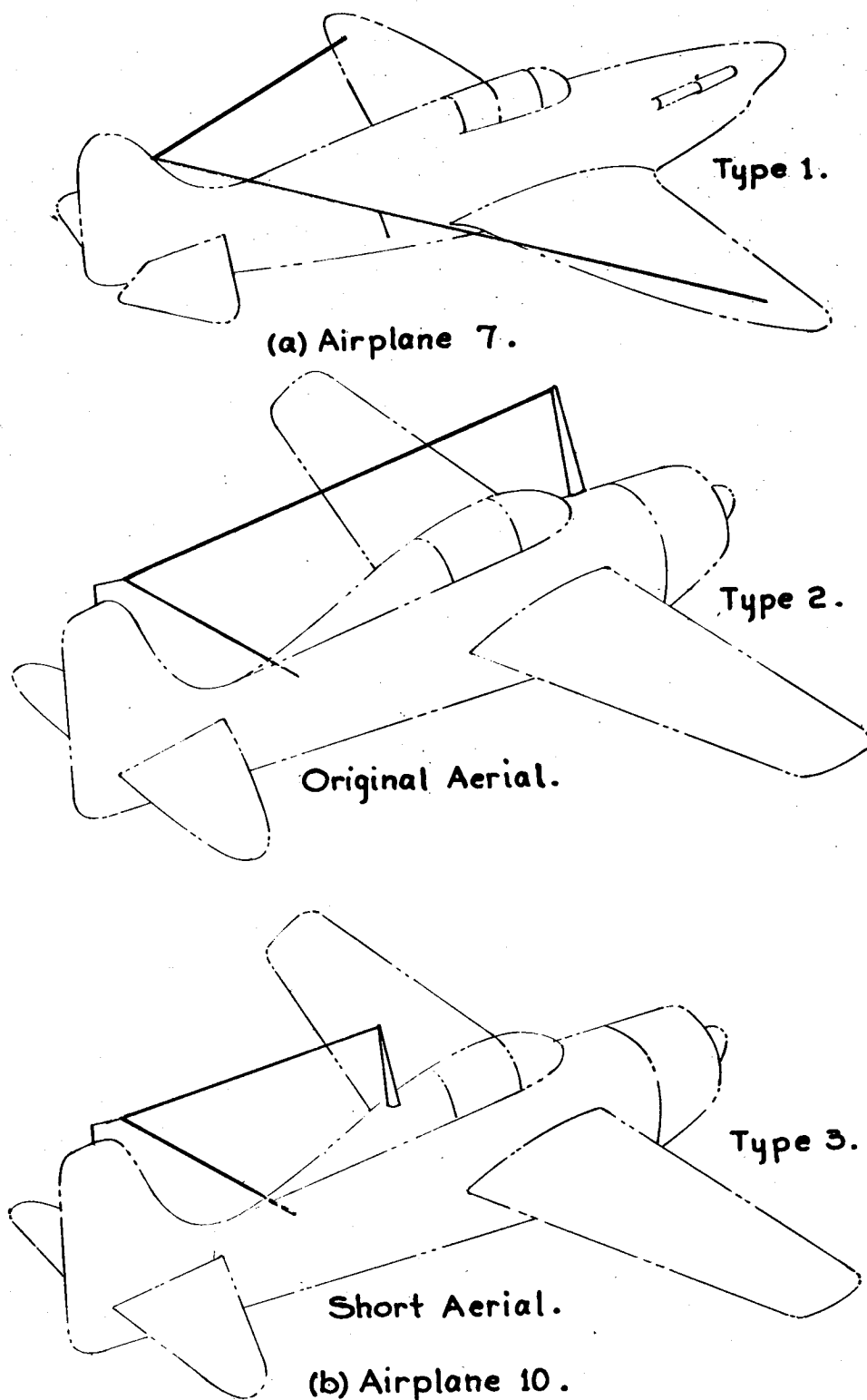
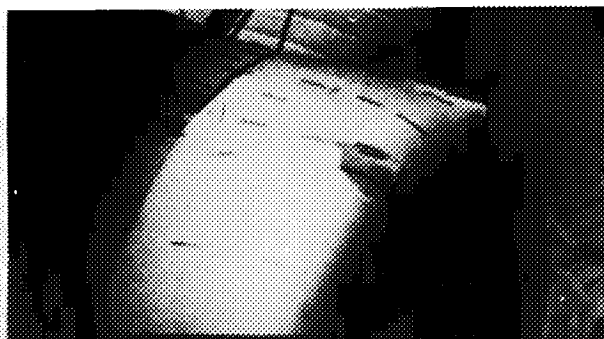
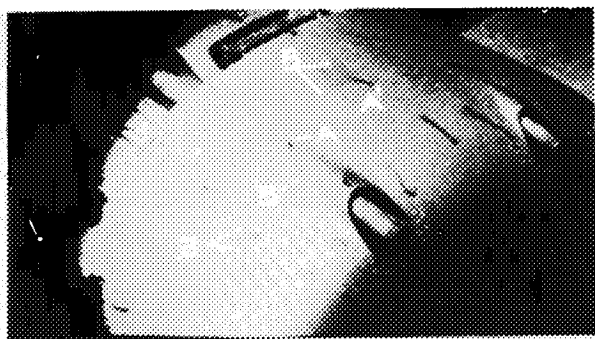


Figure 35.-Aerial installations.

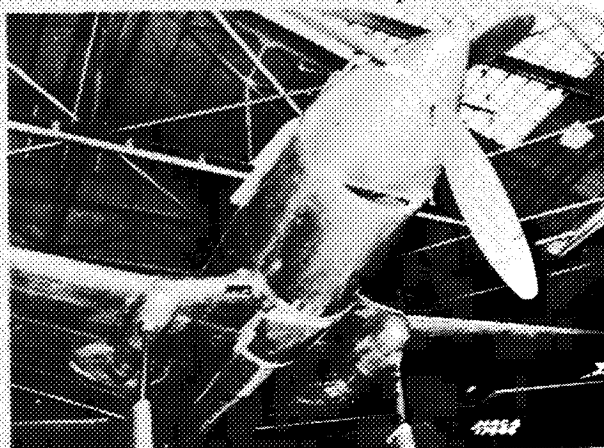
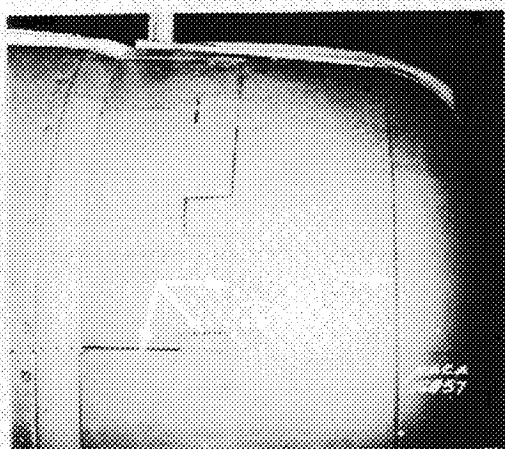
MCA-20925

NACA

Fig. 36

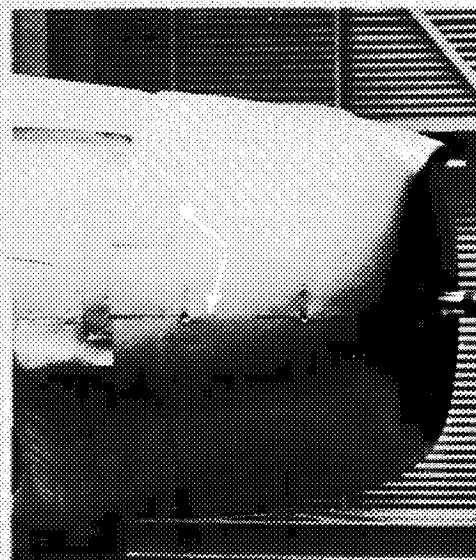
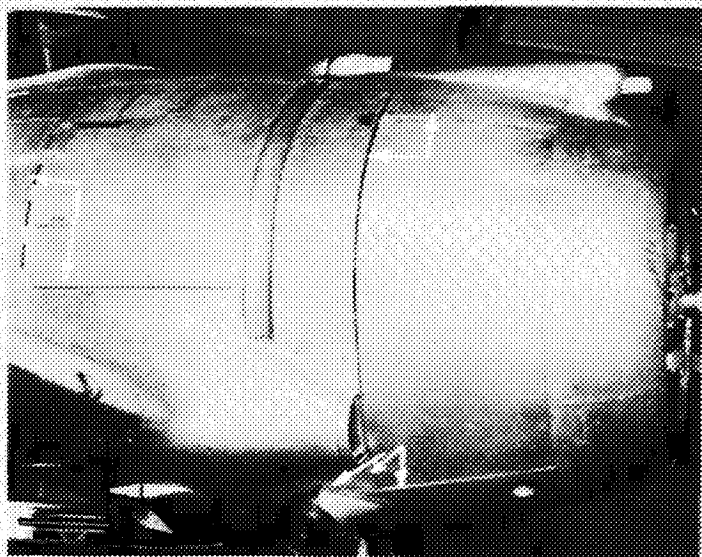


Original installation. Tubes faired & cowling gaps sealed.  
 (a) Gun blast tube installation on airplane 3. (Note: A indicates fixed ends of tufts & B their free ends for original condition.)



(b) Cowling gaps on airplane 5.

(c) Spinner gaps on airplane 7.



(d) Cowling gaps on airplane 8.

(e) Cowling gaps on airplane 10.

Figure 36.—Sources of leakage.



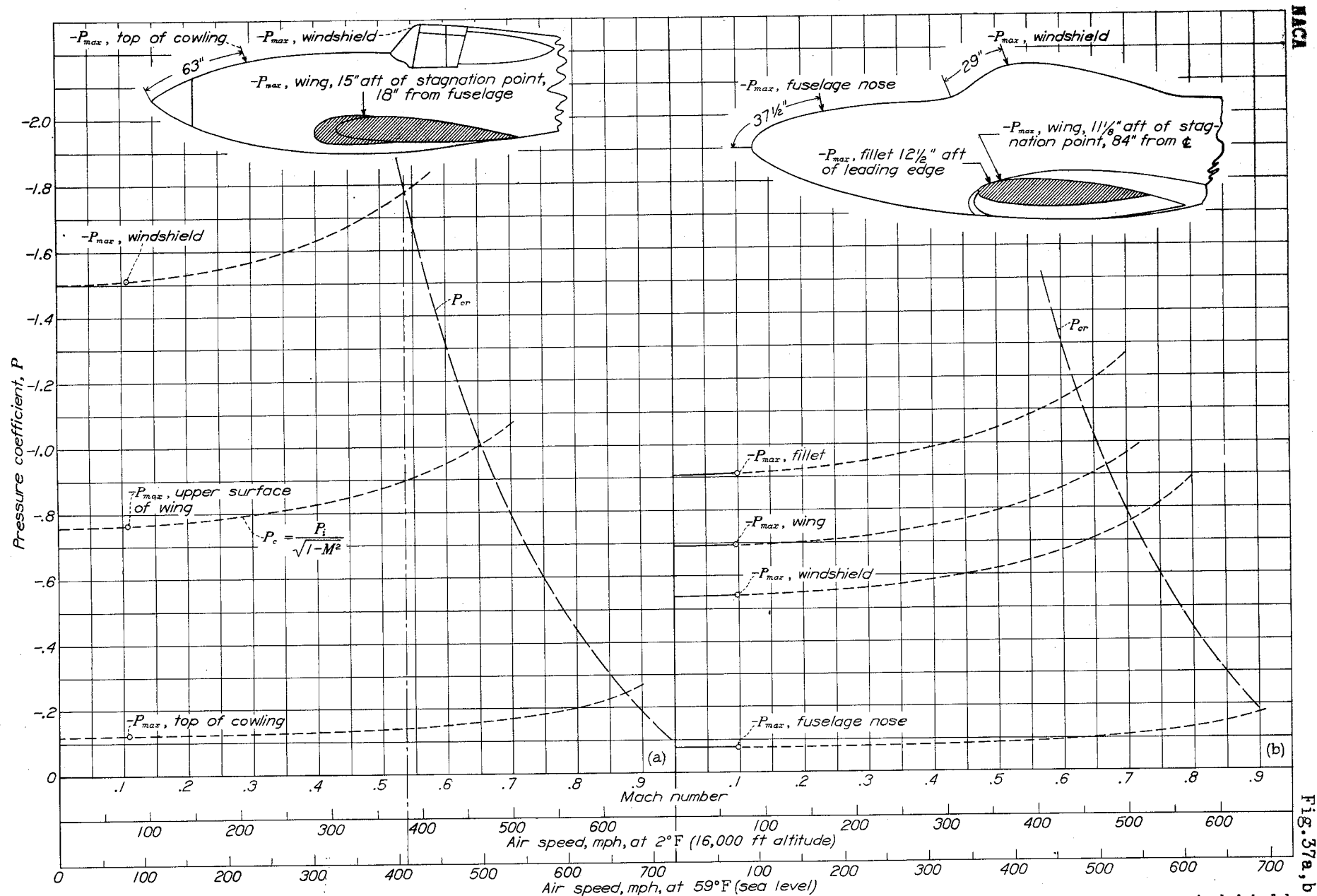


Figure 37a.- Critical speed for windshield, wing, and nose of airplane 7.

Figure 37b.- Critical speed for airplane nose, windshield, wing, and fillet, airplane 9.

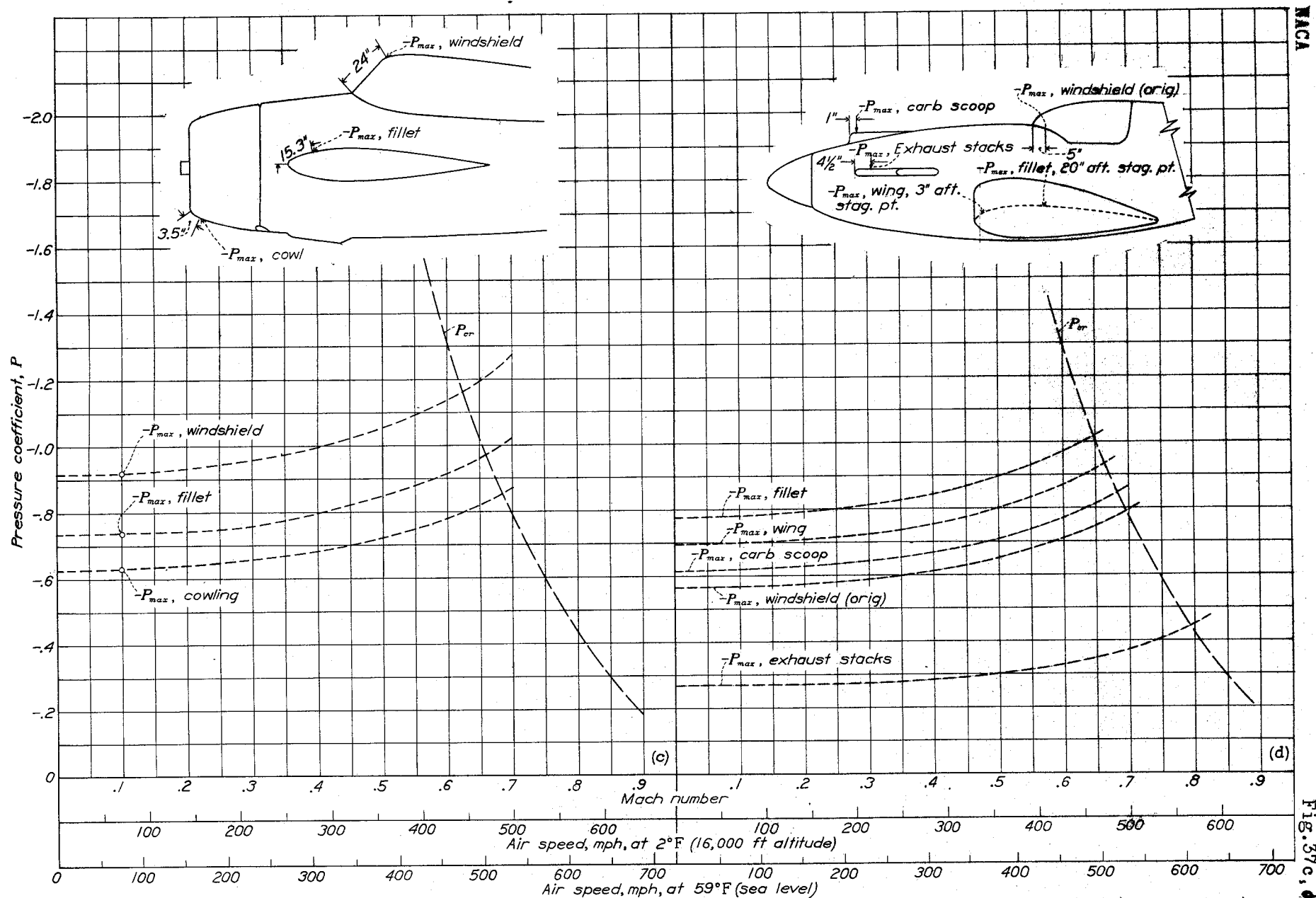


Figure 37c.- Determination of the critical compressibility speeds. Airplane 10.

Figure 37d.- Critical speed for various components of airplane 11.